

For Reference

NOT TO BE TAKEN FROM THIS ROOM

Ex libris
UNIVERSITATIS
ALBERTAENSIS



T H E U N I V E R S I T Y O F A L B E R T A

RELEASE FORM

NAME OF AUTHOR: NORMAN PATRICK FREITAG

TITLE OF THESIS: VAPOR-LIQUID EQUILIBRIA IN TERNARY
 SYSTEMS OF HYDROGEN AND CARBON DIOXIDE
 WITH A LIGHT ALKANE

DEGREE FOR WHICH THESIS WAS PRESENTED: DOCTOR OF PHILOSOPHY

YEAR THIS DEGREE GRANTED FALL 1982

Permission is hereby granted to THE UNIVERSITY OF
ALBERTA LIBRARY to reproduce single copies of this
thesis and to lend or sell such copies for private,
scholarly or scientific research purposes only.

The author reserves other publication rights, and
neither the thesis nor extensive extracts from it may
be printed or otherwise reproduced without the author's
written permission.

THE UNIVERSITY OF ALBERTA

VAPOR-LIQUID EQUILIBRIA IN TERNARY SYSTEMS
OF HYDROGEN AND CARBON DIOXIDE WITH A
LIGHT ALKANE

by



NORMAN PATRICK FREITAG

A THESIS

SUBMITTED TO THE FACULTY OF GRADUATE STUDIES AND RESEARCH,
IN PARTIAL FULFILMENT OF THE REQUIREMENTS FOR THE DEGREE
OF DOCTOR OF PHILOSOPHY

DEPARTMENT OF CHEMICAL ENGINEERING

EDMONTON, ALBERTA

FALL, 1982



Digitized by the Internet Archive
in 2019 with funding from
University of Alberta Libraries

<https://archive.org/details/Freitag1982>

THE UNIVERSITY OF ALBERTA

FACULTY OF GRADUATE STUDIES AND RESEARCH

The undersigned certify that they have read, and recommend to the Faculty of Graduate Studies and Research, for acceptance, a thesis entitled VAPOR-LIQUID EQUILIBRIA IN TERNARY SYSTEMS OF HYDROGEN AND CARBON DIOXIDE WITH A LIGHT ALKANE submitted by NORMAN PATRICK FREITAG in partial fulfilment of the requirements for the degree of Doctor of Philosophy.



To my Parents,
LOUIE and DOROTHEA FREITAG

ABSTRACT

The equilibrium compositions and refractive indices of the vapor and liquid phases were measured for the hydrogen-carbon dioxide-methane system at 227.4 and 258.2 K, for the hydrogen-carbon dioxide-n-pentane system at 273.2 and 323.2 K, and for the hydrogen-n-pentane system at 273.2, 323.2 and 373.2 K at pressures up to 27 600 kPa. The molar volumes of the co-existing phases were calculated from the refractive index measurements combined with pure component Lorentz-Lorenz refractivities obtained from the literature.

The lower-temperature portion of the data for the hydrogen-carbon dioxide-methane system was obtained with an existing, constant-volume, stirred, equilibrium cell. The remaining, larger portion of the data was obtained with a constant-volume, vapor-recirculation cell that was built for this purpose.

Vapor pressure and density data for pure hydrogen were taken from the literature and were examined in order to select appropriate methods of hydrogen parameter calculation that can be used with several commonly used cubic equations of state. Two suitable approaches, the modification of Gunn, Chueh and Prausnitz, and the use of the unmodified experimental parameters, were identified and were compared by employing them in the Peng-Robinson equation of state to predict the experimental data.

The modification of Gunn et al. provided no significant improvement over the use of unmodified parameters.

The use of temperature-dependent binary interaction parameters provided no improvement over the use of constant interaction parameters. The accuracy of vapor-liquid equilibrium predictions of the hydrogen concentrations was substantially poorer than for the other compounds that were present.

ACKNOWLEDGEMENT

I wish to express my thankfulness to Dr. D. B. Robinson for consistently and willingly providing his invaluable judgement and advice, and especially for the patience shown during the periods in which progress on this project was slow.

I would also like to thank Dr. H. J. Ng, Mr. Hans Rempis and Dr. H. Kalra for their help in solving many of the technical problems associated with the taking and processing of the data, and to Dr. D. Y. Peng for making available his computer program for phase equilibrium predictions. In addition, I appreciated the services of the instrument and machine shop staff of the Chemical Engineering Department, especially John Van D., Bob S. and Keith F. who suggested many useful ideas, and who regarded the less feasible of my ideas with appropriately light-hearted humor.

Foremost among those who provided personal support was my wife Henrietta, whose spirit survived continual disappointment and inconvenience, and who shared increasingly in my moments of joy or gloom. I am also grateful to my parents and family for their steady encouragement, and to many friends including Ron Reed for his inspiring insights, Tom Oosterhuis and Nolan Van Gaalen for helping me to place my work into perspective, and including fellow friends and philosophers R. & C. Sloboda, B. Cocks, J. & J. Vandall, N. & Y. Senturk, S. Graham, R. & B. Johnstone, D. Lynch and N. Jensen, to name a few.

Finally, I wish to thank Linda Franke for her able service in typing this thesis.

TABLE OF CONTENTS

CHAPTER		PAGE
I.	INTRODUCTION.	1
II.	LITERATURE SURVEY	3
	A. Vapor-Liquid Equilibrium Data	3
	B. Refractivity Data	4
	C. Prediction of Vapor-Liquid Equilibria	8
	C-1. Composite Methods	9
	C-2. Cubic Equations of State.	10
	C-3. Extended Virial Equations of State.	13
	C-4. Reference Equations of State.	15
	C-5. Treatment of Quantum Gases.	16
III.	EXPERIMENTAL METHOD	21
	A. Equipment Design.	21
	A-1. The Two Equipment Sets.	21
	A-2. Lower-Temperature Equipment (Cold Cell)	22
	A-3. Higher-Temperature Equipment (Warm Cell)	23
	A-3-a. New Equilibrium Cell.	23
	A-3-b. Air Bath.	27
	A-3-c. Vapor Recirculation Pump.	27
	A-3-d. Charging and Sampling Equipment	32
	B. Temperature Measurement.	34
	C. Pressure Measurement	34
	D. Composition Measurement.	35
	D-1. Lower-Temperature Equipment.	35
	D-2. Higher-Temperature Equipment	38
	D-2-a. The Methane-Containing System.	38

CHAPTER	PAGE
D-2-b. The n-Pentane-Containing Systems.	38
E. Refractive Index Measurement	40
F. Materials.	43
G. Experimental Procedures.	43
G-1. Lower-Temperature Equipment.	43
G-1-a. Charging and Equilibrating . .	43
G-1-b. Measurements	45
G-2. Higher-Temperature Equipment	46
G-2-a. Charging and Equilibrating . .	46
G-2-b. Refractive Index Measurement .	47
G-2-c. Sampling and Analysis.	48
IV. EXPERIMENTAL RESULTS	50
A. The Hydrogen-n-Pentane System.	50
B. The Hydrogen-Methane-Carbon Dioxide System .	53
C. The Hydrogen-Carbon Dioxide-n-Pentane System	58
D. Estimated Accuracy	61
D-1. Temperature Measurement.	61
D-2. Pressure Measurement	62
D-3. Composition Measurement.	63
D-4. Refractive Index and Molar Volume Measurement.	69
V. PROPERTY PREDICTION.	74
A. Choice of Predictive Method.	74
A-1. Corresponding States Test.	74
A-2. Vapor Pressure Tests	82
A-3. The Peng-Robinson Correlation.	84

CHAPTER	PAGE
A-4. Binary System Composition Tests. . . .	86
B. Determination of Binary Interaction Parameters	89
C. Comparison of Prediction Methods	92
D. Discussion	102
VI. Conclusions.	105
A. Vapor-Liquid Equilibrium Data.	105
B. Predictions with Cubic Equations of State. .	105
REFERENCES	107
APPENDIX A. THERMOCOUPLE AND PRESSURE GAUGE CALIBRATIONS.	110
APPENDIX B. GAS CHROMATOGRAPH CALIBRATIONS.	119
APPENDIX C. EXPERIMENTAL DATA	137
APPENDIX D. CALCULATION OF MOLAR VOLUME	152
APPENDIX E. DIMENSIONS OF NEW EQUILIBRIUM CELL. . . .	156
APPENDIX F. THE PENG-ROBINSON EQUATION OF STATE . . .	162

LIST OF TABLES

Table	Description	Page
1	Literature Sources for Vapor-Equilibrium Data on the Binary Systems Relevant to this Work	5
2	Parts List for the Vapor Recirculation Pump Assembly Drawing	30
3	Average Errors of Predicted Compressibility Factors of Hydrogen for Various Modifications to the Calculation of Corresponding States Parameters	78
4	Characterization of the Modifications for Calculation of Corresponding States Parameters	79
5	Temperature-Independent Binary Interaction Parameters for the Unmodified and the Gunn Approaches for Hydrogen	91
6	Average Absolute Per Cent Deviations Between Experimental and Calculated Equilibrium Ratios	96
7	Average Absolute Per Cent Deviations Between Experimental and Calculated Bubble Point Pressures	97
8	Average Absolute Per Cent Deviations Between Experimental and Calculated Dew Point Pressures	98
9	Average Absolute Per Cent Deviations Between Experimental and Calculated Liquid Molar Volumes	99
10	Average Absolute Per Cent Deviations Between Experimental and Calculated Vapor Molar Volumes	100
A-1	Thermocouple Calibration for the Lower-Temperature Equilibrium Cell	112
A-2	Thermocouple Calibration for the Higher-Temperature Equilibrium Cell	113
A-3	Calibration of 13 800 kPa Pressure Gauge	115
A-4	Calibration of 20 700 kPa Pressure Gauge	116

Table	Description	Page
A-5	Calibration of 34 500 kPa Pressure Gauge	117
A-6	Calibration of 2070 kPa Pressure Gauge	118
C-1	Experimental Equilibrium Ratios and Phase Compositions for the Hydrogen-Methane-Carbon Dioxide System	138
C-2	Experimental Refractive Indices and Molar Volumes for the Hydrogen-Methane-Carbon Dioxide System	142
C-3	Experimental Equilibrium Ratios and Phase Compositions for the Hydrogen-Carbon Dioxide-n-Pentane System	144
C-4	Experimental Refractive Indices and Molar Volumes for the Hydrogen-Carbon Dioxide-n-Pentane System	147
C-5	Experimental Equilibrium Phase Properties of the Hydrogen-n-Pentane System	149

LIST OF FIGURES

Figure	Description	Page
1	Essential Features of the Warm Cell	24
2	Schematic Representation of the Auxiliary Equipment for the Warm Cell	28
3	Vapor Recirculation Pump Assembly	29
4	Schematic Representation of the Angle Measurement Involved in the Determination of the Refractive Index	41
5	Equilibrium Phase Compositions of the Hydrogen-n-Pentane System	51
6	Equilibrium Ratios for Hydrogen and n-Pentane in the Hydrogen-n-Pentane System	52
7	Equilibrium Phase Compositions of the Hydrogen-Methane-Carbon Dioxide System at -45.8°C	54
8	Equilibrium Phase Compositions of the Hydrogen-Methane-Carbon Dioxide System at -15°C	56
9	Equilibrium Phase Compositions of the Hydrogen-Carbon Dioxide-n-Pentane System at 0.0°C	59
10	Equilibrium Phase Compositions of the Hydrogen-Carbon Dioxide-n-Pentane System at 50.0°C	60
11	Chromatograph Calibration - Relationship Between Peak Area and Transducer Signal for Methane in Nitrogen Carrier Gas	121
12	Chromatograph Calibration - Relationship Between Peak Area and Transducer Signal for Methane in Helium Carrier Gas	122
13	Chromatograph Calibration - Relationship Between Peak Area and Transducer Signal for Hydrogen in Nitrogen Carrier Gas	123
14	Chromatograph Calibration - Relationship Between Peak Area and Transducer Signal for Carbon Dioxide in Helium Carrier Gas	124
15	Calibration of the Pressure Transducers	125

Figure	Description	Page
16	Chromatograph Calibration - Relationship Between Peak Area and Transducer Signal for Hydrogen in Argon Carrier Gas	127
17	Chromatograph Calibration - Relationship Between Peak Area and Transducer Signal for Methane in Argon Carrier Gas	128
18	Chromatograph Calibration - Relationship Between Peak Area and Transducer Signal for Carbon Dioxide in Argon Carrier Gas	129
19	Composition Dependence of the Constant a in the Equation Relating Hydrogen to n-Pentane Peak Areas	132
20	Composition Dependence of the Constant b in the Equation Relating Hydrogen to n-Pentane Peak Areas	133
21	Composition Dependence of the Constant a in the Equation Relating Carbon Dioxide to n-Pentane Peak Areas	134
22	Composition Dependence of the Constant b in the Equation Relating Carbon Dioxide to n-Pentane Peak Areas	135
23	Front View of Equilibrium Cell	157
24	Side View of Equilibrium Cell	158
25	Top and Rear Views of Equilibrium Cell	159
26	Dimensions of the Window Cover Plate for the Equilibrium Cell	160
27	Dimensions of the Mirrors and Window for the Equilibrium Cell	161

NOMENCLATURE

Symbol	Description
a, b, c	Various constants
f	Fugacity
k_{ij}	Binary interaction parameter of component pair i and j
m	Molecular weight, or a constant
n	Refractive index
u	Intermolecular potential function
x	Mole fraction of liquid phase
y	Mole fraction of vapor phase
z	Mole fraction of arbitrary phase
A	Chromatograph peak area
E_{Hj}	Constant used to calculate the b constant in equation of state calculations for mixtures containing hydrogen
K	Equilibrium ratio
P	Pressure
P_c	Critical pressure
P_r	Reduced pressure (P/P_c)
R	Gas constant
R_{LL}	Lorentz-Lorenz refractivity
T	Absolute temperature
T'	Effective absolute temperature
T_c	Critical temperature
T_r	Reduced temperature (T/T_c)
V	Molar volume or voltage
\bar{V}	Partial molar volume
Z	Compressibility factor (PV/RT)

Symbol	Description
α	The coefficient of the constant a in certain cubic equations of state
β, γ, δ	Various angles
γ°	Fugacity coefficient
ρ	Density
ω	Acentric factor
θ	Constant with units of temperature
κ	A constant used to calculate α in the Peng-Robinson equation of state

I - INTRODUCTION

In recent years the sudden shift in cost and availability of conventional oil supplies has fostered a surge of interest in the conversion of heavy oil, bitumen and coal into readily useable fuels. Most or perhaps all of the currently feasible processes for carrying out such conversions involve the introduction of hydrogen in its molecular form. Efficient design of these processes requires good estimates of the pressure, temperature and composition relationships of the complex mixtures involved.

The determination of these relationships has been hampered by the following two factors. Firstly, there is a lack of reliable ternary and multicomponent phase equilibrium data with which to check thermodynamic property estimates. Secondly, the methods used for predicting vapor-liquid equilibrium conditions appear to be less reliable for mixtures containing hydrogen than they are for many other commonly encountered mixtures.

This investigation was aimed at both of these concerns. It was decided to obtain vapor-liquid equilibrium data for one binary and two ternary mixtures involving hydrogen and following that to examine briefly the methods of fluid property prediction for these systems and to evaluate them using experimental data.

The number of possible ternary combinations that could be studied was very large; hence the scope of the study had to be limited to a selection of typical mixtures. A

review of the literature indicated little previous work on mixtures containing carbon dioxide and hydrogen with light alkanes. In order to obtain basic data on some mixtures of this type, it was decided to study the behavior of the hydrogen-carbon dioxide-methane and hydrogen-carbon dioxide-n-pentane ternaries.

The binary system that was studied, hydrogen-n-pentane, was chosen because no satisfactory phase equilibrium data for this system existed in the literature. Such data are needed to obtain the binary parameters used in most of the recent methods of predicting ternary and multicomponent equilibria.

As volumetric data may be required for process design and are also useful for comparing predictive methods, it was decided to measure the refractive indices of the co-existing phases in addition to the pressure, temperature and composition. The density could then be calculated using the measured composition together with the appropriate pure component information.

II - LITERATURE SURVEY

A. Vapor-Liquid Equilibrium Data

A literature search was carried out for vapor-liquid equilibrium data on systems containing hydrogen with one or more of the following components: non-cyclical hydrocarbons of ten or fewer carbon atoms, carbon dioxide, nitrogen, carbon monoxide and water. Adequate and sometimes plentiful information has been published on the binary systems of hydrogen with each of the normal alkanes from methane to n-octane, except for n-pentane.

The single available source (13) on the hydrogen-pentane system provides only three data points at one temperature. The data are presented graphically. The article refers only to "pentane" and does not indicate whether a pure isomer or a mixture of isomers was used. Also, data presented in the same article for the hydrogen-n-butane system display serious errors according to a later study (23). Frohlich and co-workers, who were testing the range of application of the Henry's constant, may have been more interested in measuring relative concentrations than in absolute concentrations.

No data were found for ternary systems of a light hydrocarbon with hydrogen and carbon dioxide. The only experimental information on systems including hydrogen, carbon dioxide and light hydrocarbons has been provided by Yorizane et al. (48) for the two multicomponent systems hydrogen-methane-carbon monoxide-carbon dioxide-propane, and hydrogen-

methane-carbon monoxide-carbon dioxide-n-butane. The data consist of dewpoint pressures and vapor compositions at 0°C. Hydrogen concentrations were determined by difference, not directly, and exhibit large scatter.

The results of the literature survey for the component pairs that appear in the systems studied in this work are presented in Table 1.

B. Refractivity Data

Information was collected from the literature on the pure-component refractivities of the compounds that were included in this work. Refractivities were needed to calculate phase densities from the measured refractive indices. The relationship between the refractive index and the density of a fluid is probably best represented by the Lorentz-Lorenz refractivity (5), given by Equation (1).

$$R_{LL} = \frac{1}{\rho} \frac{n^2 - 1}{n^2 + 2} \quad (1)$$

In the above equation, ρ is the density, n is the refractive index and R_{LL} is the Lorentz-Lorenz refractivity, which is usually very nearly constant, varying only slightly with temperature and density.

Highly accurate determinations of R_{LL} have been carried out by Diller (11) for hydrogen, and by Olson (31) for methane. Because these refractivities were reported for wavelengths different from that used in this study, small corrections were made based on the experimental data of Peck and Huang for hydrogen (32), and the data of Watson and

TABLE 1

LITERATURE SOURCES FOR VAPOR-LIQUID EQUILIBRIUM
DATA ON THE BINARY SYSTEMS RELEVANT TO THIS WORK

SYSTEM	REFERENCE
CO ₂ -CH ₄	<p>Donnelly, H. G., and Katz, D. L., Ind. Eng. Chem, 1954, <u>46</u>, 511.</p> <p>Sterner, C. J., Advan. Cryog. Eng., 1961, <u>6</u>, 467.</p> <p>Davis, J. A., Rodewald, N., and Kurata, F., AIChE J. 1962, <u>8</u>, 537.</p> <p>Hensel, W. E., and Massoth, F. E., J. Chem. Eng. Data, 1964, <u>9</u>, 352.</p> <p>Kaminishi, G., Arai, Y., Saito, S., and Maeda, S., J. Chem. Eng. Japan, 1968, <u>1</u>, 109.</p> <p>Kaminishi, G., and Toriumi, T., Rev. Phys. Chem. Jap., 1968, <u>38</u>, 79.</p> <p>Neumann, A., and Walch, W., Chem.-Ing.-Techn., 1968, <u>40</u>, 201.</p> <p>Toriumi, T., and Kaminishi, G., Asahi Garasu Kogyo Gijutsu Shorei-Kai Kenkyu Hokoku, 1968, <u>14</u>, 67.</p> <p>Arai, Y., Kaminishi, G., and Saito, S., J. Chem. Eng. Japan, 1971, <u>4</u>, 113.</p> <p>Hsi, C., and Lu, B. C. Y., Can. J. Chem. Eng., 1972, <u>50</u>, 144.</p> <p>Davalos, J., Anderson, W. R., Phelps, R. E., and Kidnay, A. J., J. Chem. Eng. Data, 1976, <u>21</u>, 81.</p> <p>Hwang, S. C., Lin, H. M., Chapplelear, P. S., and Kobayashi, R., J. Chem. Eng. Data, 1976, <u>21</u>, 493.</p> <p>Mraw, S. C., Hwang, S. C., and Kobayashi, R., J. Chem. Eng. Data, 1978, <u>23</u>, 135.</p>
CO ₂ -n-C ₅ H ₁₂	<p>Poettmann, F. H., and Katz, D. L., Ind. Eng. Chem., 1945, <u>37</u>, 847.</p>

TABLE 1 (Continued)

- Besserer, G. J., and Robinson, D. B., J. Chem. Eng. Data, 1973, 18, 416.
- Massoudi, R., and King, A. D., J. Phys. Chem., 1973, 77, 2016.
- H₂-CH₄ Freeth, F. A., and Verschoyle, T. T. H., Proc. Roy. Soc. London, 1931, A130, 453.
- Shtekkel, F. A., and Tsin, N. M., Zh. Khim. Prom., 1939, 16, 24.
- Fastovskii, V. G., and Gonikberg, M. G., Acta Physicochim. URSS, 1940, 12, 485.
- Fastovskii, V. G., and Gonikberg, M. G., Zh. Fiz. Khim., 1940, 14, 427.
- Likhter, A. I., and Tikhonovich, N. P., Zh. Tekhn. Fiz., 1940, 10, 1201.
- Levitskaya, E. P., Zh. Tekhn. Fiz., 1941, 11, 197.
- Benham, A. L., and Katz, D. L., AIChE J., 1957, 3, 33.
- Mueller, W. H., Leland, T. W., and Kobayashi, R., AIChE J., 1961, 7, 267.
- Solbrig, C. W., and Ellington, R. T., Chem. Eng. Progr. Symp. Ser., 1963, 59 (44), 127.
- Kirk, B. S., and Ziegler, W. T., Advan. Cryog. Eng., 1965, 10, 160.
- Yorizane, M., Yoshimura, S., Masuoka, H., and Toyama, A., Proc. 1st Int. Cryogenic Engineering Conf., 1967, 57.
- Sagara, H., Arai, Y., and Saito, S., J. Chem. Eng. Japan, 1972, 5, 339.
- Streett, W. B., Tsang, C. Y., Deiters, U., and Colado, J. C. G., EFCE Publ. Ser. 11 (Phase Equilib. Fluid Prop. Chem. Ind., Proc., Part 1), 1980, 39.
- Hong, J. H., and Kobayashi, R., J. Chem. Eng. Data, 26, 127 (1981).

TABLE 1 (Continued)

H ₂ -CO ₂	Verschaffelt, J. E., <i>Communs. Kamerlingh Onnes Lab., Univ. Leiden</i> , 1900, No. 65.
	Pollitzer, F., and Strebel, E., <i>Z. Phys. Chem.</i> , 1924, <u>110</u> , 768.
	Abdulaev, Ya. A., <i>Zh. Fiz. Khim.</i> , 1939, <u>13</u> , 768.
	Abdulaev, Ya. A., <i>Kholodilnaya Prom.</i> , 1936, <u>17</u> (2) 26.
	Mills, R. J., and Miller, F. J. L., <i>Can. Chem. Proc. Ind.</i> , 1945, <u>29</u> , 651.
	Greco, G., Casale, C., and Negri, G., <i>Ind. Chim. Belge, Spec. No.</i> , 1955, <u>20</u> , 251.
	Kaminishi, G., and Toriumi, T., <i>Kogyo Kagaku Zasshi</i> , 1966, <u>69</u> , 175.
	Barrick, P. L., Heck, C. K., and Spano, J. O., <i>U. S. Air Force Syst. Command Res. Technol. Div. Techn. Rep.</i> 66-390, 1966.
	Spano, J. O., Heck, C. K., and Barrick, P. L., <i>J. Chem. Eng. Data</i> , 1968, <u>13</u> , 168.
	Estrin, B. M., and Snyrev, Yu. L., <i>Zh. Prikl. Khim.</i> , 1969, <u>42</u> , 699.
	Yorizane, M., Yoshimura, S., and Masuoka, H., <i>Kagaku Kogaku</i> , 1970, <u>34</u> , 953.
	Yorizane, M., <i>Asahi Garasu Kogyo Gijutsu Shorei-Kai Kenkyu Hokoku</i> , 1971, <u>18</u> , 61.
	Groll, G., and Strigl, R., <i>Linde Ber. Tech. Wiss.</i> , 1976, <u>38</u> , 26.
	Streett, W. B., Tsang, C. Y., Deiters, U., Colado, J. C. G., <i>EFCE Publ. Ser. 11 (Phase Equil. Fluid Prop. Chem. Ind., Proc., Part 1)</i> , 1980, 39.
	Tsang, C. Y., and Streett, W. B., <i>Chem. Eng. Sci.</i> , 1981, <u>36</u> , 993.

Ramaswamy for methane (46). Refractivities for the same wavelength as used in this study have been published by Besserer and Robinson (6) for both carbon dioxide and n-pentane.

C. Prediction of Vapor-Liquid Equilibria

Approaches to the problem of predicting vapor-liquid equilibrium properties for systems of non-polar and slightly polar substances fall into two categories. The first is the use of composite methods of prediction. The second category is the application of equations of state.

The principal difference between equation of state and composite approaches is that composite approaches use a different model or set of equations to describe each of the vapor and liquid phases, whereas in equation of state methods the same equation is used to describe both phases. Treating both phases with the same equation has the advantage of being consistent with the principle of continuity of the vapor and liquid states. It is well known that a vapor can be changed into a liquid without ever exhibiting a meniscus or change of phase, provided the transition path passes through the supercritical region. The same is true for the reverse path. It follows therefore that an accurate mathematical description of vapors and liquids must be continuous in regions above the critical point (and by definition, at the critical point as well).

The many equations of state that have been proposed can be divided into three groups: cubic, extended

virial, and reference equations. These groups are described very briefly later in this chapter. More detailed discussions are available in the excellent reviews presented recently by Leland (25) and by Harmens (18). A good outline of earlier developments in the field can be found in the older, more general review by Tsonopoulos and Prausnitz (45).

C-1. Composite Methods

All the methods in this category apply separate models for each of the vapor and liquid phases. These models are usually based on a fugacity equation such as Equation (2) in which the fugacity f_i of component i is represented by the product of a standard state fugacity f_i^O , a composition z_i and an activity coefficient γ_i^O :

$$f_i = \gamma_i^O z_i f_i^O \quad (2)$$

Success depends mainly on the ability of the models to predict γ_i^O , the correction factor for non-ideality. Composite methods collapse at pressures near and above the critical point because the vapor and liquid models are inevitably inconsistent with the continuity of the two phases in this region.

The most commonly used methods in this category are the Chao-Seader (9) and Grayson-Streed (15) correlations. The Grayson-Streed correlation is basically a refitting of the constants of the Chao-Seader method using a more extensive data set that extends the range to higher temperatures. The Grayson-Street correlation appears to be more accurate in general. Both methods make use of the Redlich-Kwong

equation of state, but only to calculate the fugacity coefficient of the vapor phase.

These correlations, along with most other composite methods, have been replaced to a large extent by methods that employ a single equation of state.

C-2. Cubic Equations of State

This group of equations, often referred to as the Van der Waals family, first came into widespread quantitative use after the Redlich-Kwong equation of state appeared in 1949 (36). Since then the Redlich-Kwong equation has been greatly improved upon. Two of the more recent cubic equations in common use are the Peng-Robinson (PR) equation (33) and the Soave modification (41) of the Redlich-Kwong equation (SRK).

These two equations have the form

$$P = \frac{RT}{V-b} - \frac{a(T)}{f(b,V)} \quad (3)$$

where $a(T)$ is the temperature-dependent constant in the second term (the 'attraction' term), and b is the other constant believed to be related to repulsive intermolecular forces. P is the absolute pressure, T is the absolute temperature, V is the molar volume of the fluid, and R is the gas constant. By convention R is not counted as one of the equation constants as it appears in all equations of state for fluids. The PR and SRK equations of state are thus two-constant equations. The denominator of the attraction term is given by Equation (4) for the SRK equation of state, and by Equation (5) for the PR equation of state.

$$f(b,V) = V(V+b) \quad (4)$$

$$f(b,V) = V(V+b) + b(V-b) \quad (5)$$

Before either the PR or SRK equations can be used, three parameters must be known for each component encountered. These are the critical temperature, critical pressure and the acentric factor of each of the components in its pure state. In addition a binary interaction parameter is usually required for each pair of components occurring in a given mixture. The binary interaction parameter is best determined by fitting the equation of state to pressure-temperature-composition data for the vapor-liquid region of the corresponding binary system.

Cubic equations of state have the advantage of relative simplicity when compared to other equations of state. The difference becomes apparent in the much shorter computing times required by cubic equations when programmed on a digital computer. The simplicity appears to be related to the cubic nature of the volume dependence in these equations. In addition, the two adjustable constants in the equation can be defined readily in terms of the three pure-component parameters. The mixing rules by which the constants for a mixture are calculated have been determined empirically for the most part. Satisfactory results can be obtained when they are used with accurate binary interaction parameters. However, Leland (25) insists that these mixing rules are still far from optimal.

It appears that all cubic equations have several

weaknesses in common. The most outstanding one is their poor ability to provide accurate volumetric predictions. Even for the Peng-Robinson equation, which is superior to the Soave-Redlich-Kwong equation in this respect, the predicted volumes are far from the accuracy that is achievable through other types of equations of state and correlations, especially for pure components. A second common difficulty is that cubic equations tend to overestimate the pressure and composition range of the two-phase region (1) and as a result the predictions are much poorer in the critical region than in other areas.

A third difficulty arises when cubic equations of state are applied to systems which contain hydrocarbons or related materials of very high molecular weight. For these materials the critical constant and the acentric factor may be experimentally inaccessible (as with materials that decompose thermally without reaching the critical temperature), or not defined (as for a complex mixture of similar materials which are collectively treated as a pseudo-component). In order to handle these substances within the framework of cubic equations, effective parameters must be estimated, an exercise that may admit substantial errors. This difficulty is the reason given by Moshfeghian et al. (30) for investigating the use of the "Parameters From Group Contributions" (PFGC) equation. As evidence of the equation's potential they present several comparisons between predictions and experiment. However, they did not publish any group

parameters.

The idea that a third constant can be added to cubic equations without increasing the required amount of pure component information, and without altering the cubic nature of these equations, has been exploited by Harmens (17). While Harmens was able to show that one of the three-constant equations which he investigated was more accurate than the PR or SRK equations, the improvement was small and it was doubtful whether the improvement justified the increased complexity.

It is interesting to note that while the equation of Harmens could reproduce the critical volume of pure components accurately (two-constant equations can not), his equation exhibited the same weaknesses in the critical region as did other cubic equations. He attributed this weakness to limitations of the cubic nature of the equation, and referred in his thesis to evidence that the critical region requires at least a fifth-order power series to be described properly.

C-3. Extended Virial Equations of State

The extended virial equations, sometimes referred to as the Benedict-Webb-Rubin (BWR) family, do not suffer from the same limitations that cubic equations display. These equations consistently include volume terms which are greater than fifth order, and have more constants than the cubic equations. For pure components the extended virial equations provide much greater accuracy than cubic equations, especially in correlating the properties in the critical

region and the molar volumes.

The first modern equation in this group was the Benedict-Webb-Rubin (BWR) equation of state (4). It contained eight constants and involved an exponential term. The most noteworthy improvements upon the BWR equation are those of Starling (43), and Lin and Hopke (27), both of whom used the same eleven-constant modification of the BWR equation. Another recent equation of state was proposed by Bender (3). It requires twenty constants, and while it is capable of high accuracy, its complexity discourages its widespread use.

The greatest weakness of the multiconstant equations appears to be their inability to maintain accuracy in the transition from pure components to mixtures. This is attributed to deficiencies in the mixing rules that are used to calculate the constants for a mixture from the pure component constants. These mixing rules are necessarily empirical and lack firm theoretical foundation. This is hardly surprising, as the pure component constants themselves are established empirically, and have no proven fundamental significance.

The difficulty with the mixing rules has been eased somewhat (17, 18) by a procedure proposed by Lee and Kesler. They employed a twelve-constant modification of the BWR equation in a corresponding states approach. The procedure requires only two complete sets of constants, one set for the "simple fluid" as originally defined by Pitzer

et al. (33) (for which the acentric factor is zero), and one set for a reference fluid that has a large acentric factor. Thermodynamic calculations are based on the relationship:

$$Z = Z^{(o)} + \frac{\omega}{\omega(r)} (Z(r) - Z^{(o)}) \quad (6)$$

In this relationship, Z is the compressibility factor and ω is the acentric factor. The superscript (o) refers to the "simple fluid" and (r) refers to the reference fluid.

To perform calculations according to the Lee-Kesler method only three constants need to be known for a mixture: the pseudocritical pressure, the pseudocritical temperature and the acentric factor. As a result only three mixing rules are required, and each of these rules is for a quantity that can be determined approximately from experiment. Harmens recommends the mixing rules used by Plöcker (35).

A disadvantage of the Lee-Kesler correlation is that it does not extend throughout the entire two-phase region (28).

C-4. Reference Equations of State

The equations of state in this group are very complicated. They include as many constants as needed to describe to a desired accuracy the PVT relationships of a pure substance. To apply these equations directly to mixtures is practically impossible because of the problems involved in defining unique sets of constants for pure components, and in relating these to the constants for a mixture. The use of these equations is limited to providing accurate informa-

tion on a reference fluid. Such an equation is then used in a correlation in much the same manner as the modified BWR equation is used in the Lee-Kesler correlation.

C-5. Treatment of Quantum Gases

It is generally recognized that the various isotopes of hydrogen, helium and neon do not fit satisfactorily into corresponding states correlations or into the common methods of vapor-liquid equilibrium prediction. Higher molecular weight substances with simple molecular structure fit much better. The reason for the differing behavior of the low molecular weight molecules is usually attributed to certain quantum mechanical effects which become more important as molecular weight decreases and as temperature decreases (38, 37). Because these small molecules have the weakest intermolecular attraction of all substances, their vapor-liquid regions exist only at temperatures much lower than for other substances. As a result their critical pressures, critical temperatures and acentric factors may be influenced significantly by these quantum mechanical effects.

In order to obtain trustworthy predictions for systems that contain any of these quantum gases, special methods must often be employed. Either the parameters for these gases are adjusted to suit a method of vapor-liquid equilibrium prediction, or an entirely new correlation is developed. Both approaches have appeared in various forms in the literature.

The previously described correlations of Chao and

Seader and of Grayson and Streed both included special provisions for hydrogen. In the framework of these methods all the pure hydrocarbons (except methane) were correlated with the same set of constants. However, hydrogen and methane, while placed within the same framework, each required a special set of constants. Even with the special attention that hydrogen received, large errors occur in the predicted K-values of hydrogen when in the presence of cyclic hydrocarbons (40). The correlations were not extended to other quantum gases.

Sebastian and co-workers (40) proposed a new correlation prepared specifically for predicting hydrogen solubilities, particularly in heavier hydrocarbons and synthetic oils. The correlation is a composite method in which γ_i^0 and f_i^0 in Equation (2) are combined into a single coefficient. The ratio of fugacity to mole fraction is calculated according to Equation (7).

$$\ln(f/x) = \ln(f/x)_{p=0} + P\bar{V}/RT \quad (7)$$

The zero pressure term and \bar{V} are each correlated by a set of equations in which temperature and the solubility parameter are used as the independent variables.

In connection with cubic equation of state methods, a variety of proposals has been made for accommodating the quantum gases. The proposed methods (usually restricted to hydrogen) fall into four categories.

The first category is the use of effective critical constants as originally proposed by Gunn, Chueh and Prausnitz

(16). In this method the values used as the critical temperature and pressure are functions of temperature. At high temperatures these effective critical constants approach the so-called classical constants. The value of the acentric factor associated with the classical constants is zero. Although this method was originally intended to fit hydrogen and helium to the corresponding state tables of Pitzer, it has since been used to provide effective parameters for hydrogen in Soave's modification of the Redlich-Kwong equation of state (18).

The second method of handling quantum fluids involves the alteration of the temperature dependence of the constant a in the attraction term of Equation (3). Soave's original correlation of the constant a with temperature was based on data for hydrocarbons below their critical temperature, as was later done with the Peng-Robinson equation. Hydrogen at room temperature is at nine times its critical temperature and to apply the Soave-type formula requires a long extrapolation. Several authors (14, 7, 12) have proposed different temperature relationships for the attraction constant so that conditions well above hydrogen's critical point can be predicted more accurately.

The third method, proposed by El-Twaty and Prausnitz (12), is to add a quadratic term to the simple rule used to calculate the constant b in Equation (3). Normally b is calculated according to

$$b_m = \sum_i Z_i b_i \quad (8)$$

where z_i is the mole fraction of component i and the subscripts m and i refer to the mixture and the pure component i , respectively. El-Twaty and Prausnitz proposed

$$b_m = \sum_i z_i b_i + z_H \sum_j z_j E_{Hj} \quad (9)$$

where E_{Hj} is a constant characteristic of the pair formed by hydrogen and component j . E_{Hj} must be determined by empirical correlation for each component j .

The fourth method of treating hydrogen in cubic equation-of-state predictions would not be worthy of mention were it not for the frequently-used convention of assuming the acentric factor of hydrogen to be zero. The method is simply to use a negative acentric factor for hydrogen in accordance with the experimentally derived figure of -0.22 . This is a rather low value in comparison with the range 0.0 to 0.5 in which most materials that are fluid at room temperature lie. It appears that many researchers have assumed that the experimental value is not reliable as a parameter. However, Mollerup (29) has reported encouraging results when suitable negative values are used for the quantum gases. His work applied only to pure components. Lin (26) has shown that for binary systems of hydrogen with hydrocarbons containing up to thirteen carbon atoms the original Soave method (using the experimental acentric factor) performs better than the Graboski-Daubert modification of the method.

Graboski and Daubert modified the SRK equation in two ways. They employed the classical critical constants and a zero acentric factor for hydrogen, and they applied a

different temperature dependence to the constant a in an attempt to reproduce better the behavior of hydrogen at temperatures far above its critical point. Lin showed that a small overall improvement could be obtained with the Graboski-Daubert modification when the temperature function for the constant a was refitted using a more extensive data set. Significant improvement occurred in predicting K -values in binaries of hydrogen and heavy hydrocarbons, but this was partly offset by poorer results for binaries with light hydrocarbons. In addition, Lin tested the modification of the critical constants according to the method of Gunn et al. Only a slight improvement was obtained.

III - EXPERIMENTAL METHOD

A. Equipment Design

A-1. The Two Equipment Sets

The experimental data were obtained on two separate sets of equipment that operated over different temperature ranges. The use of more than one piece of equipment was preferable because of the large temperature range over which vapor-liquid equilibrium occurs for the different systems studied.

The lowest experimental isotherm (-45.8°C , hydrogen-methane-carbon dioxide) was studied with already existing equipment. This equipment was capable of operating at temperatures from about -100°C to near ambient conditions.

The measurements near and above ambient temperature were carried out on a new apparatus designed and constructed for this purpose. The operating temperature ranges of the two sets of equipment overlapped each other, allowing results from the two sets of equipment to be checked for reliability. Part of the second-lowest isotherm (-15°C , hydrogen-methane-carbon dioxide) was studied on both sets of equipment but the rest of the data were obtained on the new, higher-temperature equipment.

To distinguish between the two cells in the remainder of the text, the lower temperature cell is referred to as the cold cell, and the higher temperature one as the warm cell.

A-2. Lower-Temperature Equipment (Cold Cell)

The cold cell has been described in detail by Kalra and Robinson (20). While it was necessary to make several modifications to the support equipment, the design and operation of the cell were essentially unchanged.

Basically, the equilibrium mixtures were contained in a type 316 stainless steel vessel having a fixed volume of about 250 cm³. The equilibrium cell contents could be observed through two, pyrex glass windows located near the upper and lower ends of the cell. Each window had an internally mounted mirror behind it to permit measurement of the refractive index of the intervening phase.

The cell contents were mixed by swirling the liquid with an externally coupled, magnetically driven stirrer. Samples of each phase could be obtained through needle valves built into the cell body.

The equilibrium cell and its peripheral equipment were located inside a large fibreglass dewar that acted as an air bath. The bath was cooled by a refrigeration system supplemented by vapor from evaporating liquid nitrogen. A constant bath temperature was maintained by operating an automatically controlled electric heater against an excess load of refrigerant.

The maximum pressure obtainable in the cold cell was 22 000 kPa at temperatures ranging from near ambient to nearly -100°C.

A-3. Higher-Temperature Equipment (Warm Cell)

A-3-a. New Equilibrium Cell

The new equilibrium cell that was constructed for investigations at higher temperatures centered around an equilibrium cell with a constant internal volume of approximately 100 cm³. The main features of the cell are shown in Figure 1, and the detailed dimensions are presented in Appendix E. The cell body was machined from a 15.3 cm diameter rod of Hastelloy C-276. A flat surface was milled along the rod and then a recess, shown in the cross section of Figure 1 as the open area to the right of the window, was milled into the flat surface. The recess dimensions were approximately 8.9 cm high by 2.6 cm wide by 6.5 cm deep. The recess was stepped out to a wider opening near its mouth in order to accommodate the window and sealing system. Care was taken to insure smooth rounded surfaces to avoid points of stress concentration.

The rectangular window (9.84 cm high by 2.54 cm wide by 1.5 cm thick) was placed in the mouth of the recess and allowed the entire internal height of the cell to be viewed. The window was held in place by a cover plate of mild steel which was bolted to the cell body. The cell contents could be viewed through a 0.95 cm wide slot in the cover plate. The slot is indicated in section A-A.

The two internal mirrors used for refractive index measurements were made by grinding and polishing the ends of two 1.25 cm diameter rods. Each of these rods was machined

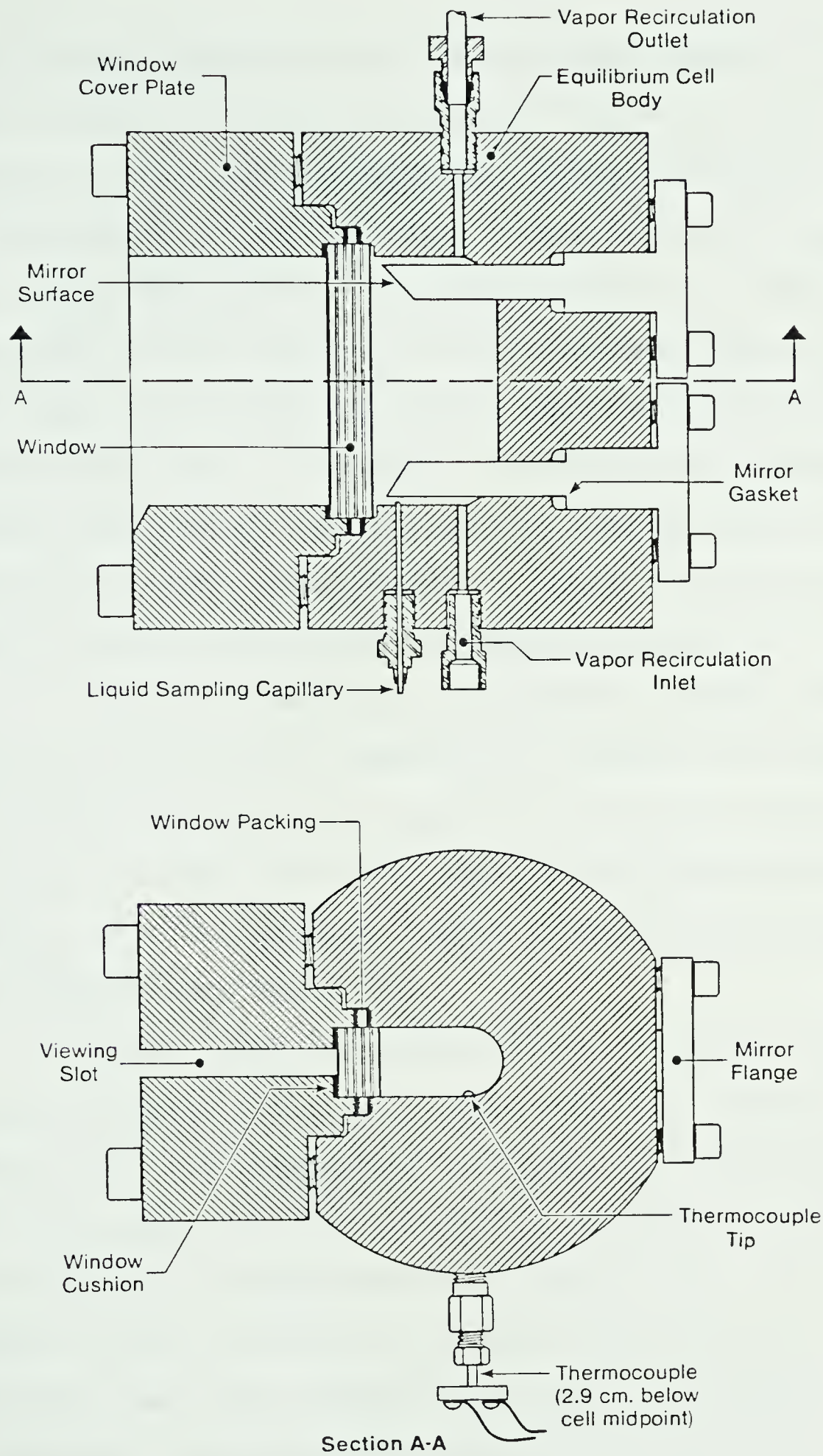


Figure 1. Essential Features of the Warm Cell

from a single piece of type 316 stainless steel. As can be seen in Figure 1, the outside end of the mirror rod widened abruptly into a 7.5 cm disk-shaped flange, by which the mirror was bolted to the cell body. Each mirror was inserted into a hole drilled into the back of the cell. The two rods protruded into the internal cavity, one near the top and the other near the bottom. As shown, the mirror surfaces were located very near to the inside surface of the window. The mirrors were sealed into the cell by compressing the circular mirror gaskets (see Figure 1), which were made of a commercial fluorocarbon polymer, against the body of the cell.

The cell contents were mixed by drawing vapor from the top of the cell and bubbling it through the liquid via the ports labelled in the figure as the vapor recirculation outlet and inlet. Two other small ports were drilled to provide for a thermocouple (shown in section A-A) and a liquid sampling line (labelled).

The window was sealed against leaks by placing a packing material along the window perimeter, as shown in section A-A, and compressing it between the cell body and the cover plate, so that the lateral distortion of the packing against the window provided a radial seal. This method, similar to the one which had worked satisfactorily on the cold cell, met with serious difficulty at pressures above 25 000 kPa. Overcoming this difficulty proved to be the foremost obstacle during the course of the experiments. A variety of materials and combinations of materials was

employed in various attempts to provide a packing arrangement that was acceptable.

Initially glass-filled teflon was used as the window packing, but at the higher temperatures it was extruded through the narrow gap between the cover plate and the cell, and the compression on the packing was lost. A graphite-strip packing was employed temporarily, but this also had several disadvantages. An excessively large force was required before the graphite would deform to provide the radial seal. Also, the adhesive used to bond the layers of graphite together tended to contaminate the cell with a greasy residue that obscured the mirrors. In addition, setting this packing in place required time-consuming, painstaking effort.

An attempt was made to use graphite impregnated asbestos. However, this material proved to be too resilient and caused the window to fracture whenever the tension on the cover plate bolts was relieved.

Finally success was achieved by placing a 3.2 mm layer of teflon between two 1.6 mm layers of a compressed asbestos gasket material (Garlock). The asbestos material was rigid enough to prevent the teflon from being extruded, but was not hard enough to crack the window when forced against it. Even this arrangement had certain drawbacks. In some instances when the compression on the window packing was increased to seal the vessel at the higher pressures, the window would crack. These cracks usually ran parallel

to the viewing surfaces of the window, and originated along the line where the packing contacted the side of the window. Evidently, the stress applied by the packing promoted the formation of cracks in the window.

The weaknesses of this type of window sealing arrangement limited the maximum operating pressure of the cell to about 28 000 kPa. The cell body, with an aluminum block substituted for the window, was able to withstand a pressure of 65 000 kPa during a room-temperature hydrostatic test.

A-3-b. Air Bath

The arrangement of the equilibrium cell and its auxiliary equipment is shown in Figure 2. An air bath was used to provide a controlled environment for the cell. Cooling was provided by a Frigidaire Freon-12 refrigeration unit. Heat was supplied by four manually controlled strip heaters having a total output of 1900 watts. The temperature was maintained by a proportional-integral temperature controller (Thermac Model TC 5192) operating a 300-watt strip heater. The air was circulated by a 30 cm fan driven by a 1/3 H.P. AC motor. The operating range of the bath was -17°C to $+135^{\circ}\text{C}$.

A-3-c. Vapor Recirculation Pump

Vapor was drawn from the top of the cell and was bubbled through the liquid by a double-acting, magnetic, piston pump. The design of the pump is shown in Figure 3, and the parts list is given in Table 2.

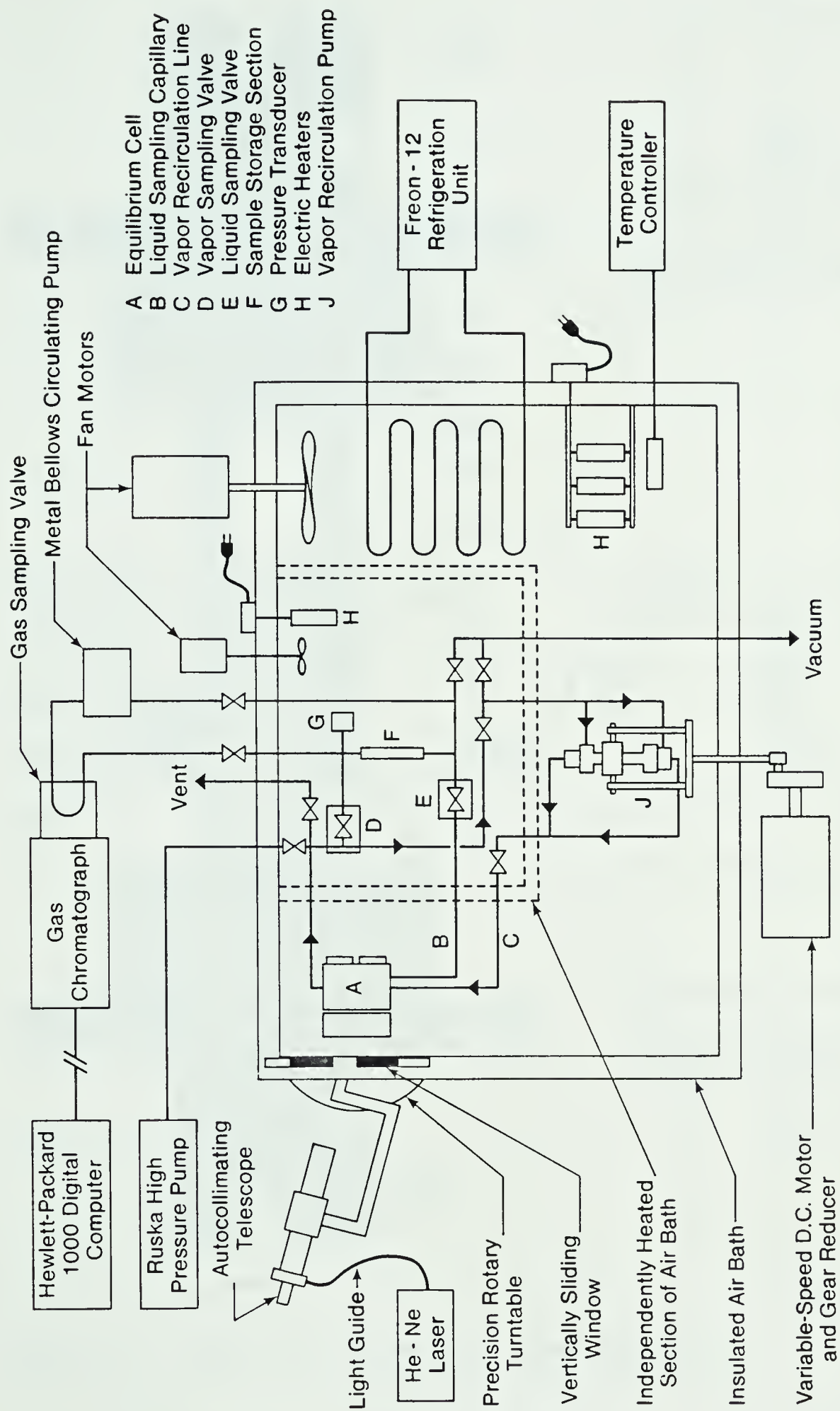


Figure 2. Schematic Representation of the Auxiliary Equipment for the Warm Cell

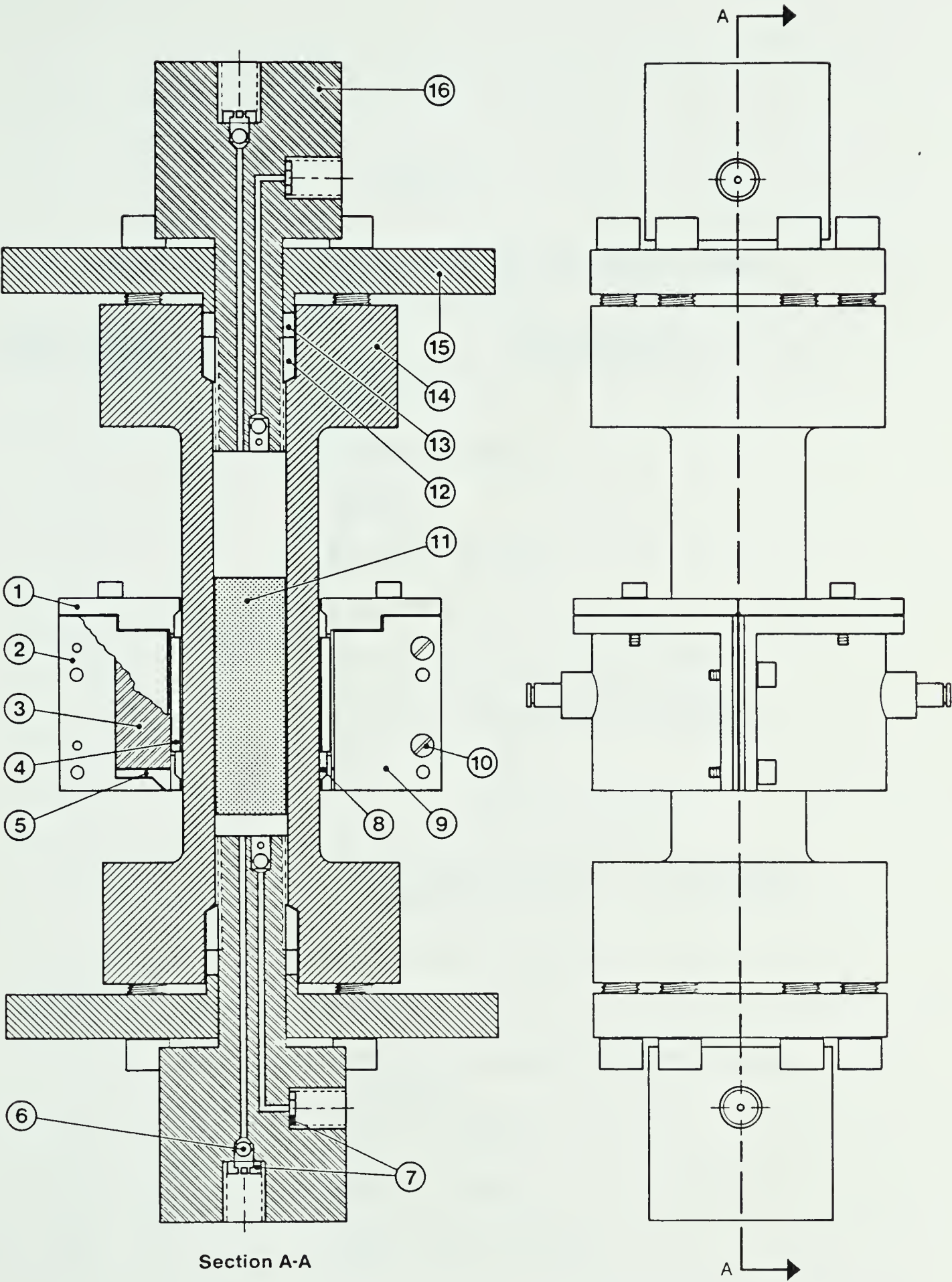


Figure 3. Vapor Recirculation Pump Assembly

TABLE 2

PARTS LIST FOR THE VAPOR RECIRCULATION PUMP
ASSEMBLY DRAWING

<u>PART NUMBER</u>	<u>DESCRIPTION</u>
1	Sleeve Cap
2	Magnet Sleeve
3	Magnet
4	Bearing Spacer
5	Pole Piece
6	Teflon Ball in Check Valve
7	Aluminum Connecting Gaskets
8	Nylon Bearing
9	Magnet Retaining Plate
10	Countersunk Screw for Securing Retaining Plate
11	Magnetized Piston
12	Retaining Nut
13	Cylinder Gasket (Glass-filled Teflon)
14	Pump Cylinder
15	Thrust Plate
16	Check Valve Body

The type 316 stainless steel pump had a free-floating, teflon-coated, magnetized piston (item 2 in Figure 3), which was drawn up and down by a set of twelve Alnico V bar magnets. The magnets (item 3) were arranged in a ring around the pump cylinder (item 14). The two check valves at each end were operated with teflon balls (item 6 indicates one of these balls) closing against conical surfaces.

The pump, indicated by item J in Figure 2, was located in the air bath and was driven from the outside by a variable-speed DC motor (Boston Gear Ratiotrol) connected to a 30/1 gear reducer (Boston Gear). The range of speeds at which the piston could be drawn back and forth was 0 to 60 times per minute, although below 10 times per minute the check valves often failed to close well enough to insure the flow of vapor through the cell.

The volume of the pump and circulating lines was approximately 30 cm³. The maximum design pressure of the pump was 63 000 kPa based upon the maximum recommended stress quoted for 316 stainless steel in ASME tables. The maximum stress was calculated by the Lamé equation. The pump passed a hydrostatic test of 50 000 kPa at room temperature. By design, the internal pressure acted to increase compression on the glass-filled teflon rings that provided the seal. This arrangement proved to be highly successful, as the pump remained free of leaks throughout the duration of the experiments.

A-3-d. Charging and Sampling Equipment

When the desired system pressure was above the pressure of the supply cylinders, the gases were charged into the warm cell with the same motor-driven Ruska pump that was employed in charging the cold cell.

Vapor and liquid samples were taken through separate needle valves. Both of the valves were essentially of the same design as those in the published description (20) of the cold cell.

The vapor samples were drawn through a needle valve, item D in Figure 2, that had been installed in the vapor recirculation line. Liquid samples passed through a 90 cm length of 0.23 mm I.D., type 316 stainless steel capillary tubing before passing through the liquid sampling needle valve, shown as item E in Figure 2. A 0.15 mm wire had been inserted along the entire length of the capillary tube in order to reduce the dead volume of the sampling line, and to improve sampling control by restricting sample flow rates. One end of the capillary tubing terminated at the valve seat very near the tip of the needle. The other end was inserted through a 1.6 mm diameter port in the bottom of the equilibrium cell (shown in Figure 1) so that the tubing extended about 1 mm above the cell floor.

The purpose of the capillary line on the liquid sampling system was to avoid partial separation of components as the sample flashed across the constriction in the sampling valve. In principle, once a steady state had been achieved

the composition of the vapor emerging from the needle valve at the end of the capillary tubing was the same as the composition of the liquid entering the tubing from the cell. Therefore one needed only to discard the portion of the sample that emerged before a steady state was achieved in order to obtain a representative sample.

In practice, however, it was found that no difference in composition could be detected whether or not the first portion of a sample was discarded. The capillary line needed only to be purged to remove material that had accumulated there when the cell was not at the equilibrium conditions being studied.

The sampling valves were housed in a separate portion of the air bath which also contained the tubing manifold and most of the valves used in charging, venting, evacuating and sample handling. This separate section could be heated independently above the temperature of the air bath, thereby preventing condensation or adsorption of n-pentane from the low pressure gaseous sample. Condensation and adsorption were a concern when the manifold was below room temperature because of the low vapor pressure of pentane at these conditions. A 10 cm squirrel-cage fan driven by a 1/40 H.P. motor provided circulation in the separate bath. Heat was furnished by a manually controlled 300-watt strip heater. A 140 kPa pressure transducer (Validyne) was connected to the sample storage tubing, and was used to observe and control the amount of sample drawn. The electrical

output from the transducer was displayed on a Hewlett-Packard Model 3455A digital voltmeter.

B. Temperature Measurement

The temperatures of the cold cell and its air bath were measured with copper-Constantan thermocouples. For the warm cell and its bath, iron-Constantan thermocouples were used. The calibrations of both sets of thermocouples were carried out in the same manner. The results for the thermocouples used in the equilibrium cells are presented in Appendix A.

The calibrations were made against a platinum resistance thermometer. For both sets of equipment, the calibrations were carried out by suspending the thermometer probe and thermocouples beside each other inside the air bath for that equipment. The voltmeter and the electrical connections to the thermocouples were the same as used during the experiments. The calibration data were fitted to polynomials of the voltage output of the thermocouple. These equations were estimated to be accurate to within 0.1°C .

C. Pressure Measurement

Equilibrium cell pressures were measured with Heise Bourdon tube gauges made from 316 stainless steel. With the cold cell, pressures at or near the 6900, 13 800 and 20 700 kPa isobars were measured on gauges whose ranges were 13 800, 20 700 and 34 500 kPa respectively.

The two gauges with the higher pressure ranges were used also on the warm cell. In addition, a fourth

gauge with a maximum pressure range of 2070 kPa was used. Pressures in the warm cell were read from the gauge with the range that was nearest to, but still above the condition studied.

All four gauges were calibrated against a Ruska dead weight gauge, and were found accurate to within 0.1% of the full scale reading when the pressure was increased from zero. Accuracy was within 0.25% of full scale when pressure was returning to zero. The calibration reports are given in Appendix A.

D. Composition Measurement

D-1. Lower-Temperature Equipment

The data obtained on this equipment were for only the hydrogen-methane-carbon dioxide ternary system. Two gas chromatographs both using thermal conductivity detectors were used for the analyses. One chromatograph measured the ratio of methane to hydrogen while the other, using a different carrier gas, measured the ratio of methane to carbon dioxide. Methane was then used as a tie component to obtain the overall composition.

Two chromatographs were used because it was not possible to obtain accurate chromatographic analyses with either of the two carrier gases (helium or nitrogen) that had been tried. (It was later discovered that satisfactory results were possible with argon as the carrier gas). When helium is used as the carrier gas in thermal conductivity detection, a chart recording of the

response for hydrogen shows that M-shaped peaks occur, often with changing polarity, over a wide range of hydrogen concentrations. While this problem can be eliminated by using a carrier gas of hydrogen mixed in helium, the weak sensitivity that ensues is unsuitable for the measurement of small hydrogen concentrations. In the same manner as for hydrogen, the thermal conductivity signal for carbon dioxide, with nitrogen as the carrier gas, also results in M-shaped peaks.

It is necessary for each component in a mixture to produce a single sharp peak in order to carry out accurate analytical work. While this requirement could not be met by using a single gas chromatograph operating with either nitrogen or helium carrier gas, it was met with the dual chromatograph system.

The gas chromatograph that measured the methane to hydrogen ratio (Hewlett Packard 7620A) operated with nitrogen as the carrier gas. The signal from the thermal conductivity detector (model 17503A) was recorded on a strip chart recorder (model 7100B), on which a disk integrator was installed to record the peak area. Component separation was achieved with a 183 cm by 2.16 mm I.D. column filled with Spherocarb packing. The nitrogen flow rate was $35 \text{ cm}^3/\text{min}$. The column temperature was 130°C , and the detector temperature was 180°C . A bridge current of 100 mA was used.

The second gas chromatograph (Hewlett Packard 5750) operated with helium as the carrier gas. The helium

flow rate was $35 \text{ cm}^3/\text{min}$ through a 366 cm by 2.16 mm I.D. column containing Porapak QS. The column temperature was maintained at 49°C , the detector temperature at 150°C , and the bridge current at 150 mA.

The chromatographs were calibrated by least-squares fitting of peak area for a pure component versus the electrical output from a $\pm 105 \text{ kPa}$ pressure transducer (Celesco Model 3PD) mounted in the sampling manifold. The peak areas from the 5750 chromatograph (helium carrier) were fitted to quadratic equations using the difference of the transducer output from zero absolute pressure as the independent variable. For peak areas from the 7620A chromatograph (nitrogen carrier) a fourth-order power series was used. The transducer outputs needed to be related to the quantity of material sampled. This was accomplished by calibrating the transducer with a closed-end manometer containing vacuum pump oil or mercury as the manometer fluid, depending on the pressure range. A cubic equation was used to represent this calibration.

The combination of the peak area and manometer calibrations permitted one to determine the pressure of a sample of pure component injected into the chromatograph. (Eight-port Hewlett Packard gas injection valves were used for this purpose). Since the volume of gas injected was always the same, the pressures associated with the peak areas represented the relative amounts of each component in the sample. These pressures were corrected for non-ideal

behavior. At the conditions used, the corrections proved to be small.

The calibrations described above are presented in Appendix A.

D-2. Higher-Temperature Equipment

The new, higher-temperature equipment (the warm cell) was used to take data on all three systems studied. For all the analyses carried out with this equipment, peak areas were found by numerical integration with a Hewlett Packard 1000 digital computer and the Hewlett Packard 3350 Series programming package.

D-2-a. The Methane-Containing System

The warm cell calibration of the methane-containing system differed from that of the cold cell in that peak areas were automatically integrated by computer, and that only one gas chromatograph was employed. Argon was used as the carrier gas. All three components were detected satisfactorily with a thermal conductivity detector. The Hewlett-Packard Model 7620A gas chromatograph, with associated equipment as described in the preceding section, was used.

The argon flow rate was 20 ml/min. Spherocarb was used in the column (183 cm, 2.16 mm I.D.) which was maintained at 110°C. The detector temperature was 135°C, and the bridge current was 80 mA.

The calibrations are shown in Appendix B.

D-2-b. The n-Pentane-Containing Systems

The same gas chromatograph calibration was used

for both the hydrogen-n-pentane and hydrogen-carbon dioxide-n-pentane systems. These components were separated in two columns joined in series. The first column (152 cm, 2.16 mm I.D.) was packed with Porapak Q, and was used to retain the pentane as the hydrogen and carbon dioxide passed on through both columns. The second column (183 cm, 2.16 mm I.D.) was packed with Spherocarb to separate the hydrogen and the carbon dioxide. After the hydrogen and carbon dioxide had been eluted, the direction of flow was reversed, and the pentane was backflushed from the first column to the detectors.

Argon was used as the carrier gas. Because the thermal conductivity detector responded only weakly to n-pentane in argon, it was necessary to employ both a flame ionization detector (F.I.D.) and a thermal conductivity detector (T.C.D.). The flow from the columns was split so that approximately seven-eighths of the gas passed through the T.C.D. which was used to detect hydrogen and carbon dioxide. Only the pentane was detectable with flame ionization. The argon flow rate was 35 cm³/min. The columns were maintained at 125°C, the T.C.D. at 135°C, and the F.I.D. oven at 150°C. The T.C.D. bridge current was 80 mA. The hydrogen and air flow rates used to sustain the flame were 37 and 500 cm³/min respectively. The flow rate of make-up argon, that augmented the portion of the column gas flowing to the F.I.D., was 46 cm³/min.

An initial attempt to obtain a calibration in the same manner as for the methane-containing system led to poor

results. Consequently, the calibration was performed with gas mixtures whose compositions were known to within a relative accuracy of about 1%. These mixtures were prepared volumetrically and/or gravimetrically, depending on which procedure provided greater accuracy for a given composition.

The T.C.D. response did not vary linearly with the quantity of material. In order to calibrate this signal a rather complicated approach was used in which the effective response factor was made to vary with both peak area and sample composition. A detailed description as well as the actual calibrations are presented in Appendix B.

E. Refractive Index Measurement

The refractive index of each of the coexisting phases was determined by measuring the angle at which a beam of light emerged from the equilibrium cell after reflection from the internal mirror. Figure 4 is a reproduction of a diagram used elsewhere (5) to illustrate this arrangement.

A beam of monochromatic light (632.8 nm) was directed from a continuous helium-neon laser (Spectra Physics Model 132) into a telescope (Gaertner M523, aperture 28 mm, focal length 250 mm) with an Abbé-Lamont autocollimating eyepiece (Gaertner L372) using an optical fibre guide.

A partially reflecting mirror directed light down the telescope towards the cell window. The telescope was mounted on a precision rotary turntable (Karl Kneise RTPH-10) and was turned by using a hand-operated vernier wheel graduated in divisions of two seconds. The maximum turntable

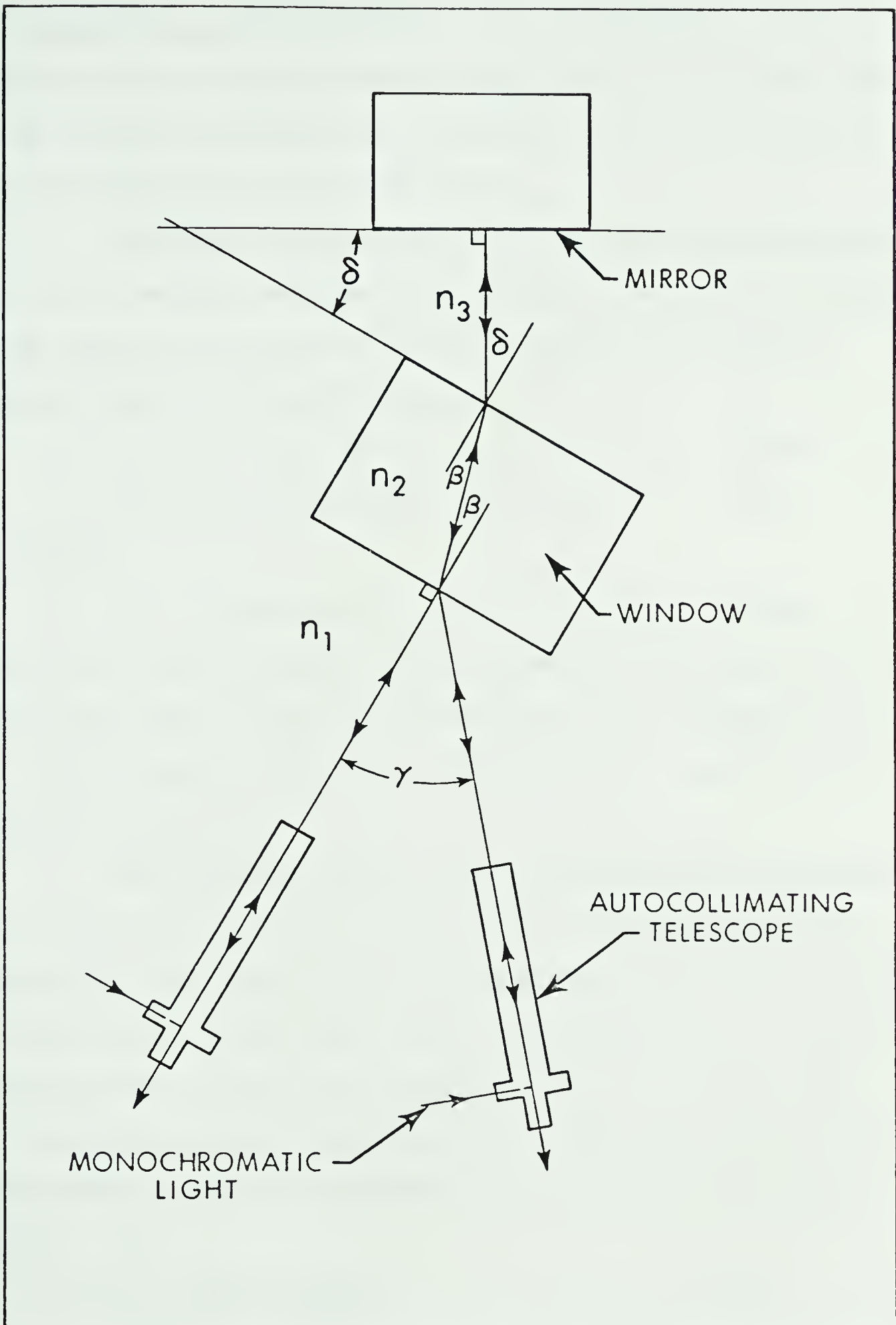


Figure 4. Schematic Representation of the Angle Measurement Involved in the Determination of the Refractive Index

error was 10 seconds over 360° . The turntable was rotated until the beam of light emerging from the cell could be observed through the telescope, indicating that the entering and returning rays were co-incident.

The angle between this ray and the line perpendicular to the window surface (γ in Figure 4) could be related to the refractive index of the fluid inside the cell by applying Snell's Law as follows:

$$n_1 \sin \gamma = n_2 \sin \beta \quad (10)$$

$$n_2 \sin \beta = n_3 \sin \delta \quad (11)$$

Therefore,

$$n_3 = n_1 \sin \gamma / \sin \delta \quad (12)$$

where n_1 is the refractive index of ambient air, n_2 is the refractive index of the window and n_3 is the refractive index of the fluid in the cell. The angles β , γ and δ are as shown in Figure 4.

The window surfaces must be parallel for Equation (12) to be valid. The internal angle δ could be found by measuring γ when the cell was filled with ambient air ($n_3=n_1$) in which case γ and δ were equal. Alternatively, γ could be measured when the cell was evacuated ($n_3=1$) in which case the refractive index of air had to be obtained from a handbook before δ could be calculated by rearranging Equation (12),

$$\delta = \sin^{-1}(n_1 \sin \gamma). \quad (13)$$

For the cold cell, the rotary table was placed below the cell and centred approximately on a vertical line

through the windows. For the warm cell the rotary table was mounted sideways, and was centred on a horizontal line passing from left to right in front of the cell window. The internal angles (δ) were approximately 30° for all the mirrors except the vapor mirror in the warm cell. For the latter, a larger angle of 42° was used, in order to improve the accuracy. On the warm cell, the maximum measurable refractive index was about 1.10 for the vapor mirror, and 1.37 for the liquid mirror. The limits for the cold cell were not known, but were never approached.

F. Materials

The hydrogen and carbon dioxide used in this study were both purchased from a local industrial supplier. The specified minimum purity was 99.99% for hydrogen and 99.9% for carbon dioxide. The methane was Matheson ultra high purity grade, and had a specified minimum purity of 99.97%.

The n-pentane was from Fisher Scientific Company and was designated as pesticide grade (suitable for pesticide residue analysis). No specified purity was quoted, but repeated gas chromatographic analyses of the material did not show any other peaks.

For each of the other three materials mentioned above, no contaminants were ever detected during analysis.

G. Experimental Procedure

G-1. Lower-Temperature Equipment

G-1-a. Charging and Equilibrating

Normally, the following procedure was used during

the investigation of the hydrogen-methane-carbon dioxide system in the cold cell. The equilibrium cell was cooled to near the desired temperature while it and the charging lines were purged and evacuated. This operation lasted about 2 to 3 hours. The cell was then charged with carbon dioxide until liquid covered a substantial portion of the lower window. While the cell contents were being mixed, methane was charged until the cell pressure reached a predetermined value. This pressure corresponded to the phase region that was to be studied, and was estimated from previous experience or from trial and error. Finally hydrogen was added until the intended pressure for the data point being studied was reached. As the cell contents approached equilibrium, small amounts of gas were added or withdrawn to maintain the pressure as closely as was possible. Differences from the designated pressure as large as 40 kPa (max. 0.6% of the total pressure) were tolerated. It was assumed that equilibrium had been attained when no pressure change was detected for at least thirty minutes with the cell at the desired temperature. Typically, two to three hours of mixing were required to reach equilibrium. For mixtures near the critical point, up to ten hours were required, even when the swirling liquid exhibited a froth-like appearance and a deep vortex.

After the desired measurements at one of the lower isobars had been completed, conditions appropriate to the next higher isobar were attained, when possible, by charging

hydrogen or methane.

G-1-b. Measurements

After equilibrium had been reached, mixing was interrupted in order to take refractive index measurements. Two to four measurements were made for each phase and then averaged. The sampling and analysis were then begun.

Portions of each sample were injected alternately into the two gas chromatographs. Normally six analyses of every sample were made with each chromatograph. Each analysis from one chromatograph was paired with one analysis from the other chromatograph, and a tie-component calculation was performed to obtain an overall composition. The resulting six values for the overall composition were averaged.

Two samples of both the liquid and vapor were taken. The cell contents were mixed between sample taking. Each composition that was reported was the mean for the two samples. The combined calculations required about three hours, and could not be done before the experimental run was completed.

When the composition obtained for the two samples of a phase disagreed by more than could be attributed to normal scatter, the result was rejected. In addition, the results were plotted on a triangular graph. When a plotted point disagreed substantially with the boundaries of the two-phase region, as described by the other points, it too was discarded. The latter situation occurred mainly before

it was realized that long periods of several hours of mixing were required to reach equilibrium. Prior to that, samples had frequently been taken under non-equilibrium conditions.

The pressure drop in the cell during liquid sampling was barely detectable. During vapor sampling, the drop was larger and ranged from 10 to 30 kPa. After a noticeable pressure drop, the system was usually returned to the original pressure by charging tiny amounts of hydrogen or methane. It was felt that errors from this procedure would be less than those caused by reduced system pressure.

G-2. Higher-Temperature Equipment

G-2-a. Charging and Equilibrating

For the portion of the hydrogen-methane-carbon dioxide data that was studied on the warm cell, the charging procedure was the same as described for the cold cell.

For the hydrogen-n-pentane and hydrogen-carbon dioxide-n-pentane systems, n-pentane was charged into the equilibrium cell after the cell had been evacuated and purged. The pentane was introduced as a vapor from a 0.2 litre bomb which had been filled with liquid n-pentane. After it had been filled, it was cooled until the pentane was frozen. Following this, air and other non-condensed contaminants were removed with a vacuum pump. Before the cell was charged, the bomb was heated and the cell was cooled so that enough pentane could be charged into the cell over a reasonably short time interval. This was necessary because the vapor pressure of n-pentane is only about 70 kPa

at room temperature.

After the pentane had been added, carbon dioxide and hydrogen were charged so that the desired two-phase composition region was reached. When the cell was being charged or vented, care was taken to open or close the valves in the vapor recirculation line so that vapor could flow only in the normal direction of circulation. Forcing the vapor to flow in the opposite direction would have damaged the check valves in the vapor recirculation pump.

Equilibrium was attained much more quickly with the use of vapor recirculation than was possible with the stirring mechanism of the cold cell. With the recirculating pump reciprocating 15 to 25 times per minute, no changes in pressure or composition were ever observed after one-half hour of mixing. Recirculation was stopped while taking samples, but could continue during refractive index measurement without interfering with the measurements.

G-2-b. Refractive Index Measurement

The angles required for calculating the refractive index were measured two to four times and averaged. In a few instances the refractive index of the observed phase was beyond the range of the equipment. When one of the mixture components was n-pentane, the mirror in the vapor phase often became obscured by a liquid film. It was discovered accidentally that a small sudden decrease of the bath temperature during vapor recirculation caused the mirror to clear briefly. Thereafter, such a decrease was deliberately

induced in order to take measurements otherwise unobtainable. The corresponding temperature drop recorded by the cell thermocouple was less than 0.5°C . The error introduced into the angle measurement was estimated to be 30 seconds at maximum, and usually less, depending on the vapor density.

G-2-c. Sampling and Analysis

Two samples of each phase were taken. If agreement was not obtained, a third and occasionally a fourth sample was taken to confirm a reproducible result. Two to four chromatographic analyses were made for each sample.

When the pressure was above 15 000 kPa, sampling had to be done very carefully to avoid removing too much material and subsequently losing equilibrium. The flow rate through the needle valve was controlled by inserting or withdrawing a needle into a small circular hole through which the sample was drawn. Ideally, the needle should be able to move smoothly from the closed to the open position. However, the needle was normally stuck in the valve seat, and upon withdrawal it would free itself suddenly. If there was any freedom of motion for the needle in the valve stem, the needle would pop out, and a sudden large flow of sample would ensue. This problem could be avoided by placing a small spring in the valve stem so that the needle was free to move only by further compressing the partly compressed spring. However, at the higher pressures, the force on the needle from the contents of the cell was large enough to push the needle back against the spring. No commercially

available metal spring with small enough dimensions to fit into the valve stem was found to be strong enough to prevent this motion. The best control was achieved by placing a small, deformable piece of polyurethane in place of the spring. However, at 100°C the polyurethane appeared to deteriorate gradually, with the resulting loss of spring strength.

Prior to the end of the experimental runs that were performed, the response to pentane from the flame ionization detector began to weaken. Corrections had to be applied to this response in order to calculate the composition for the last two data points (13 790 and 27 580 kPa at 100°C). This was accomplished by carrying out chromatographic analyses of a gas mixture of known composition, between the analyses of the samples drawn from the cell. Using the peak areas for the samples of known composition, it was possible to calculate the factor by which the pentane peak area needed to be multiplied in order for the original calibration to be correct. The same factor was then applied to the pentane peak areas from the analyses of the experimental samples. The corrected peak area was subsequently used in the original calibration to calculate the composition of the samples from the cell.

IV - EXPERIMENTAL RESULTS

A. The Hydrogen-n-Pentane System

The hydrogen-n-pentane binary system was studied at 0.0, 50.0 and 100.0°C. A total of thirty-two data points, all taken with the warm cell, were obtained for this system. A data point consisted of the measured pressure, temperature, and compositions of both the liquid and vapor phases when in equilibrium with each other. The results are shown in Figure 5 in which the mole fraction of hydrogen in each phase is plotted versus pressure at each temperature. Three characteristics of this system are immediately apparent. Firstly, the solubility of hydrogen in the liquid phase increases with temperature, as is normal for hydrogen-containing systems. Secondly, at the highest pressures attained, nearly 28 000 kPa, the system is obviously still far from its critical point, and only the vertical lines describing the vapor composition in the figure provide any indication of the retrograde region. Thirdly, the pentane concentration in the vapor phase is very small at 0°C, a consequence of the low vapor pressure of pentane.

The equilibrium ratios, or K-factors, defined as the ratio of the mole fraction of a component in the vapor phase to the mole fraction of the same component in the liquid phase, are shown in Figure 6. The data display only a small amount of experimental scatter.

The compositions are provided also in tabular form in Table C-5 found in Appendix C. Included in the same table

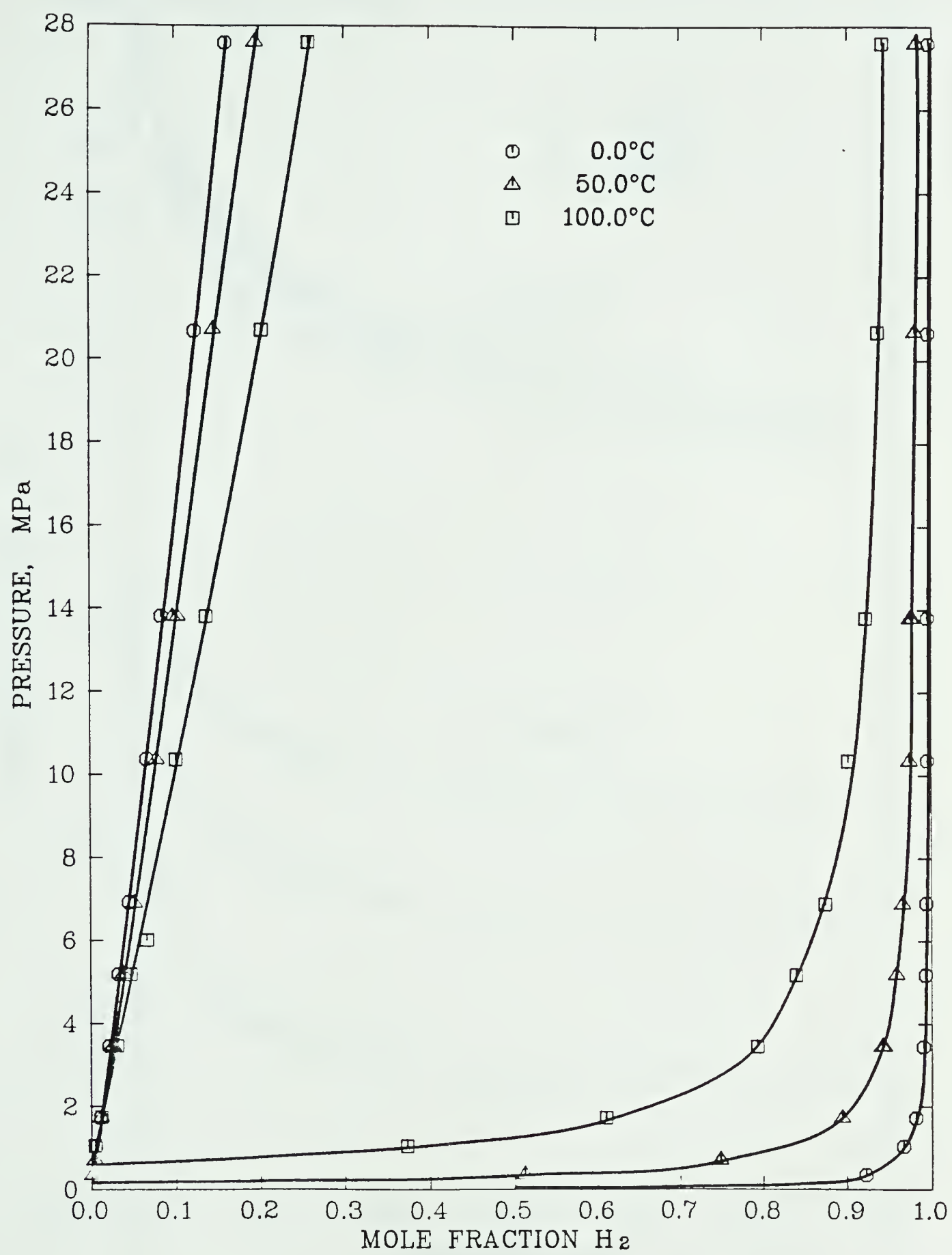


FIG. 5 EQUILIBRIUM PHASE COMPOSITIONS OF THE HYDROGEN-n-PENTANE SYSTEM

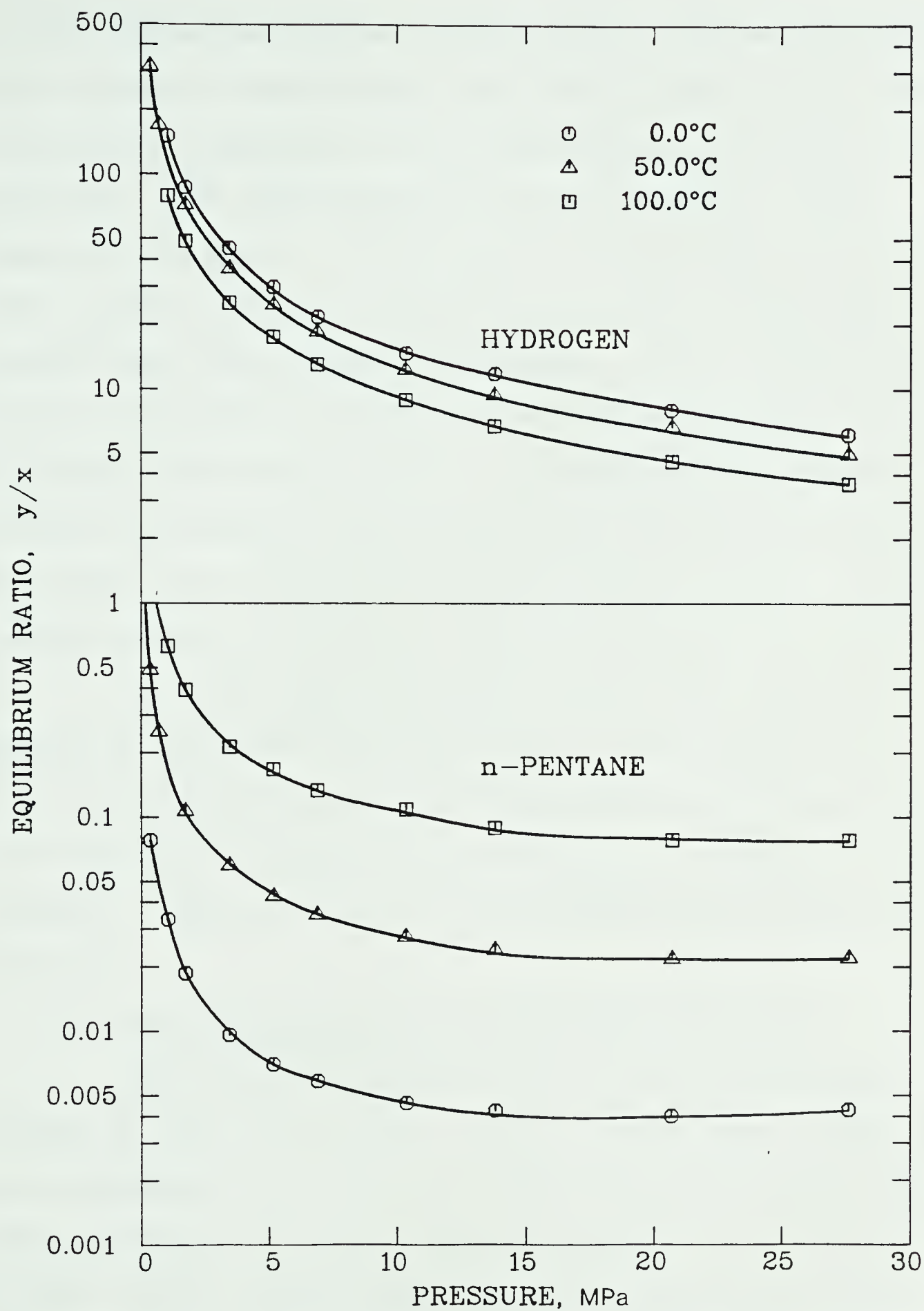


FIG. 6 EQUILIBRIUM RATIOS FOR HYDROGEN AND n-PENTANE IN THE HYDROGEN-n-PENTANE SYSTEM

are the refractive indices of each phase, and the calculated molar volumes. Considerable uncertainty exists in the concentration of hydrogen in the liquid phase at 0°C and low pressures. The affected results are presented in parentheses in the table. A combination of very small concentrations together with the difficulties of lower-temperature analyses made high accuracy impossible. Only a few of the data are affected this way. For low pressure points at the two higher temperatures, errors were substantially reduced because the sampling procedure had been improved and because the higher vapor pressure of pentane allowed larger, higher-pressure samples to be drawn without condensation occurring.

At the lowest pressures studied, the refractive indices of the vapor phase were also of poor accuracy because the angles of refraction that needed to be measured were very small and approached the range of precision of the equipment. These values also are listed in parentheses in Table C-5.

B. The Hydrogen-Methane-Carbon Dioxide System

The hydrogen-methane-carbon dioxide system was studied at -45.8 and -15.0°C. Three isobars were studied at each temperature, and for each isobar the compositions were varied to cover the entire two-phase region. All the data for the -45.8°C isotherm were obtained with the cold cell, for which isobars of 6900, 13 790, and 20 680 kPa were chosen. The compositions in mole fractions for these points are presented graphically in Figure 7.

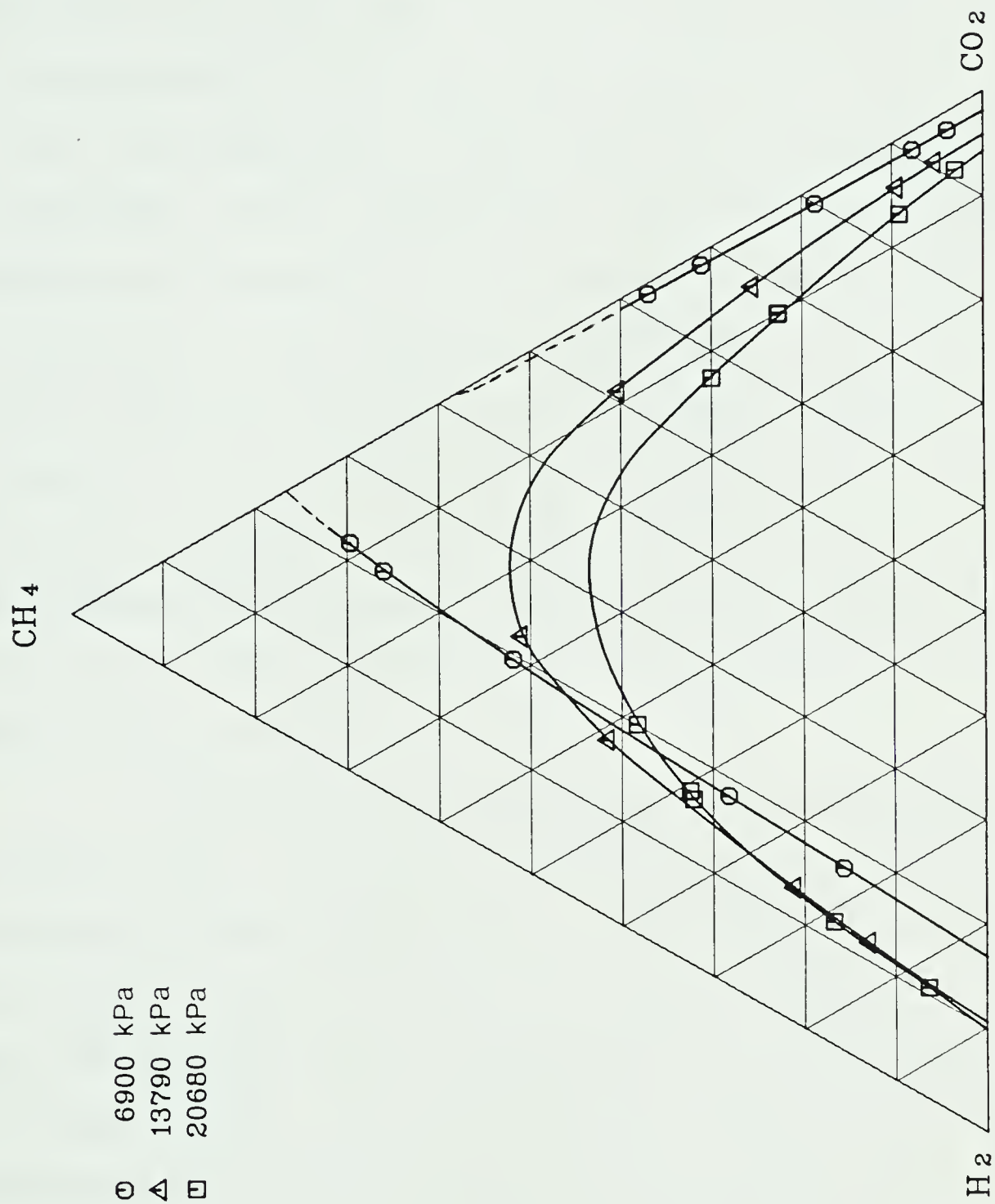


FIG. 7 EQUILIBRIUM PHASE COMPOSITIONS OF THE HYDROGEN - METHANE - CARBON DIOXIDE SYSTEM AT -45.8°C

Similarly, three isobars were studied on the warm cell for the higher isotherm. Pressures of 6900, 13 790 and 27 580 kPa were selected. The somewhat larger pressure range reflects the moderately higher pressures that could be obtained in the warm cell. However, the 13 790 kPa isobar was studied twice, once with each equilibrium cell, in order to test the consistency of data from the two different sets of equipment. These compositions, measured at the higher isotherm, are presented in the triangular plot of Figure 8. An indication of the degree of consistency of the data from the two equilibrium cells can be obtained by observing the two-phase boundary lines running through each of the two data sets collected at 13 790 kPa. A small but noticeable disagreement exists between the vapor phase compositions from the two cells. The extent of disagreement is examined later in this chapter.

A total of thirty-one data points were obtained for this system. For most of these points refractive index measurements were obtained also. Four additional data points were taken in order to locate the binary compositions at which the isobaric plots terminate along the perimeter of the phase diagram. As an example, the methane-carbon dioxide binary point that terminates the two-phase loci of the 6900 kPa isobar can be seen along the right edge of the triangle in Figure 8. It shows that the mole fractions of methane are about 0.23 and 0.51 in the liquid and vapor phases respectively. At the higher pressures represented by

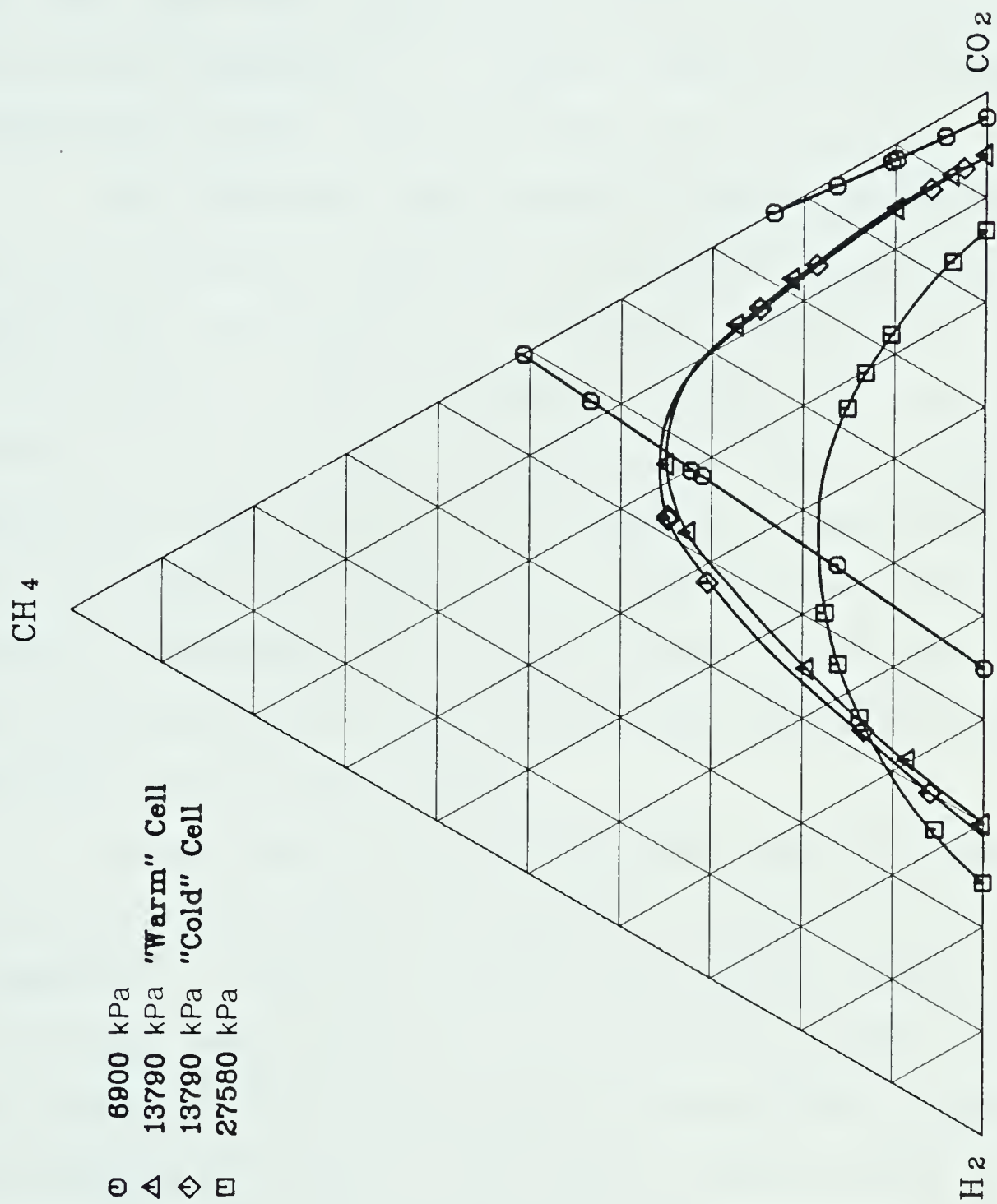


FIG. 8 EQUILIBRIUM PHASE COMPOSITIONS OF THE HYDROGEN-METHANE-CARBON DIOXIDE SYSTEM AT -15°C

the other two isobars, methane-carbon dioxide mixtures are always supercritical at this temperature, and the two-phase locus does not extend to the two-component boundary. Instead, the vapor and liquid arms of the locus converge at the critical composition, at which a substantial hydrogen concentration exists, as can be seen from the figure.

The limiting, two-component compositions (and the associated refractive indices) were measured whenever it appeared that accurate values could not be obtained by interpolation of data in the literature. However, for the isobars studied on the cold cell, hydrogen-carbon dioxide binary compositions could not be obtained because a measurable amount of methane was required as a tie-component for the analysis. Ultimately, one methane-carbon dioxide point and three hydrogen-carbon dioxide points were obtained as complementary data for this system.

These binary data were included among the hydrogen-methane-carbon dioxide data presented in Tables C-1 and C-2 in Appendix C. Table C-1 contains the measured compositions and K-values, while Table C-2 contains the measured refractive indices and the experimentally derived molar volumes of the corresponding points. The tables include partial data points, for which the composition of only one phase was obtained. However, such partial points are not shown on the figures so that the experimental tie lines can be found more easily in Figures 7 and 8. Tie lines for any isobar can be found by joining the first experimental liquid point on the

graph with the first vapor point, then joining the second points of each phase, and so forth, provided one starts with the vapor point and the liquid point nearest to one side of the diagram. It is necessary to choose a side that represents a binary system in which both liquid and vapor exist at that pressure and temperature.

C. The Hydrogen-Carbon Dioxide-n-Pentane System

The hydrogen-carbon dioxide-n-pentane system was studied at 0.0 and 50.0°C. Only the warm cell was employed for this system. At each temperature three isobars were studied: 6900, 13 790 and 27 580 kPa. Data were collected so that the complete composition range of the vapor-liquid region was covered for each isobar. A total of twenty-five data points was obtained. These points are plotted in Figures 9 and 10. Three additional hydrogen-carbon dioxide binary data points are plotted in order to locate the ends of the loci for the two-phase boundaries. Also, six of the hydrogen-n-pentane binary data points, presented earlier in this chapter, are shown again along the lower edge of the triangular plots. Not shown is one ternary liquid phase composition for which the composition of the co-existing vapor phase was not obtained. However, this liquid composition is included in Table C-3 in Appendix C.

The refractive indices were measured in all cases except for one vapor phase, at which the refractive index was beyond the measurable range of the warm cell. These refractive indices together with the calculated molar volumes

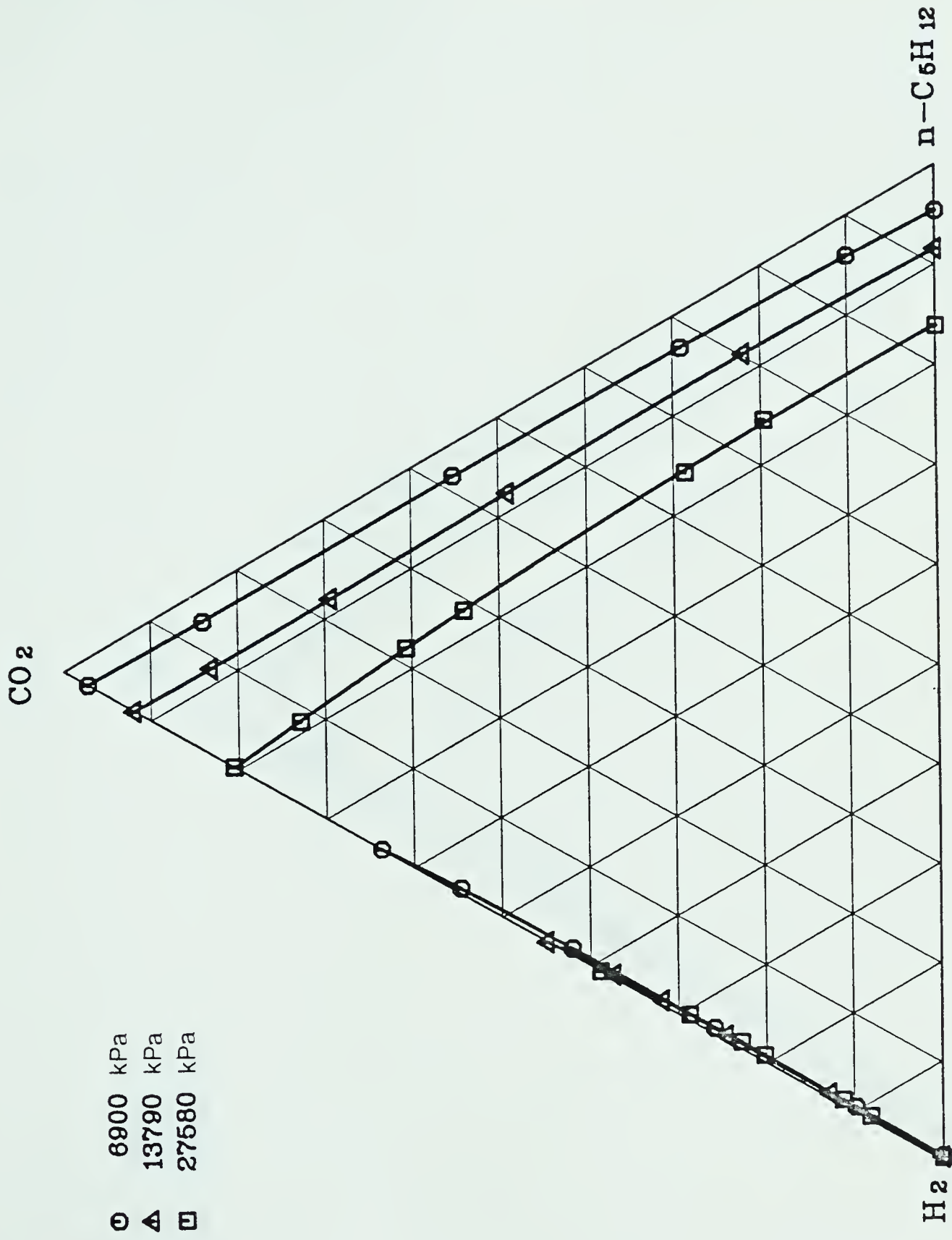


FIG. 9 EQUILIBRIUM PHASE COMPOSITIONS OF THE HYDROGEN-CARBON DIOXIDE-n-PENTANE SYSTEM AT 0.0°C

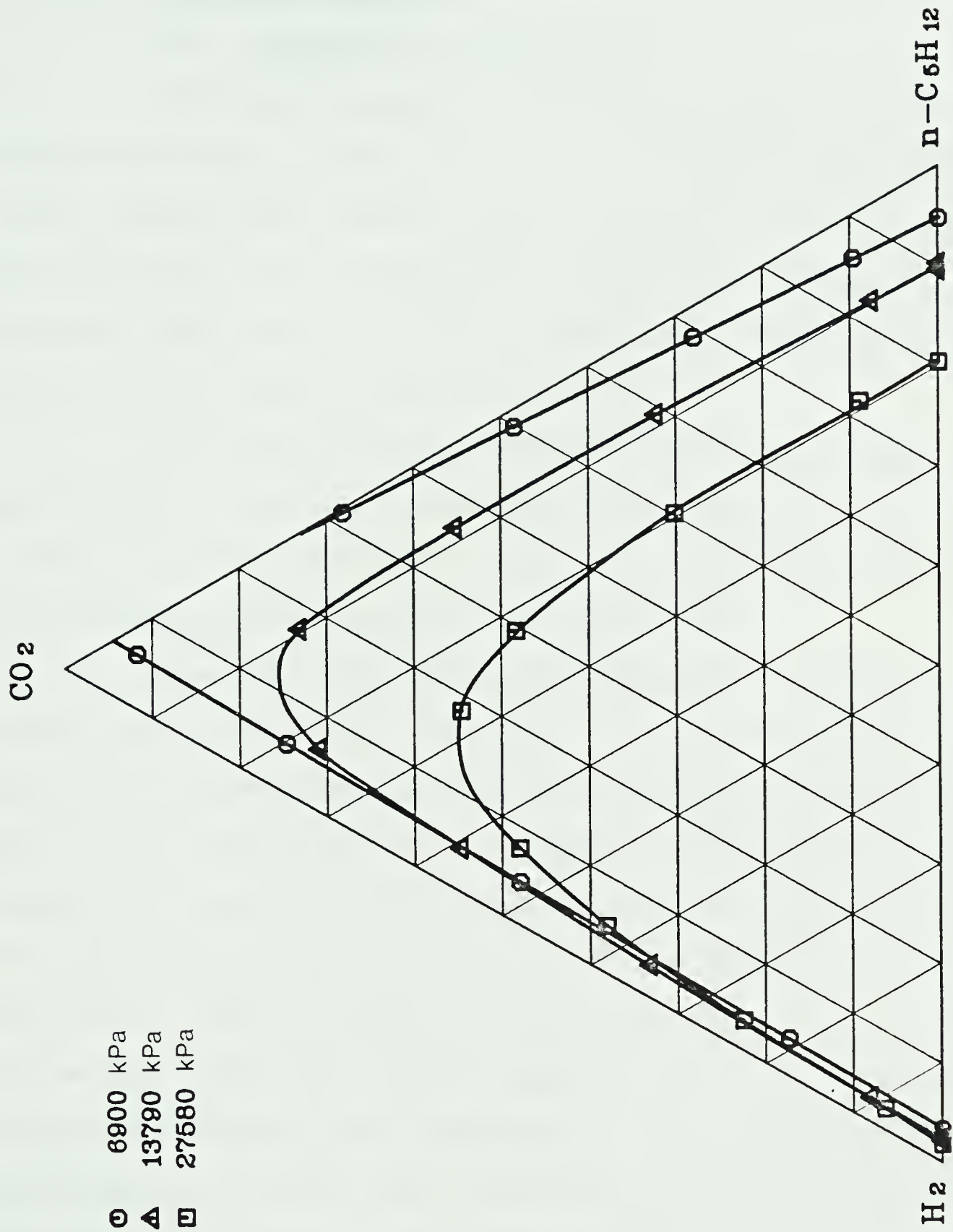


FIG. 10 EQUILIBRIUM PHASE COMPOSITIONS OF THE HYDROGEN-CARBON DIOXIDE-n-PENTANE SYSTEM AT 50.0°C

are presented in Table C-4 in Appendix C.

D. Estimated Accuracy

D-1. Temperature Measurement

The main sources of error in the measurement of temperature were: inaccuracy of the thermocouple calibrations, temperature variation with location in the air bath, the influence of an overcooled or overheated stream of recycled vapor (warm cell only), and fluctuations in the bath and cell temperatures themselves.

A statistical analysis was made of the random deviations of the points used to obtain the calibration curves. It indicated that the error of the fitted calibration curves was very likely less than 0.1°C .

The effect of thermal inhomogeneity in the air baths was more difficult to assess. During operation of the warm cell, it was observed that the temperature measured by the air bath thermocouple was slightly different from the temperature measured by the equilibrium cell thermocouple. (No such differences were observed during operation of the cold cell.) The difference between the bath and cell temperatures was larger for greater differences between the ambient temperature and the bath temperature. The greatest observed difference was 0.8°C , which occurred when the bath temperature was about 100°C . This temperature disagreement is believed to be due to thermal losses from the bath air through the bath walls, and to small air leaks in the bath walls, which allowed mixing of ambient

air with the bath air. The bath thermcouple had been suspended roughly 50 cm from the cell on the upstream side of the air flow. It is believed that a small amount of ambient air did mix with the bath air in this section, probably because of leaks along the sliding window in the bath wall (see Figure 2). The large, highly-conductive mass of the equilibrium cell itself certainly diminished any inhomogeneity of the bath air temperature, and it is hard to conceive of associated disturbances inside the cell causing more than a 0.05°C difference from the thermocouple reading.

Observed changes in the cell temperature upon starting or stopping vapor recirculation indicated that the disturbance due to vapor returning at a temperature different from the cell temperature was not more than several hundredths of a degree. Furthermore, observed variation of the cell temperature reading during constant vapor recirculation was never more than $\pm 0.06^{\circ}\text{C}$, and was usually less.

When all the above sources of error are considered, the maximum possible error in the reported temperatures is estimated to be $\pm 0.25^{\circ}\text{C}$.

D-2. Pressure Measurement

Three possible sources of error in pressure measurement were identified. These were: hysteresis in the bourdon tube gauges, calibration error, and fluctuations of the pressure in the equilibrium cell due to sampling.

The effect of hysteresis upon pressure readings when the pressure rises from zero was specified by the

manufacturer (Heise) to be within 0.1% of full scale. The calibrations made against a dead weight gauge were also within 0.1% of full scale. Pressure changes due to sampling and recharging were consistently under 0.2% of the system pressure. It is estimated that the maximum possible error from all sources is 0.5% of the reported pressures. The reported pressures, as found in Appendix C, are not necessarily the same as the nominal pressures for an isobar. For example, the pressure recorded for individual data points for the 6900 kPa (nominal pressure) isobar of the hydrogen-methane-carbon dioxide system at -45.8°C (Table C-1 in Appendix C) varies from 6888 to 6936 kPa. Such differences between the nominal and reported pressures were still small and were at most 0.6%. Consequently, for data of a certain isobar the maximum error that could occur when the nominal pressure is used is estimated to be 1%.

D-3. Composition Measurement

The errors that occur during composition analysis can vary considerably with the components to be analyzed, the relative amounts of each component, and the procedure and method used in measuring these concentrations. The degree of uncertainty differs from one system to another, and from one calibration to another. Analyses are often less accurate when very small concentrations are encountered. As a result, it is more difficult to estimate the possible errors in composition measurement than in temperature or pressure measurement.

The error estimates that follow are based mainly upon the random scatter observed during calibrations. The few available tests for systematic error were considered also. Each system is treated separately.

For the data taken with the cold cell (part of the results for the hydrogen-methane-carbon dioxide system) the standard deviations of points from the smoothed calibration curves (see Figures 11 to 14 in Appendix B) were about 2% relative for each component over most of the calibrated range. For the calibration curve of the pressure transducer that was used to measure the pressure (and hence the relative amounts) of the pure component samples, the standard deviation in the range in which most of the experimental measurements were taken was under 0.5%. The use of two gas chromatographs, from which the results needed to be combined before the overall composition was obtained, led to slightly larger uncertainties than could be achieved on single-chromatograph analyses. Finally, the slowness of the technique used for mixing the contents of the cold cell often made it difficult to determine whether equilibrium had been achieved or merely approached closely. Based on these considerations, the estimate for the maximum possible error was 8% relative. This limit applies to the difference from unity of mole fraction composition, or to the composition itself, whichever is less. For example, a composition given as 0.800 is considered to be accurate to 8% of (1.000 - 0.800), or to ± 0.016 mole fraction.

The portion of the hydrogen-methane-carbon dioxide data that was taken with the warm cell is believed to be of high quality. Only one gas chromatograph was employed, and it was possible to operate it isothermally under very stable conditions. Calibration data for individual components had approximately the same standard deviations as for the cold cell calibration just described i.e. about 2%. The calibration was checked nearly a year after it had been made by analyzing a gas mixture of known composition. When the measured mole fractions were compared with those obtained during the mixture preparation, the results were all within 3% relative. In view of the 1% uncertainty in the compositions obtained during mixture preparation, and that the chromatograph conditions had to be re-established after having used the equipment for other measurements, the agreement is extraordinarily good. It is believed that the reported compositions of the warm cell data for this system are accurate to within 4% relative.

Another test of the accuracy of the hydrogen-methane-carbon dioxide data is found by comparing the data from the cold cell and the warm cell for the intermediate isobar at -15°C (Figure 8). As pointed out previously, the entire two-phase region of this isobar was studied twice, once with each equilibrium cell. Comparison of these two sets of data resulted in the observations described below.

The vapor phase compositions differ noticeably. The disagreement becomes larger as the critical point is

approached. Smoothed compositions taken from the shown curves are essentially in agreement at low methane concentrations, but the concentrations in the critical region differ by as much as 10% relative. When the liquid phase concentrations of hydrogen and methane were plotted against each other for each data set, the same trend and magnitude of disagreement were observed. The possibility that non-equilibrium conditions in the cold cell caused this disagreement was considered, but was rejected because the expected erroneously low hydrogen concentration in the liquid phase was not observed. Concentrations of hydrogen from the cold cell data were 0 to 10% higher than from the warm cell data for both the liquid and vapor phases. At most, a 2% relative disagreement could be attributed to non-equilibrium conditions in the cold cell data.

For the two systems that contained n-pentane as one component the same calibration was used, and hence the estimates of possible error are identical. As this calibration was conducted in a very different manner than the other two calibrations, the bases for accuracy estimates differed accordingly.

Gas mixtures of known composition (see Appendix B) were used for the chromatographic calibrations. These compositions were known to within $\pm 2\%$, and usually to within $\pm 1\%$, relative accuracy. As a test for random error, the raw calibration data were fed back into the final system of equations that represented the calibrations. The disagreement

with known compositions as well as the magnitude of random scattering were observed, and were found to be of generally the same magnitude as for the other systems already described. Perhaps the greatest source of error in the calibration of the pentane-containing systems was changing relative sensitivities of the two detectors employed. The success of the calibration required that the sensitivities of response of a thermal conductivity detector (T.C.D.) and a flame ionization detector (F.I.D.) did not vary significantly over the course of the experiments. However, the sensitivity of the F.I.D. was observed to drop, particularly towards the end of the data acquisition. (The remedial action that was taken is outlined in Chapter III). For the data taken at 0°C, for which no independent tests of the calibration accuracy were made, a change in detector sensitivities of a few per cent could have gone undetected. On the other hand, an attempt to reproduce three of the data points of the hydrogen-n-pentane system at 50°C was successful for two of the points (See Table C-5 in Appendix C). The data referred to are at pressures of 693, 3450 and 13 790 kPa. It was concluded that the detector response had remained stable over the intervening period (one month operation) until the two data points were successfully reproduced. Noticeable disagreement occurred in the reported compositions of the pair of data points at 13 790 kPa. Mole fractions of n-pentane in the vapor of 0.0214 and 0.0238 were reported for the initial and reproduced measure-

ments respectively. This represents a difference of 10.1% of the larger value. Similarly, the reported mole fractions of hydrogen in the liquid phase were 0.1035 and 0.0975 respectively, a difference of 5.8%. When the vapor compositions were plotted on suitably scaled graphs and a smoothed curve was drawn, it became obvious that the reproduced vapor composition (0.0238 mole fraction n-pentane) was in serious disagreement with the rest of the data. A similar graph for the liquid compositions showed that the liquid composition for the reproduced data point was also in disagreement with the other data points, although not as badly. While a re-examination of the record for the reproduced data point at 13 790 kPa revealed no obvious cause for this unusually large disagreement, the results for this point are untypical of the other experimental data and are probably erroneous. Examination of smoothed compositions obtained by using the Peng-Robinson equation of state also confirmed this conclusion.

During the first portion of the data acquisition for the systems containing n-pentane, the gaseous samples obtained after they had been drawn from the cell were not mixed before chromatographic analysis. At first it was suspected that inhomogeneities in the composition of these samples (caused by enrichment of components with low molecular weight as they passed through tiny orifices in the sampling valve and manifold) contributed to serious errors in the analysis. However, the successful reproduction of

results for two of the binary conditions demonstrated that the influence of inhomogeneities was negligible for the sample handling procedure used.

For most of the data for these two systems the overall maximum uncertainty of the data was estimated to be $\pm 5\%$ relative. The data at 0°C could conceivably be in error by as much as $\pm 7\%$ relative. Furthermore, much larger random errors occurred when only small quantities of a component existed in a sample. As a result, errors up to $\pm 10\%$ relative could exist for compositions below a mole fraction of 0.010.

The error estimates quoted in this section are for the maximum errors believed possible. They do not include improvements that could be expected from data smoothing.

D-4. Refractive Index and Molar Volume Measurement

The accuracy of individual refractive index measurements varied widely, depending on the conditions of the window and mirror at the time. When a single undistorted image of the laser beam could be observed through the autocollimating telescope the estimated accuracy of the refractive index was usually about ± 0.00015 . In such instances, the sources of uncertainty were the inaccuracies of the measured angles, and more important, the uncertainty of the internal angle between the mirror surface and the window surface (δ in Figure 4). While repeated measurements could identify this angle to within 10 seconds of arc, the angle itself would change slightly because the window would tilt

inside the packing as the cell was subjected to changing internal pressure or, to a lesser extent, temperature. As a result, the uncertainty of the internal angle was ± 15 to ± 30 seconds, depending on the temperature and pressure changes the cell had undergone in the time since the previous internal angle measurement.

Unfortunately, the uncertainty in the refractive index was often increased for the following reasons. Firstly, the windows through which the optical measurements were taken would sometimes crack or chip near a surface, thereafter causing distortion of the beam of light passing through it. Secondly, several of the windows had surfaces that were measurably non-parallel. While corrections were made for this influence, the inaccuracies involved in measurement of the angle of non-parallelism contributed a small amount to the total uncertainty. Finally, obscuring of the window surfaces, especially by liquid film on the vapor-side mirror sometimes caused the reflected beams to appear very diffuse or to disappear entirely. This led to additional uncertainty, either through the difficulty involved in measuring angles using unclear images, or from disturbances to the system that occurred when steps were taken to disperse the film.

In order to assess the overall possible errors, estimates were made of the possible error from each of the above contributions for each measured value of the refractive index. The results varied widely. Calculated

uncertainties were usually between 0.00015 and 0.001 for vapor phase refractive indices, and between 0.0003 and 0.0013 for the liquid phase values. Through experience and minor equipment modifications, greater accuracy was gradually obtained. As a result, the refractive indices of the last data taken, the 50 and 100°C isotherms of the hydrogen-n-pentane and the hydrogen-carbon dioxide-n-pentane systems, are all believed accurate to within 0.0005.

In the tables in Appendix C the results are quoted to four decimal places, except when uncertainties greater than 0.0013 exist, in which case only three decimal places are quoted.

Estimation of the accuracy of the experimental molar volumes required additional considerations. Obviously the quality of the results depends partly on the accuracy of the value of the refractive index used in the equation for the Lorentz-Lorenz refractivity. This equation is

$$R_{LL} = \frac{n^2-1}{n^2+2} \frac{1}{\rho} \quad (14)$$

where R_{LL} is the Lorentz-Lorenz refractivity, n is the refractive index, and ρ is the fluid density.

A second source of uncertainty involves the assumption that the molar refractivity of a mixture is equal to the mole average of the pure component refractivities. This approximation has been investigated by several authors for a variety of system types. The results were summarized by Besserer (5). The approximation is accurate to within about $\pm 1\%$.

A third source of error involves the uncertainty in the mole fraction composition. The amount that the compositional errors affect the values for the molar volumes depends upon the mixture compositions and the difference between pure component refractivities. For example, even fairly large relative errors in the composition of hydrogen when it is in a low concentration will affect the calculated value of the molar volume very little, because of hydrogen's low value of R_{LL} . As a second example, consider simultaneous errors in methane and carbon dioxide concentrations. Because these two components have refractivities that are nearly the same, a large error in the concentration of one will be nearly balanced in the volume calculation by an equal and opposite error in the other.

As a consequence of the above factors the magnitude of the uncertainty for the molar volumes is often much less than for the compositions. For vapor phase volumetric data except at pressures below 3000 kPa the estimated uncertainties fall between $\pm 1\%$ and $\pm 4\%$. At pressures below 3000 kPa, which applies only to the hydrogen-n-pentane system, the difference of the refractive indices from unity is very small, causing the uncertainty from angle measurement to become overwhelmingly large, especially at the lowest pressures.

On the other hand, the liquid-phase volumetric data were all estimated to be accurate to within $\pm 2\%$, and most within $\pm 1\%$.

The volumetric data, presented in Appendix C, are given to the precision at which the last figure should have large uncertainty. Values with unusually large uncertainty appear in parentheses.

V - PROPERTY PREDICTION

A. Choice of Predictive Method

Phase equilibrium predictions based upon a current engineering approach were compared with the experimental data. Consideration was restricted to cubic equations of state because they are simpler than other methods and usually display approximately the same accuracy when used for predicting vapor-liquid equilibrium compositions of mixtures. The Peng-Robinson equation of state was chosen as the method of prediction as it has been shown to be of similar or superior accuracy when compared with most other cubic equations of state (33, 44, 18).

The question of how to incorporate hydrogen into the framework of the predictions was more difficult to answer. In order to distinguish between the various possibilities outlined in Chapter II, data (28) on the vapor pressure and density of normal hydrogen were examined.

A-1. Corresponding States Test

The treatment of quantum gases as proposed by Gunn, Chueh and Prausnitz (16) (referred to in this chapter as the method, or approach, of Gunn) was given foremost attention because of encouraging results from preliminary predictions carried out for this study, and because of the success reported by Harmens (18). In the method of Gunn, the critical temperature and critical pressure of a pure fluid are each treated as temperature-dependent functions. Thus these two quantities no longer correspond to the true critical values,

but must be viewed as effective values. Equations (15) and (16) are the expressions used to calculate the effective critical temperature T_c , and the effective critical pressure P_c :

$$T_c = \frac{T_c^0}{1 + \frac{21.8}{mT}} \quad (15)$$

$$P_c = \frac{P_c^0}{1 + \frac{44.2}{mT}} \quad (16)$$

T is the temperature in kelvins and m is the molecular weight. T_c^0 and P_c^0 are the classical (not experimental) critical constants, which for hydrogen are 43.6 K and 20.2 atm (2047 kPa) respectively. These constants portray the corresponding states behavior of a material in the high-temperature limit. The acentric factor is assumed to be zero.

A qualitative similarity was noticed between Gunn's approach and the quantum corrections successfully applied by Rosenfeld and Thieberger (38) to predictions of the melting curves of several substances of low molecular weight. This similarity was investigated further. A computer program was written for interpolating compressibility factors from corresponding states tables in the same manner as described by Gunn et al. The tables that were employed were those of Chao and Greenkorn (8), who extended the tables of Pitzer to lower reduced temperatures.

Smoothed experimental densities of normal hydrogen (28) were chosen so that the entire region within the limits of the Chao and Greenkorn tables was covered. The points were more heavily concentrated in the regions of the table

in which the compressibility factor changed rapidly. The vicinity of the two phase locus was avoided because of the difficulties caused by the discontinuous nature of this line. Eighty-one data points were selected at temperatures from 14 to 121 K and pressures from 200 to 10 000 kPa.

The average absolute deviation (A.A.D.) between the smoothed density data and the densities predicted by the tables was calculated in terms of per cent of the experimental values. Several approaches to hydrogen parameter calculation were used. These approaches included the method of Gunn, simple models based upon an effective energy approach to quantum corrections, and several cases of modified acentric factors in conjunction with unaltered critical parameters.

In the effective energy approach, an effective temperature was employed to indicate the temperature at which a material would exist if all molecular motion, from both thermal and quantum mechanical contributions, were taken as thermal motion alone. The method is based loosely upon the following intermolecular pair potential suggested by Rosenfeld and Thieberger:

$$u_{\text{eff}}(r) = u(r) + \frac{c}{mT} \nabla^2 u(r) \quad (17)$$

where $u(r)$ = Intermolecular potential function

$u_{\text{eff}}(r)$ = Effective intermolecular potential function

applying to classical equations of state

m = Molecular mass

T = Absolute temperature

c = a constant that combines several fundamental constants and integers.

Difficulty was encountered when relating the effective internal energy to effective temperature because of the complicated variation of the heat capacity of hydrogen, especially near the critical point. Within this approach the best results were obtained when the effective temperature was given by:

$$T' = T + \theta \frac{|T - T_c|}{T^2} \quad (18)$$

where T' = Effective absolute temperature

T = Absolute temperature

T_c = Experimental critical temperature

θ = 30 K

All of the variables in Equation (18) are in kelvins.

A comparison of the different approaches is provided in Table 3. The parameter calculations that were employed with each approach are outlined in Table 4.

As can be seen from Tables 3 and 4, no modification was found that was significantly more accurate than the approach of Gunn. Indeed, the best result was obtained by optimizing the value for the acentric factor within the Gunn approach. Varying the constants in the denominators of Equations (15) and (16) produced no further improvement. The optimized Gunn approach was the only modification that led to a positive acentric factor.

The results for the various modifications did not differ widely. The effective temperature approach provided

Table 3. Average Errors of Predicted Compressibility
 Factors of Hydrogen For Various Modifications
 to the Calculation of Corresponding States
 Parameters

<u>Modification</u>	<u>Std. Dev. (%)</u>	<u>A.A.D. (%)</u>
Optimized Gunn	2.0	1.3
Effective T	2.3	1.6
Gunn	2.5	1.5
Optimal ω	2.7	2.1
Unmodified	3.1	2.1
Simple Fluid	7.7	5.9

Table 4. Characterization of the Modifications for Calculation
of Corresponding States Parameters

Modification	T(K)	T _C (K)	P _C (kPa)	ω
Optimized Gunn	Actual	Eqn. (15)	Eqn. (16)	+0.06
Effective T	Eqn. (18)	33.19	1315	-0.24
Gunn	Actual	Eqn. (15)	Eqn. (16)	0
Optimal ω	Actual	33.19	1315	-0.28
Unmodified	Actual	33.19	1315	-0.22
Simple Fluid	Actual	33.19	1315	0

approximately the same accuracy as the Gunn approach. Surprisingly, the use of no modifications whatsoever was only moderately less accurate than Gunn's method. When the acentric factor was changed to the optimized value of -0.28 only a slight improvement over the unmodified approach was realized. However, the assumption that hydrogen is a "simple fluid" as defined by Pitzer et al. (34) (acentric factor equal to zero), and that its experimental T_C and P_C do not have to be corrected, led to poor results.

It is worthwhile to point out the disadvantages associated with the various modifications. The modification of Gunn required that two of the three parameters used in the corresponding states correlation be temperature dependent. This leads to increased complexity and longer computation times, especially for applications that require derivatives with respect to temperature. Furthermore, the critical point predicted by the original modification of Gunn, which was based on data at supercritical temperatures between 35 and 150 K, does not coincide with the experimental critical point. At the true critical temperature and pressure, the method of Gunn predicts a reduced temperature (T/T_C) of 1.009 and a reduced pressure (P/P_C) of 1.067. Accordingly, errors are inherent in the vicinity of T_C and P_C . All of the other modifications of parameter calculation predict the critical temperature and pressure correctly.

The effective temperature approach requires only one parameter to vary with temperature. It exhibits

essentially the same accuracy as the method of Gunn, which employs two parameters to be temperature dependent. While the increased simplicity suggests that the effective temperature approach is preferable to Gunn's approach, neither method produces a large increase in accuracy. It appears that a temperature dependence for any of these parameters is of small importance.

For each of the approaches investigated in this portion of the study, there were regions of temperature in which the correlations deviated noticeably from the smoothed data. The scatter between data and correlation was always largest in the critical region. Below 25 K the experimental data and the correlated densities diverged sharply for most of the methods examined. In these cases the correlated densities were consistently too high and reached 5 to 8% error around 15 K. Only the effective temperature approach handled the subcritical temperature region well. This was the only instance in which a temperature dependent parameter provided a large improvement. However, the method was slightly poorer than the other approaches at temperatures above 65 K, at which a bias of 1 to 2% towards low densities was observed.

A relationship was found between the accuracy of the correlation at different temperatures and the value used for the acentric factor when the other parameters were unmodified. Near 120 K an acentric factor of -0.16 provided the best correlation, but at lower temperatures, successively lower acentric factors were required. At the critical

point an acentric factor of -0.35 was needed for exact agreement while at the lowest temperatures studied (15 K) a value of -0.45 was the most suitable. The trend did not apply at reduced temperatures between 1.0 and 1.1 because in this range the influence of acentric factor on correlated values is negligibly small. Because of the above result and the reasonable success obtained by using approaches that included a large negative acentric factor, it was decided to examine in more detail the choice of an appropriate value for the acentric factor of hydrogen.

A-2. Vapor Pressure Tests

According to Pitzer (34), the simpler and smaller molecules approach the hypothetical "simple fluid", for which he assigned an acentric factor of zero. By implication, the quantum fluids should have acentric factors that are also nearly zero. The effective critical parameters method of Gunn is in accordance with this reasoning although Gunn and co-workers do not state why they chose ω to be zero.

The acentric factor ω is defined as

$$\omega = -\log_{10}(P_r) - 1.000 \quad (19)$$

where P_r is the reduced vapor pressure at the reduced temperature (T/T_c) of 0.7. A plot was made of $\log_{10}(P_r)$ of hydrogen versus $1/T_r$, the inverse of the reduced temperature. The vapor pressure data were taken from smoothed tables published by NASA (28).

By reading the value of $\log_{10}(P_r)$ at $T_r = 0.7$ the acentric factor for normal hydrogen was confirmed to be -0.22.

However, the plot for hydrogen displayed concave upward curvature. For most non-polar and slightly polar substances a similar plot shows a line that is very nearly straight over the entire range from the triple point to the critical point. For these substances the slope of the $\log(P_r)$ versus $1/T_r$ plot could be used to calculate the acentric factor indirectly. This is not true for hydrogen. If straight lines are drawn from the critical point to various points on the plot of the vapor pressure, and the straight line is treated as the vapor pressure curve, values between -0.15 and -0.29 are obtained for the acentric factor. This shows the large extent to which the vapor pressure of hydrogen fails to conform to the behavior exhibited by other materials.

A plot of $\log(P_r)$ versus $1/T_r$ was also made for the vapor pressure of helium. The acentric factor was found to be -0.61. The curvature of this plot was even greater than for the plot for hydrogen.

The concave upward curvature of the plots described above is qualitatively consistent with the effective intermolecular pair potential given by Equation (17). The term that contains the Laplacian operator in this equation represents the quantum mechanical correction. It predicts that the quantum effect varies inversely with temperature, and that it is volume dependent. At either high temperatures or low densities the correction is negligible. However, at higher densities and at lower temperatures it becomes increasingly important. If this is true, then from the view-

point of classical mechanics, the liquid would appear to have a greater internal energy than would be expected at the observed temperature. Therefore, because the difference in internal energy between the liquid and vapor states is correspondingly smaller than the value that classical mechanics would indicate, vaporization of a quantum fluid would occur more readily, and the vapor pressure would appear to be anomalously high. The effect would increase with decreasing temperature causing a plot of $\log(P_r)$ versus $1/T_r$ to become concave upward, provided classical mechanics leads to a linear plot.

Unfortunately, Equation (17) gives little indication of the temperature below which quantum effects become significant for vapor pressure or density calculations.

A-3. The Peng-Robinson Correlation

A third test was carried out using a relationship from the Peng-Robinson equation of state (details presented in Appendix F). The form of this relationship had been developed earlier by Soave who found that the temperature dependence of the constant a in the Redlich-Kwong equation of state (see Equation (3)) could be represented as follows:

$$\alpha_i^{0.5} = 1 + m_i (1 - T_{ri}^{0.5}) \quad (20)$$

where $\alpha_i = a_i/a_{ci}$

a_{ci} = value of the constant a for component i at the critical point

T_{ri} = the reduced temperature of component i

m_i = a constant characteristic of component i .

The values of m_i were correlated with the acentric factor. For the Peng-Robinson equation of state, which employs the same form of relationship for the constant a , m_i was replaced by κ_i , which was calculated in a different manner, but was similarly correlated with the acentric factor according to Equation (21).

$$\kappa_i = 0.37464 + 1.54226\omega - 0.26992\omega^2 \quad (21)$$

If a plot of $\alpha_i^{0.5}$ against $T_{ri}^{0.5}$ results in a straight line, the slope (κ_i) of this line can be used in equation (21) to determine the acentric factor. The value of α can be determined at any given temperature on the vapor pressure curve by equating the fugacities of the two phases (the condition for equilibrium). α_i was calculated in this manner for normal hydrogen at temperatures from the triple point to the critical point. The results showed α_{H_2} to be nearly 1.0 over the entire temperature range. The maximum value was 1.0169 at $T_r = 0.70$ and the minimum was 0.9975 at the triple point ($T_r = 0.42$). When $\alpha_{H_2}^{0.5}$ was plotted against $T_r^{0.5}$, a locus with a slight curvature was obtained. A straight line was drawn through the points so that it passed through $\alpha = 1$ at $T_r = 1$ (at which α_{H_2} must be unity). The slope of the line κ_i was inserted into Equation (21) which was then solved for ω . A value of -0.21 was obtained.

An estimate of the range of possible values of ω could be calculated from the minimum and maximum slopes of the straight lines that could be drawn through the slightly curved plot of $\alpha^{0.5}$ against $T_r^{0.5}$. The highest value of

the acentric factor obtained in this fashion was -0.16 . This corresponded to a straight line that was tangent to the curve at $T_r = 1$. The lowest value was -0.24 , and it corresponded to a straight line passing through both $T_r = 1$ and the triple point.

The above findings indicate that the experimentally determined acentric factor for hydrogen is a reasonable value to use at reduced temperatures between 0.4 and 1. Again, little indication was provided about the suitability of negative acentric factors at higher reduced temperatures, where most of the systems of interest to engineers exist.

A-4. Binary System Composition Tests

The final test in this search for a suitable acentric factor involved a comparison of the Gunn and unmodified approaches in the prediction of binary phase compositions. Soave (41) has reported that negative values for ω are more suitable in vapor-liquid equilibrium calculations with the SRK equation of state, provided pressures do not exceed 2000 psia (13 800 kPa).

Data from the literature (39, 47) were selected for two systems, hydrogen-methane at 174 K and hydrogen-carbon dioxide at 273 K. Each of these data sets extended over almost the entire vapor-liquid region. Attempts were made to correlate each data set by using the Peng-Robinson equation of state. The optimal binary interaction parameters for each approach were found by trial and error, and the resulting compositions were compared graphically with the data on

pressure-composition diagrams.

Neither the unmodified approach nor the modification of Gunn could correlate the entire vapor-liquid region successfully. Compositions at pressures below the retrograde region could be represented accurately, but both approaches seriously overestimated the extent of the critical region, especially for the hydrogen-carbon dioxide data. While the use of lower acentric factors reduced the predicted critical pressure to more realistic levels, the two-phase region simultaneously became too narrow. Apparently, neither approach is capable of predicting the shape of the phase envelope over the retrograde region, even when the lower pressure regions are ignored.

A comparison similar to the above was performed with the hydrogen-n-pentane data obtained in this work. Although these data do not extend significantly into the retrograde region, they do permit comparison over a reasonably wide temperature range (273 to 373 K). Four of the modifications that are described in Table 4 were tested: the unmodified approach, the 'optimum ω ' modification, the Gunn modification, and the simple fluid assumption.

One method, the simple fluid assumption, was clearly inferior to the others. While this method was able to correlate the compositions of any one isotherm, the interaction parameters had unusually low values (below -1), and were strongly dependent on temperature. A temperature dependence was essential, as predictions made with an interaction

parameter for a different temperature led to very poor results.

For each of the other three cases, a single value of the interaction parameter provided reasonably accurate results over the 100°C temperature range, although a slight temperature dependence was observed. The interaction parameters were approximately -0.4 for the method of Gunn, 0.3 for the unmodified method, and 0.4 for the 'optimum ω ' approach, in which ω equals -0.28. The similarity of the results gave little indication as to which approach could be recommended above the others, except, perhaps, that the unmodified approach is more in keeping with the general tendency for binary interaction parameters to have small positive values.

Overall, the various tests revealed a range of possible approaches to the treatment of hydrogen in predictions based on two-constant cubic equations of state. At one extreme is the method of Gunn which employs the simple fluid assumption ($\omega=0$) together with temperature-dependent critical parameters. The effective critical parameters are intended to account for the increased quantum mechanical influences in light molecules. At the other extreme is the use of the unadjusted experimental critical parameters together with a negative acentric factor that is in the neighborhood of the experimental value. The use of this approach assumes that hydrogen is not a simple fluid, and that quantum mechanical effects are negligible.

The effective temperature approach that was described earlier borrows elements from both extremes and can be viewed as a compromise.

In view of the uncertainty as to which extreme is more appropriate for engineering calculations, it was decided to compare predictions based on each of these extremes with the data obtained in this study. Accordingly, the various properties that had been measured were predicted by the method of Gunn and by the unmodified method, in conjunction with the Peng-Robinson equation of state.

B. Determination of Binary Interaction Parameters

Before predictions could be made for the two ternary systems that were studied, the interaction parameters had to be determined for five binary systems. For the hydrogen-n-pentane system these parameters were obtained from the data presented in Chapter IV. For the other binary systems data on vapor-liquid equilibrium compositions were taken from the literature. The single methane-carbon dioxide data point and the few hydrogen-carbon dioxide data points that were taken in this study were not used for the determination of interaction parameters. Instead, the parameters obtained with the literature data were used later to predict these points.

As already shown, the predictive methods are incapable of accurately representing the entire two-phase envelope. Thus a choice had to be made of the features to be emphasized in property prediction. Because the ternary data

to be predicted involved some measurements in the retrograde region, it was decided to fit the binary data so that the lower-pressure portion of the retrograde region was considered together with the data at pressures below the retrograde region. This involved a compromise in accuracy between these two regions, but permitted one to test whether either approach could accommodate the two regions better than the other. However, data in the vicinity of the critical point were excluded.

The binary data were chosen to cover a temperature range as near to the ternary data isotherms as possible. The criterion for best fit was the minimization of per cent standard deviation between predicted and measured compositions. For each data point only the composition of the component in lower concentration was used in the calculations.

The best overall values of k_{ij} , the binary interaction parameter, that were obtained are shown in Table 5 together with the sources and the temperature range of the data. The interaction parameters were found to have a weak temperature dependence in all but one of the instances in which hydrogen was a member of the binary pair. This temperature dependence was expressed as a linear equation, which was found for each pair by least squares fitting of the interaction parameters at different temperatures. The resulting temperature-dependent values of k_{ij} are given by Equations (22) to (26) in which T is the absolute temperature in kelvins, and k_{ij} as the interaction parameter for the indicated binary

Table 5. Temperature-Independent Binary Interaction Parameters for
the Unmodified and the Gunn Approaches for Hydrogen

<u>System</u>	<u>k_{ij} (Unmod.)</u>	<u>k_{ij} (Gunn)</u>	<u>Temp. Range (K)</u>	<u>Sources</u>
H ₂ -CH ₄	0.07	-0.10	91-183	(19, 22)
H ₂ -CO ₂	0.14	-0.42	220-290	(44, 47)
CH ₄ -CO ₂	0.10	(0.10)	230-288	(10, 21, 2)
H ₂ -n-C ₅ H ₁₂	0.34	-0.40	273-373	This work
CO ₂ -n-C ₅ H ₁₂	0.13	(0.13)	278-378	(6)

system:

$$\text{H}_2\text{-CH}_4 \text{ (Unmodified): } k_{ij} = -0.095 + 0.00130T \quad (22)$$

$$\text{(Gunn): } k_{ij} = 0.081 - 0.00166T \quad (23)$$

$$\text{H}_2\text{-CO}_2 \text{ (Unmodified): No temperature dependence}$$

$$\text{(Gunn): } k_{ij} = 0.898 - 0.00547T \quad (24)$$

$$\text{H}_2\text{-n-C}_5\text{H}_{12} \text{ (Unmodified): } k_{ij} = -0.189 + 0.0017T \quad (25)$$

$$\text{(Gunn): } k_{ij} = 0.222 - 0.0021T \quad (26)$$

In conducting the k_{ij} determination for the hydrogen-carbon dioxide system, the data of Spano, Heck and Barrick (42) were excluded after initial consideration, because they disagreed noticeably with the data of the two other investigators.

In determining k_{ij} for the hydrogen-methane binary, the data of Sagara et al. (39) were excluded because the k_{ij} 's were somewhat different from the k_{ij} 's found from the data of other investigators. However, the cause of this difference was not disagreement between the data, but rather that Sagara's data did not extend to the higher pressure regions included in the data from other investigators.

C. Comparison of Prediction Methods

Predictions were made of five types of variables that were available from the data collected for this study:

- a. Equilibrium ratio $K_i (y_i/x_i)$
- b. Bubble point pressure for the liquid phase composition,
- c. Dew point pressure for the vapor phase composition,
- d. Liquid molar volume,

e. Vapor molar volume.

For each of the two approaches to the treatment of hydrogen, predictions were made for both the case of constant k_{ij} (Table 5), and temperature-dependent k_{ij} (Equations (22) to (26)). Thus, a total of four sets of predictions were made. The summarized results are presented in Tables 6 to 10. When examining Tables 6, 7 and 8 one should note that the composition-pressure variables for the hydrogen-n-pentane system are for correlations rather than predictions, because the experimental compositions were used to obtain the binary interaction parameters for this system. The results for all other systems and variables are pure predictions; the experimental data were not used in any way to obtain the calculated values.

The predicted properties of the single methane-carbon dioxide point (6900 kPa, -15.0°C) that was taken are not included in the tables, but are expressed below as per cent difference from the experimental measurements:

K_{CH_4} :	3.2%
K_{CO_2} :	-2.8%
Bubble Point Pressure:	0.3%
Dew Point Pressure:	-7.4%
Liquid Molar Volume:	-2.9%
Vapor Molar Volume:	-2.2%

Only one method of prediction applied to the methane-carbon dioxide point, as the interaction parameter was found to be essentially temperature independent, and the calculation is

Table 6. Average Absolute Per Cent Deviations Between
Experimental and Calculated Equilibrium Ratios

System	Method	No. Points	A.A.D. (%)			
			H ₂	CH ₄	CO ₂	n-C ₅ H ₁₂
H ₂ -CO ₂	Gunn (a)	6	8.5	-	5.7	-
	Gunn (b)	6	9.7	-	3.1	-
	Unmodified (a)	6	10.4	-	1.7	-
H ₂ -n-C ₅ H ₁₂	Gunn (a)	31	3.9	-	-	7.7
	Gunn (b)	31	4.7	-	-	7.1
	Unmodified (a)	31	9.8	-	-	4.4
	Unmodified (b)	31	5.1	-	-	5.8
H ₂ -CH ₄ -CO ₂	Gunn (a)	31	15.8	5.6	6.6	-
	Gunn (b)	31	12.8	5.3	5.6	-
	Unmodified (a)	31	10.8	5.8	4.1	-
	Unmodified (b)	31	11.7	5.3	4.4	-
H ₂ -CO ₂ -n-C ₅ H ₁₂	Gunn (a)	25	8.2	-	4.4	9.3
	Gunn (b)	25	9.7	-	6.3	7.7
	Unmodified (a)	25	10.0	-	7.8	7.2
	Unmodified (b)	25	10.2	-	8.0	6.1
Combined Ternaries	Gunn (a)	56	12.4	-	5.9	-
	Gunn (b)	56	11.4	-	5.9	-
	Unmodified (a)	56	10.4	-	5.8	-
	Unmodified (b)	56	11.0	-	6.0	-

Table 7. Average Absolute Per Cent Deviations Between
Experimental and Calculated Bubble Point Pressures

<u>System</u>	<u>Method</u>	<u>No. Points</u>	<u>A.A.D. (%)</u>
H ₂ -CO ₂	Gunn (a)	6	5.9
	Gunn (b)	6	7.9
	Unmodified (a)	6	7.7
H ₂ -n-C ₅ H ₁₂	Gunn (a)	32	4.2
	Gunn (b)	32	5.0
	Unmodified (a)	32	10.6
	Unmodified (b)	32	5.7
H ₂ -CH ₄ -CO ₂	Gunn (a)	31	7.0
	Gunn (b)	31	6.3
	Unmodified (a)	31	6.1
	Unmodified (b)	31	6.2
H ₂ -CO ₂ -n-C ₅ H ₁₂	Gunn (a)	26	4.6
	Gunn (b)	26	5.2
	Unmodified (a)	26	7.1
	Unmodified (b)	26	5.8
Combined Ternaries	Gunn (a)	57	5.9
	Gunn (b)	57	5.8
	Unmodified (a)	57	6.6
	Unmodified (b)	57	6.0

Table 8. Average Absolute Per Cent Deviations Between
Experimental and Calculated Dew Point Pressures

<u>System</u>	<u>Method</u>	<u>Convergent Points</u>	<u>A.A.D. (%)</u>
H ₂ -CO ₂	Gunn (a)	7	11.7
	Gunn (b)	7	8.3
	Unmodified (a)	7	5.3
H ₂ -n-C ₅ H ₁₂	Gunn (a)	30	11.6
	Gunn (b)	32	11.1
	Unmodified (a)	32	7.5
	Unmodified (b)	30	9.5
H ₂ -CH ₄ -CO ₂	Gunn (a)	29	16.4
	Gunn (b)	30	14.0
	Unmodified (a)	26	10.2
	Unmodified (b)	26	11.3
H ₂ -CO ₂ -n-C ₅ H ₁₂	Gunn (a)	24	23.5
	Gunn (b)	24	19.2
	Unmodified (a)	22	19.6
	Unmodified (b)	20	13.4
Combined Ternaries	Gunn (a)	53	19.6
	Gunn (b)	54	16.4
	Unmodified (a)	48	14.5
	Unmodified (b)	46	12.2

Table 9. Average Absolute Per Cent Deviations Between
Experimental and Calculated Liquid Molar Volumes

<u>System</u>	<u>Method</u>	<u>No. Points</u>	<u>A.A.D. (%)</u>
H ₂ -CO ₂	Gunn (a)	6	3.0
	Gunn (b)	6	2.6
	Unmodified (a)	6	2.2
H ₂ -n-C ₅ H ₁₂	Gunn (a)	29	2.3
	Gunn (b)	29	2.3
	Unmodified (a)	29	2.1
	Unmodified (b)	29	2.0
H ₂ -CH ₄ -CO ₂	Gunn (a)	27	7.1
	Gunn (b)	27	6.9
	Unmodified (a)	27	6.6
	Unmodified (b)	27	6.5
H ₂ -CO ₂ -n-C ₅ H ₁₂	Gunn (a)	25	2.0
	Gunn (b)	25	2.0
	Unmodified (a)	25	2.0
	Unmodified (b)	25	2.0
Combined Ternaries	Gunn (a)	52	4.6
	Gunn (b)	52	4.5
	Unmodified (a)	52	4.4
	Unmodified (b)	52	4.3

Table 10. Average Absolute Per Cent Deviations Between
Experimental and Calculated Vapor Molar Volumes

<u>System</u>	<u>Method</u>	<u>No. Points</u>	<u>A.A.D. (%)</u>
H ₂ -CO ₂	Gunn (a)	7	1.6
	Gunn (b)	7	2.1
	Unmodified (a)	7	4.9
H ₂ -n-C ₅ H ₁₂	Gunn (a)	21	2.5
	Gunn (b)	21	2.5
	Unmodified (a)	21	3.8
	Unmodified (b)	21	3.7
H ₂ -CH ₄ -CO ₂ (Cold Cell)	Gunn (a)	18	5.2
	Gunn (b)	18	6.1
	Unmodified (a)	18	9.0
	Unmodified (b)	18	7.7
H ₂ -CH ₄ -CO ₂ (Warm Cell)	Gunn (a)	11	3.2
	Gunn (b)	11	2.8
	Unmodified (a)	11	4.2
	Unmodified (b)	11	3.7
H ₂ -CO ₂ -n-C ₅ H ₁₂	Gunn (a)	24	1.8
	Gunn (b)	24	2.0
	Unmodified (a)	24	3.8
	Unmodified (b)	24	3.8
Combined Ternaries	Gunn (a)	53	3.4
	Gunn (b)	53	3.6
	Unmodified (a)	53	5.6
	Unmodified (b)	53	5.1

not affected by the method for treatment of hydrogen.

The results for the hydrogen-carbon dioxide data points were included in the tables even though there were only three or four points at each of the temperatures, -15.0 and 0.0°C . This temperature difference is too small to identify any influence of temperature upon the predictions. For the other systems there was a larger difference between isotherms. The actual temperatures and the distribution of points between them are given in Chapter IV and in Appendix C. Within each system, approximately the same number of data points were taken at each temperature.

In Tables 6 to 10 "Gunn (a)" and "Unmodified (a)" refer to the use of the constant binary interaction parameters from Table 5, and "Gunn (b)" and "Unmodified (b)" refer to the use of the temperature-dependent interaction parameters from Equations (22) to (26).

The results presented in Table 8 for the accuracy of the different methods for dew point pressure prediction are somewhat misleading, because convergence could not be obtained for all the data points. In the cases of failure the cause was that only a single phase was predicted for the experimental composition and temperature, regardless of the pressure. When the system temperature was reduced by a few degrees, or the composition was changed slightly, convergence often became possible. However, the predicted dew point pressures for such points were always greatly in error, and the methods that converged more reliably had higher average

errors as a consequence.

It was often uncertain whether an experimental condition represented a normal or retrograde dew point. When both types of dew points were predicted to exist, the one nearest to the experimental pressure was chosen.

With regard to the molar volumes of the equilibrium phases (Tables 9 and 10) the predicted values were usually too small for both the vapor and liquid phases. For the hydrogen-methane-carbon dioxide system the predicted liquid molar volumes were somewhat better at -15.0°C than at -45.8°C . The molar volumes for this system were generally not predicted as well as for the hydrogen-carbon dioxide-n-pentane system.

The predictions could be used also as a test of the consistency of molar volumes obtained from the two sets of equipment. As pointed out previously, the 13 800 kPa isobar for the hydrogen-methane-carbon dioxide system at -15.0°C was studied over the entire concentration range on both the cold cell and the warm cell. For consistent results, the average deviations between prediction and experiment should be nearly the same for two sets of data for this isobar.

When the test was applied to the vapor volumes, a 5 to 6% disagreement between the data from the two cells was found. The molar volumes obtained from the cold cell were consistently smaller than those from the warm cell. The difference is believed to have resulted from the unusually

severe optical distortion that was experienced during measurement of vapor refractive indices with the cold cell. The distortion arose from the chipping and cracking of the high pressure window that was used for vapor phase observation. This accounts also for the unusually large A.A.D. between predictions and the cold cell data, as can be seen from Table 10.

For liquid molar volumes the agreement between the data from the two cells was within 1%. Similarly, excellent consistency was observed for the equilibrium ratios and the bubble point pressures. The latter implies consistency of liquid and vapor compositions. The failure of the various methods to predict dew points for all of the vapor compositions made the comparison of dew point predictions to be of little value for consistency tests.

The differences between the accuracy of the Gunn and the unmodified approaches to prediction of hydrogen systems were small and varied with the property being predicted. The unmodified approach was slightly better for predicting equilibrium ratios and liquid volumes. The approach of Gunn, Chueh and Prausnitz was slightly more accurate for predicting bubble point pressures and vapor volumes, and was also able to predict the existence of the dew point more reliably. However, the prediction of dew point pressures was inaccurate for either method. Also, for both methods the predicted equilibrium ratios for hydrogen were considerably less accurate than for the other components.

In general, neither approach for the treatment of hydrogen parameters was clearly more accurate than the other.

Overall, the use of temperature dependence in the binary interaction parameters provided almost no advantage for the systems that were studied. Very little improvement was obtained in the correlation of the equilibrium ratios for the hydrogen-n-pentane system. For the other systems the variable interaction parameters provided no consistent improvement for the prediction of either equilibrium ratios or bubble point pressures. For the volumetric predictions, a very small reduction of errors was observed with either approach.

D. Discussion

Several generalizations can be drawn from the results of the predictions and preliminary tests. Firstly, methods of predicting vapor-liquid equilibrium compositions with the Peng-Robinson equation of state are substantially less accurate for hydrogen than for most other light, non-polar or slightly polar materials. The poorer accuracy occurs even when special provisions are made for hydrogen. While this study did not include materials with molecular weights greater than that of pentane, poorer accuracy for hydrogen in systems of heavier compounds has been noted frequently in the literature for a variety of prediction methods. In view of the poorer accuracy reported also for other cubic equations of state (14, 26, 44), it appears that the difficulty with hydrogen is common to most cubic equations.

Secondly, hydrogen does not conform to the same three-parameter corresponding states rule that was originally advanced by Pitzer for low molecular weight, non-polar gases and liquids. This was demonstrated by the difficulty encountered in all of the efforts to match hydrogen densities with densities from corresponding states tables. (The relatively poor accuracy of predictive methods is further evidence). The disagreement was greater in the critical region, but was obvious at other conditions as well.

Thirdly, it is probably more realistic to assign hydrogen a negative acentric factor that is far from zero. This is based on the observation that the use of the experimentally determined acentric factor of -0.22 , together with the experimental values for T_c and P_c , lead to correlations and predictions that are nearly as accurate as those with an acentric factor of zero and effective, temperature-dependent values for T_c and P_c . It is possible that an acentric factor somewhat different from -0.22 might be better if quantum effects could be accounted for accurately.

Finally, within the accuracy afforded by the corresponding states tables of Chao and Greenkorn, significant influences of quantum effects upon the density of hydrogen occur only at temperatures below 25 or 30 K. This implies that quantum corrections are not necessary for reduced temperatures of hydrogen that are substantially above 1. Furthermore, attempts to explain the difference in behavior between quantum gases and other gases at supercritical

conditions are apt to be unsuccessful if they rely solely upon quantum mechanical corrections.

The question that remains is how to describe the unique behavior of quantum gases for purposes of accurate property prediction. Only broad guidelines appear to be available. It is the author's opinion that corrections to the procedures for calculating the constants in cubic equations of state are not likely to be successful. Changes to the equation model appear to be more promising. The modification of Van der Waals-type equations to incorporate terms that are fourth order or perhaps even fifth order in volume may be necessary for an accurate description of fluid behavior. Such a change would unfortunately destroy the computationally desirable cubic nature of such equations, and might require new methods to calculate any additional constants that would appear in the equation.

VI - CONCLUSIONS

A. Vapor-Liquid Equilibrium Data

Experimental measurements were made of the equilibrium compositions and refractive indices of the following binary and two ternary systems, for which no extensive information has previously appeared in the literature.

Measurements for the hydrogen-n-pentane binary system were made at pressures from 350 to 27 600 kPa for the 273.2, 323.2 and 373.2 K isotherms.

Measurements of the same variables were made for the hydrogen-methane-carbon dioxide system at the 227.4 K isotherm, at which the 6900, 13 800 and 20 600 kPa isobars were studied; and at the 258.2 K isotherm, at which the 6900, 13 700 and 27 600 kPa isobars were studied.

Similarly, measurements were made of the hydrogen-carbon dioxide-n-pentane system at the 273.2 and 323.2 K isotherms, at which the 6900, 13 800 and 27 600 kPa isobars were studied.

For all three of the above systems, the molar volumes of both of the co-existing phases were calculated from the experimental refractive indices and compositions.

B. Predictions with Cubic Equations of State

The vapor-liquid equilibrium properties of systems that contain hydrogen in combination with lower alkanes and carbon dioxide cannot be predicted as accurately as similar systems that do not include hydrogen when an equation of state from the Van der Waals family is employed.

The use of temperature-dependent binary interaction parameters provides no significant improvement over constant interaction parameters for binary pairs that involve hydrogen with carbon dioxide or a light alkane.

The acentric factor of hydrogen should be assigned a value in the neighborhood of -0.22 in order for predicted properties to be in best accord with correlations based on the acentric factor, and to minimize the need for special corrections to the other parameters used for hydrogen.

REFERENCES

1. Anderson, T. F., and Prausnitz, J. M., Ind. Eng. Chem., Process Des. Dev., 1980, 19, 9.
2. Arai, Y., Kaminishi, G., and Saito, S., J. Chem. Eng. of Japan, 1971, 4, 113.
3. Bender, E., Proc. 5th Symp. Thermophys. Prop., ASME, New York, 1970, 227.
4. Benedict, M., Webb, G. B., and Rubin, L. C., Chem. Eng. Prog., 1951, 47, 419.
5. Besserer, G. J., "The Use of Refractive Index Measurements in High Pressure Vapor-Liquid Equilibrium Studies" 1972, Ph. D. Dissertation in Chemical Engineering, University of Alberta.
6. Besserer, G. J., and Robinson, D. B., J. Chem. Eng. Data, 1973, 18, 416.
7. Boston, J. F., and Mathias, P. M., EFCE Publ. Ser. 11 (Phase Equilib. Fluid Prop. Chem. Ind., Proc., Part 2), 1980, 821.
8. Chao, K. C., and Greenkorn, R. A., "Thermodynamics of Fluids - An Introduction to Equilibrium Theory", 1975, Marcel Dekker Inc., New York, New York, Appendix B, 297-313.
9. Chao, K. C., and Seader, J. D., AIChE J., 1961, 7, 598.
10. Davalos, J., Anderson, W. R., Phelps, R. E., and Kidnay, A. J., J. Chem. Eng. Data, 1976, 21, 81.
11. Diller, D. E., J. Chem. Phys., 1968, 49, 3096.
12. El-Twaty, A. I., and Prausnitz, J. M., Chem. Eng. Sci., 1980, 35, 1765.
13. Frohlich, P. K., Tauch, E. J., Hogan, J. J., and Peer, A. A., Ind. Eng. Chem., 1931, 23, 548.
14. Graboski, M. S., and Daubert, T. E., Ind. Eng. Chem. Process Des. Dev., 1979, 18, 300.
15. Grayson, H. G., and Streed, C. W., Sixth World Petroleum Congress, June 1963, Paper 20, Section VII, Frankfurt, Germany.
16. Gunn, R. D., Chueh, P. L., and Prausnitz, J. M., AIChE J., 1966, 12, 937.

17. Harmens, A., "A Three-Parameter Cubic Equation of State for Normal Fluids", Ph. D. Dissertation, 1980, Technical University of Berlin.
18. Harmens, A., EFCE Publ. Ser. 11 (Phase Equilib. Fluid Prop. Chem. Ind., Proc. Part 2), 1980, 379.
19. Hong, J. H., and Kobayashi, R., J. Chem. Eng. Data, 1981, 26, 127.
20. Kalra, H., and Robinson, D. B., Cryogenics, 1975, 15, 409.
21. Kaminishi, G., Arai Y., Saito, S., and Maeda, S., J. Chem. Eng. Japan, 1968, 1, 109.
22. Kirk, B. S., and Ziegler, W. T., Advan. Cryog. Eng., 1965, 10, 160.
23. Klink, A. E., Cheh, H. Y., and Amick, E. H. Jr., AIChE J., 1975, 21, 1142.
24. Lee, B. I., and Kesler, M. G., AIChE J., 1975, 21, 510.
25. Leland, T. W., EFCE Publ. Ser. 11 (Phase Equilib. Fluid Prop. Chem. Ind., Proc., Part 2), 1980, 283.
26. Lin, H. M., Ind. Eng. Chem. Process Des. Dev., 1980, 19, 501.
27. Lin, C. J., and Hopke, S. W., "Application of the BWRS Equation to Methane, Ethane, Propane, and Nitrogen Systems", paper presented at the 74th National AIChE Meeting, March 1973, New Orleans.
28. McCarthy, R. D., "Hydrogen Technological Survey - Thermophysical Properties", 1975, Scientific and Technical Information Office, National Aeronautics and Space Administration, Washington, D. C.
29. Mollerup, J., EFCE Publ. Ser. 11 (Phase Equilib. Fluid Prop. Chem. Ind., Proc., Part 2), 1980, 963.
30. Moshfeghian, M., Shariat, A., and Erbar, J. H., "Thermodyn. Aqueous Syst. Ind. Appl.", ACS Symp. Ser., 1980, 133, 333.
31. Olson, J. D., J. Chem. Phys., 1975, 63, 474.
32. Peck, E. R., and Huang, S., J. Opt. Soc. Am., 1977, 67, 1550.
33. Peng, D. Y., and Robinson, D. B., Ind. Eng. Chem. Fundam., 1976, 15, 59.

34. Pitzer, K. S., Lippmann, D. Z., Curl, R. F. Jr., Huggins, C. M., and Petersen, D. E., J. Am. Chem. Soc., 1955, 77, 3433.
35. Plöcker, U., Knapp, H., and Prausnitz, J. M., Ind. Eng. Chem. Proc. Des. Dev., 1978, 17, 324.
36. Redlich, O., and Kwong, J. N. S., Chem. Rev., 1949, 44, 233.
37. Rosenfeld, Y., J. Chem. Phys., 1980, 73, 5760.
38. Rosenfeld, Y., and Thieberger, R., Phys. Rev. A., 1977, 15, 1269.
39. Sagara, H., Arai, Y., and Saito, S., J. Chem. Eng. Japan, 1972, 5, 13.
40. Sebastian, H. M., Lin, H. M., and Chao, K. C., AIChE J., 1981, 27, 138.
41. Soave, G., Chem. Eng. Sci., 1972, 27, 1197.
42. Spano, J. O., Heck, C. K., and Barrick, P. L., J. Chem. Eng. Data, 1968, 13, 168.
43. Starling, K. E., "Applications of Multiproperty Analysis in Equation of State Development and Thermodynamic Property Prediction", Proc. 49th Annual NGPA Convention, March 1970, Denver.
44. Tsang, C. Y., and Streett, W. B., Chem. Eng. Sci., 1981, 36, 993.
45. Tsonopoulos, C., and Prausnitz, J. M., Cryogenics, 1969, 9, 315.
46. Watson, H. E., and Ramaswamy, K. L., Proc. Roy. Soc. A., 1936, 156, 144.
47. Yorzane, M., Asahi Garasu Kogyo Gijutsu Shoreikai Kenkyu Hokoku, 1971, 18, 61.
48. Yorzane, M., Yoshimura, S., and Masuoka, H., Bull. Jap. Petrol. Inst., 1972, 14, 105.

APPENDIX A

THERMOCOUPLE AND PRESSURE GAUGE CALIBRATIONS

A. Thermocouples

The thermocouple calibration data are presented in Tables A-1 and A-2. The data were smoothed by least-squares fitting to cubic equations, and the equations were subsequently used to determine the experimental temperatures. Equation (A-1) was used for the cold cell thermocouple, and Equation (A-2) was used for the warm cell thermocouple. For these equations, T is the temperature in degrees Celsius and V is the thermocouple output in millivolts.

$$T = 0.9521V^3 - 0.8869V^2 + 26.0168V + 0.107 \quad (\text{A-1})$$

$$T = 0.01011V^3 - 0.2345V^2 + 19.9196V + 0.173 \quad (\text{A-2})$$

The maximum absolute disagreement between Equation (A-1) and the calibration was 0.137°C , and the standard deviation was 0.052°C . For Equation (A-2) the corresponding values were 0.052°C and 0.028°C .

Table A-1. Thermocouple Calibration for the Lower-Temperature Equilibrium Cell

Thermocouple Output (mV)	Platinum Resistance Thermometer Temperature (°C)
0.986	25.00
0.979	24.82
0.307	7.97
0.008	0.32
-0.426	-11.10
-0.652	-17.29
-0.654	-17.34
-0.990	-26.60
-1.324	-36.08
-1.678	-46.45
-2.080	-58.77
-2.137	-60.42
-2.148	-60.95
-2.430	-69.68
-2.610	-75.49

Table A-2. Thermocouple Calibration for the Higher-Temperature Equilibrium Cell

Thermocouple Output (mV)	Platinum Resistance Thermometer Temperature (°C)
-0.902	-18.00
-0.901	-17.98
-0.889	-17.73
-0.802	-15.98
-0.646	-12.79
-0.329	- 6.39
-0.326	- 6.34
0.413	8.36
0.414	8.42
0.963	19.18
0.978	19.47
1.066	21.14
1.067	21.15
1.109	21.99
1.967	38.51
2.394	46.62
2.491	48.50
2.596	50.45
2.686	52.22
2.749	53.40
3.008	58.23
3.198	61.77
3.215	62.08
3.353	64.70
3.378	65.15
3.510	67.65
3.634	69.95
4.206	80.60
4.774	91.06
5.761	109.12
6.569	123.72
7.341	137.77
7.352	137.97

B. Pressure Gauges

(Units for pressure gauge calibrations are pounds per square inch.)

TABLE A-3. Calibration of 13 800 kPa Pressure Gauge

PRESSURE CALIBRATION			
CPE NO.	1367	MANUFACTURER	Heise
SER. NO.	C-28831-R	ITEM	Gauge
DATE	78-9-22	RANGE	0-2000
WETTED PARTS	316	ACCURACY	0.150 FS
CALIBRATED BY	DS	TESTING INST.	Ruska

CALIBRATOR	P INCREASE	P DECREASE
0	-	0
210	-	210
410	-	412
610	-	612
810	-	812
1010	-	1012
1210	-	1212
1410	-	1412
1610	-	1671
1810	-	1811
1910	-	-

REMARKS

TABLE A-4. Calibration of 20 700 kPa Pressure Gauge

PRESSURE CALIBRATION			
CPE NO.	2067	MANUFACTURER	Heise
SER. NO.	H-39686	ITEM	Gauge
DATE	Nov 27/77	RANGE	0-3000 psi
WETTED PARTS	316 SS	ACCURACY	+ .1% FS
CALIBRATED BY	R.H.	TESTING INST.	Ruska
CALIBRATOR	P INCREASE	P DECREASE	
0	-	-	
200	-	-	
400	-	-	
600	-	-	
800	-	-	
1200	1197	1205	
1500	-	1505	
1800	-	1807	
2100	-	2106	
2400	-	2406	
2700	-	2706	
3000	-	-	
REMARKS	All pressures \pm .1% F.S. indicated		

TABLE A-5. Calibration of 34 500 kPa Pressure Gauge

PRESSURE CALIBRATION			
CPE NO.	2828	MANUFACTURER	Heise
SER. NO.	C-63479	ITEM	Gauge
DATE	Apr. 23/77	RANGE	0-5000 psi
WETTED PARTS	216 SS	ACCURACY	0-3000 .1%
CALIBRATED BY	R.G.H.	TESTING INST.	3000↑ .5% Ruska

CALIBRATOR	P. INCREASE		P. DECREASE	
0	-		0	0
250	-		250%	.05%
750	-		752.5	.05%
1250	-		1255	.1%
1750	-		1755	.1%
2500	-		2510	.2%
3000	-		3010	.2%
3500	-		3510	.2%
4000	-		4005	.1%
4500	4447.5	.05%	4505	.1%
5000				
REMARKS				

TABLE A-6. Calibration of 2070 kPa Pressure Gauge

81-09-21	Heise Gauge	0-300 PSI
<u>D.W.G.</u>		<u>GAUGE</u>
0		0
46		45.6
106		105.6
146		-
186		-
206		-
246		-
286		-

Errors equal to or greater than .3 PSI are indicated

Don. S.

APPENDIX B

GAS CHROMATOGRAPH CALIBRATIONS

A. The Hydrogen-Methane-Carbon Dioxide System on the Lower-Temperature Equipment

The following equations were used to represent the calibrations of peak area A in terms of the change in pressure transducer output V from zero absolute pressure (A is in arbitrary units, and V is in volts):

Methane in nitrogen carrier:

$$A = -13.532V^4 + 177.25V^3 - 944.44V^2 + 15\,811.1V \quad (B-1)$$

Methane in helium carrier:

$$A = -10.909V^2 + 2761.15V \quad (B-2)$$

Hydrogen:

$$A = 76.147V^4 - 822.01V^3 + 962.28V^2 + 61\,832.2V \quad (B-3)$$

Carbon dioxide:

$$A = -2.965V^2 + 3843.69V \quad (B-4)$$

These equations are represented by the solid lines in Figures 11 to 14. The individual calibration points are presented as square symbols.

The pressure transducer calibration was represented by the cubic equation:

$$P = 0.000626V^3 - 0.0412V^2 + 71.675V \quad (B-5)$$

where P is pressure in mm of mercury at 0°C. It is shown as the lower solid line in Figure 15.

B. The Hydrogen-Methane-Carbon Dioxide System on the Higher-Temperature Equipment

The following equations were used to represent the

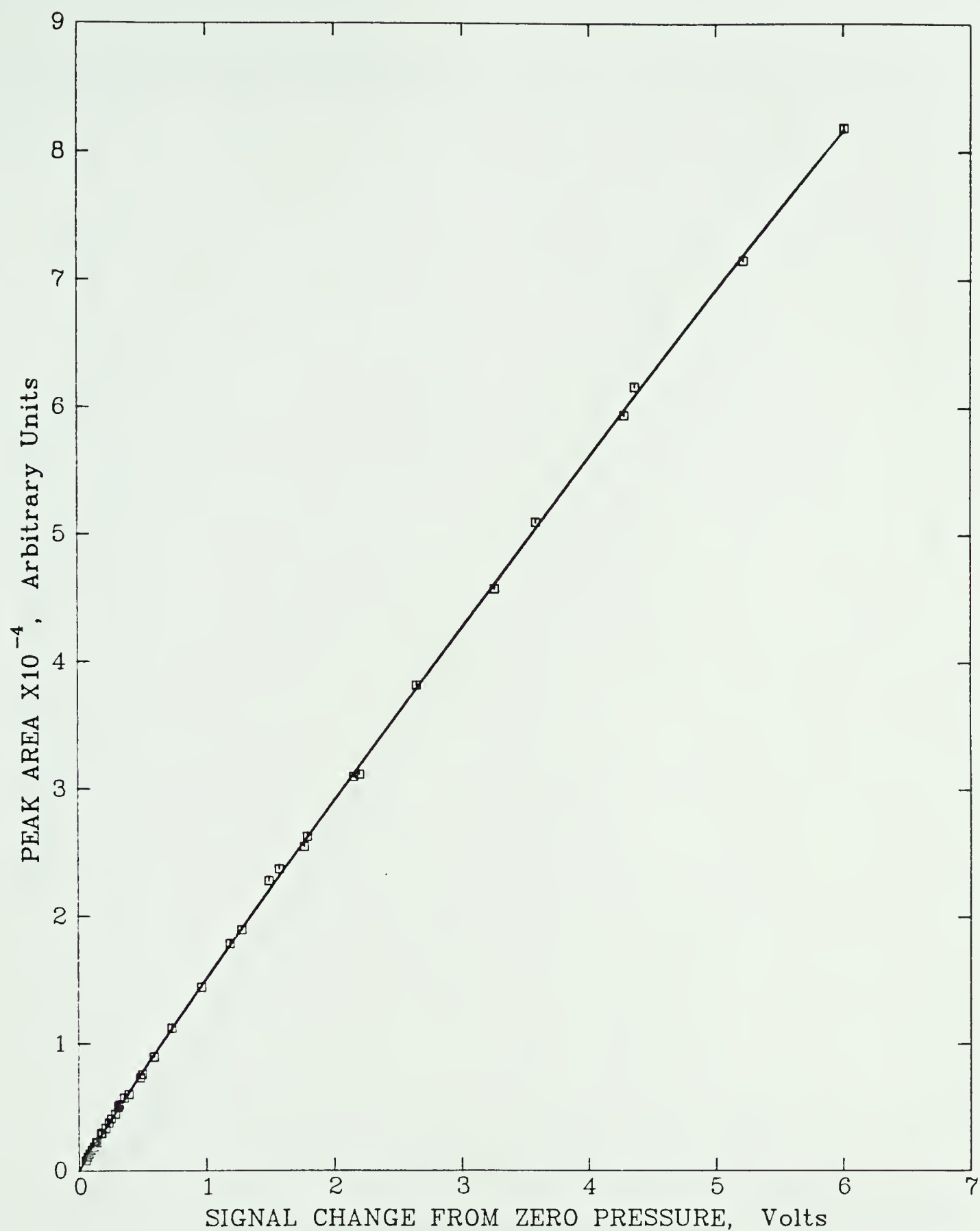


FIG. 11 CHROMATOGRAPH CALIBRATION — RELATIONSHIP BETWEEN PEAK AREA AND TRANSDUCER SIGNAL FOR METHANE IN NITROGEN CARRIER GAS

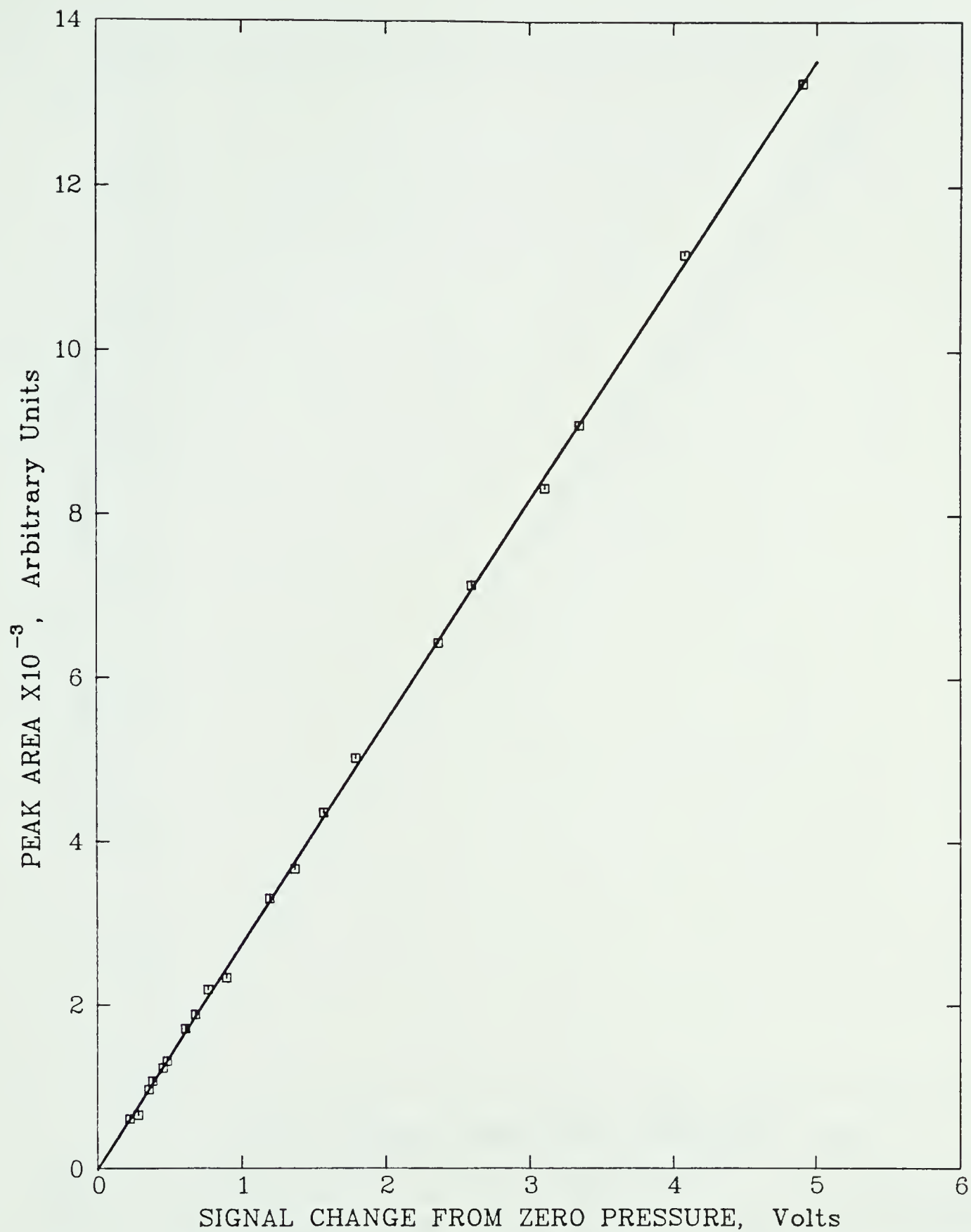


FIG. 12 CHROMATOGRAPH CALIBRATION — RELATIONSHIP BETWEEN PEAK AREA AND TRANSDUCER SIGNAL FOR METHANE IN HELIUM CARRIER GAS

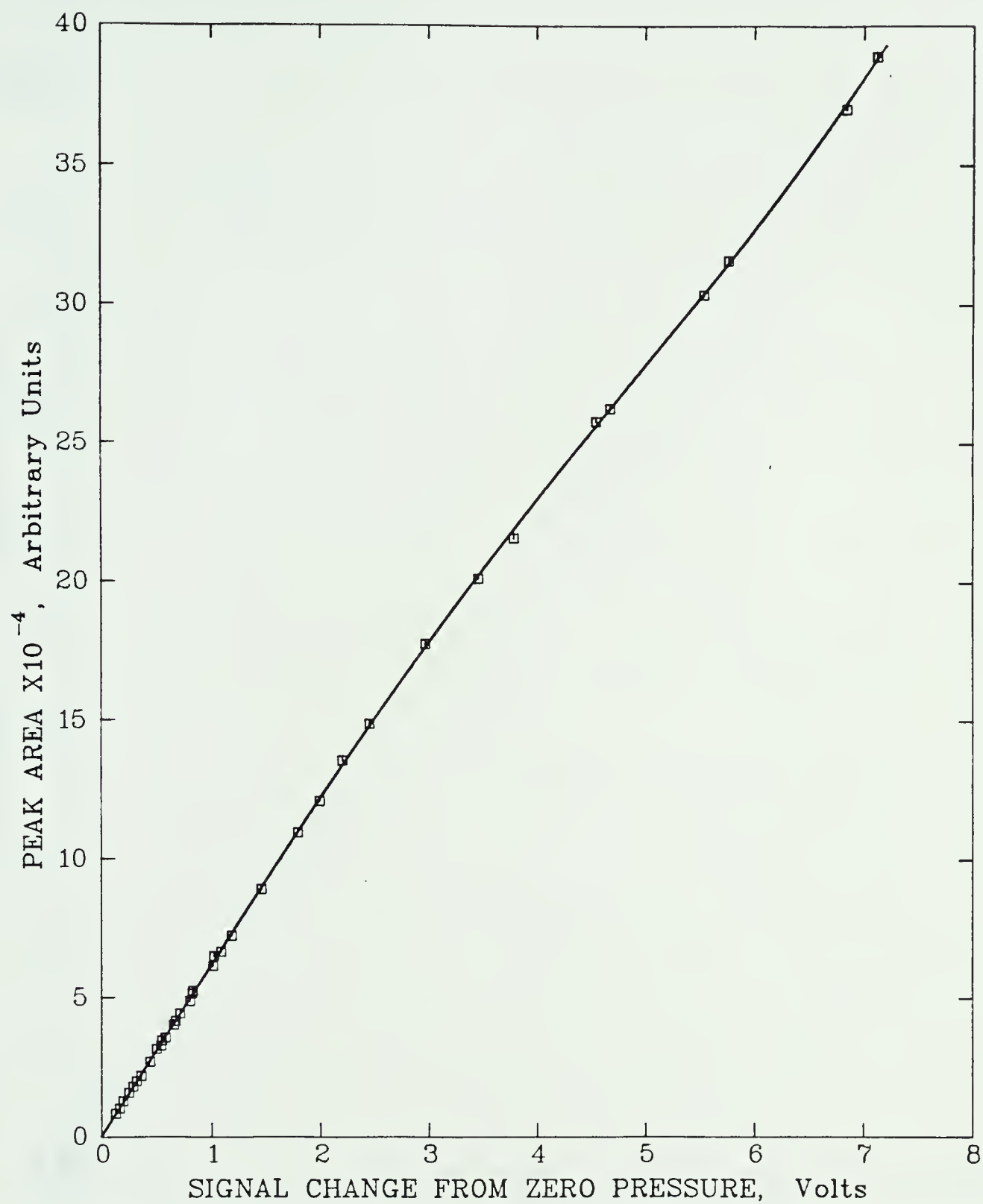


FIG. 13 CHROMATOGRAPH CALIBRATION — RELATIONSHIP BETWEEN PEAK AREA AND TRANSDUCER SIGNAL FOR HYDROGEN IN NITROGEN CARRIER GAS

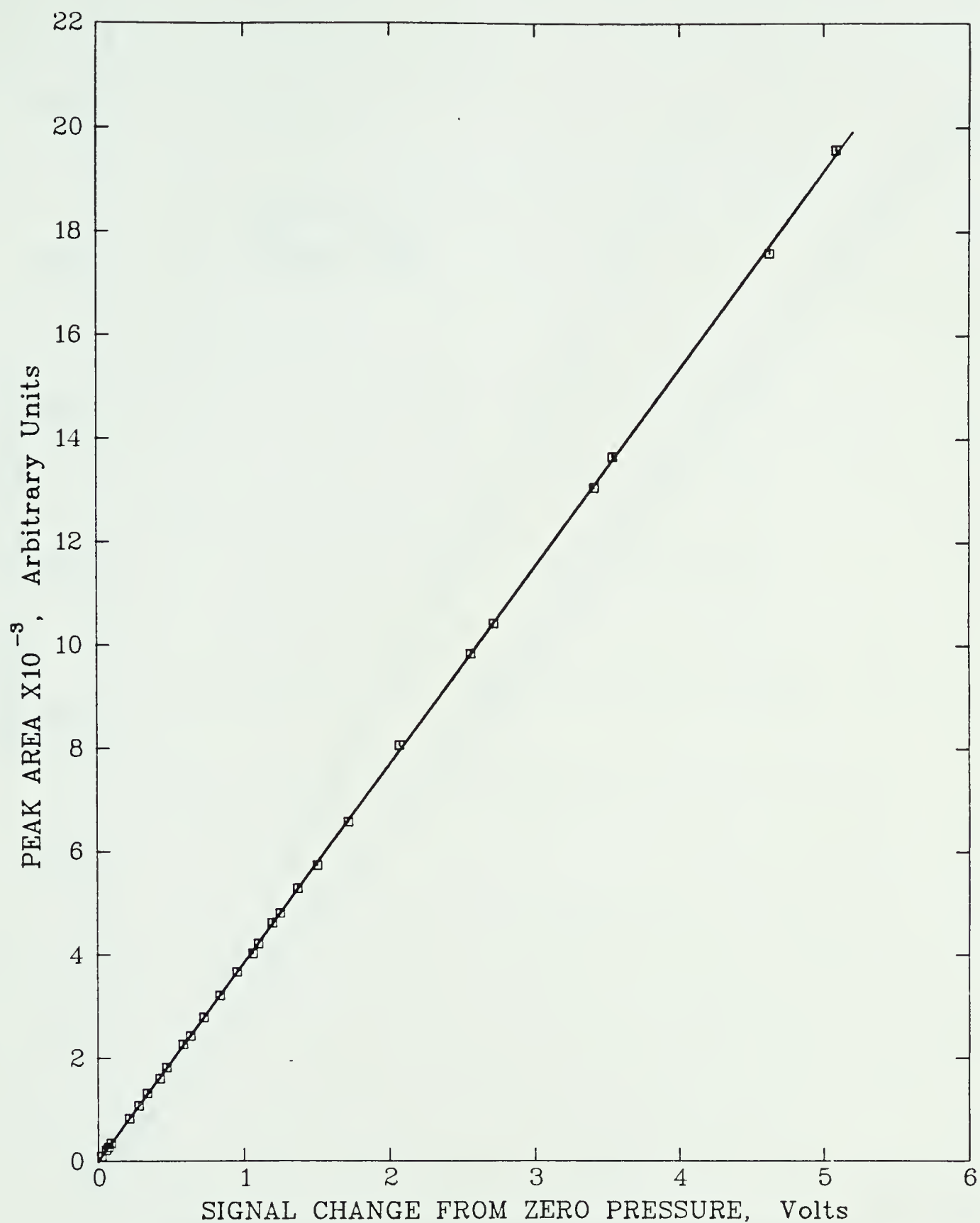


FIG. 14 CHROMATOGRAPH CALIBRATION — RELATIONSHIP BETWEEN PEAK AREA AND TRANSDUCER SIGNAL FOR CARBON DIOXIDE IN HELIUM CARRIER GAS

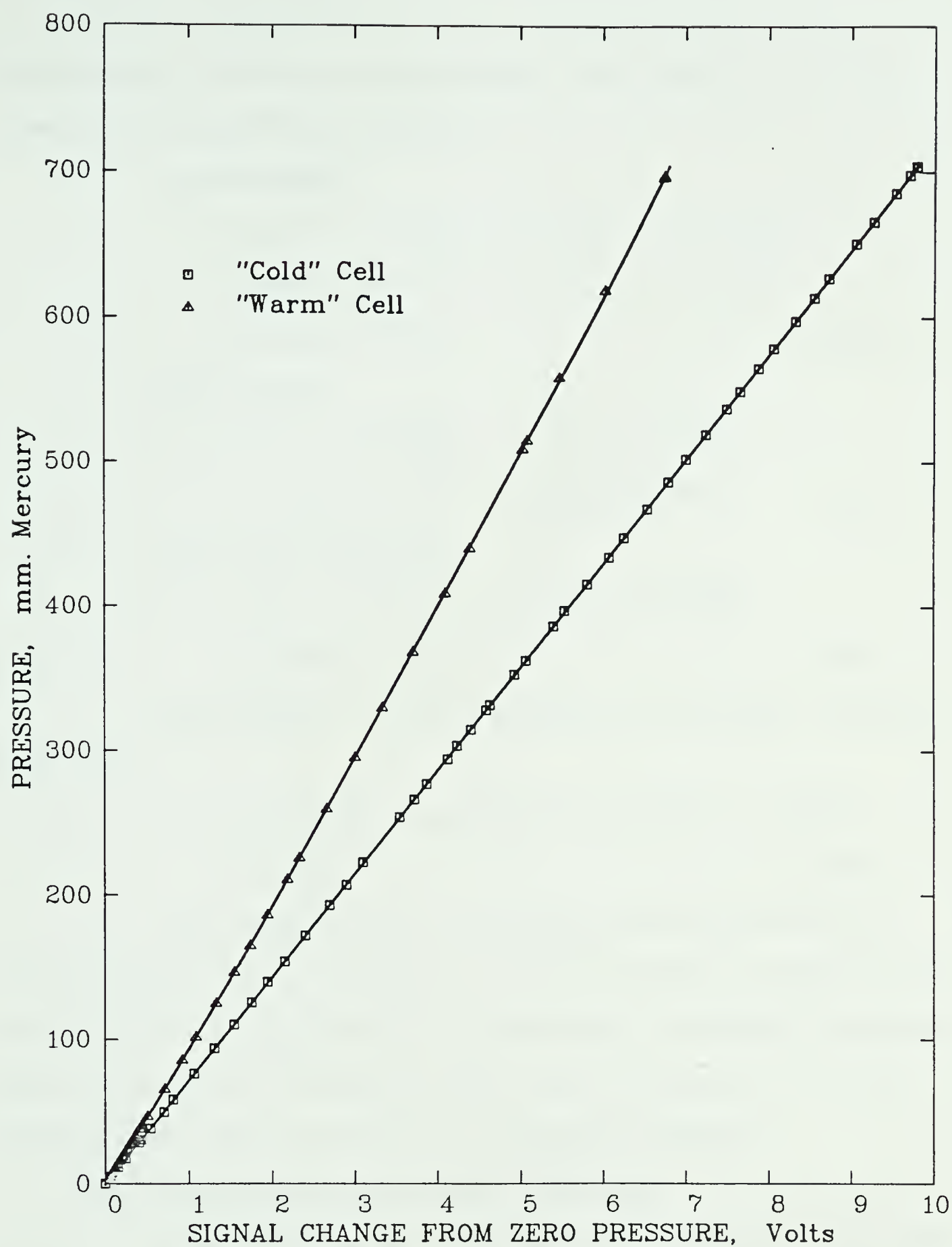


FIG. 15 CALIBRATION OF THE PRESSURE TRANSDUCERS

calibrations for use in calculation (the symbols are as defined in the previous section):

For hydrogen:

$$V = -9.254 \times 10^{-32} A^5 + 4.7997 \times 10^{-25} A^4 \\ - 8.852 \times 10^{-19} A^3 + 1.0097 \times 10^{-12} A^2 \\ + 2.734 \times 10^{-6} A \quad (B-6)$$

For methane:

$$V = 7.130 \times 10^{-24} A^4 - 6.595 \times 10^{-18} A^3 \\ + 1.504 \times 10^{-12} A^2 + 1.286 \times 10^{-5} A \quad (B-7)$$

For carbon dioxide:

$$V = 1.246 \times 10^{-16} A^3 - 1.876 \times 10^{-11} A^2 \\ + 5.2047 \times 10^{-5} A \quad (B-8)$$

The equation for the pressure transducer calibration was:

$$P = 0.032665V^5 - 0.49003V^4 + 2.3026V^3 - 1.786V^2 \\ + 93.53V \quad (B-9)$$

The equations for the peak area of each of the three components are shown as the solid lines in Figures 16 to 18, and the equation for the pressure transducer calibration is shown as the upper solid line in Figure 15. The calibration data are shown as triangular symbols.

C. The Systems Containing n-Pentane

A calibration was obtained using only the analyses of mixtures of known compositions. It was found that the relationship between peak areas could be expressed by the equation:

$$A_1 (x_2/x_1) = aA_2 + bA_2^2 \quad (B-10)$$

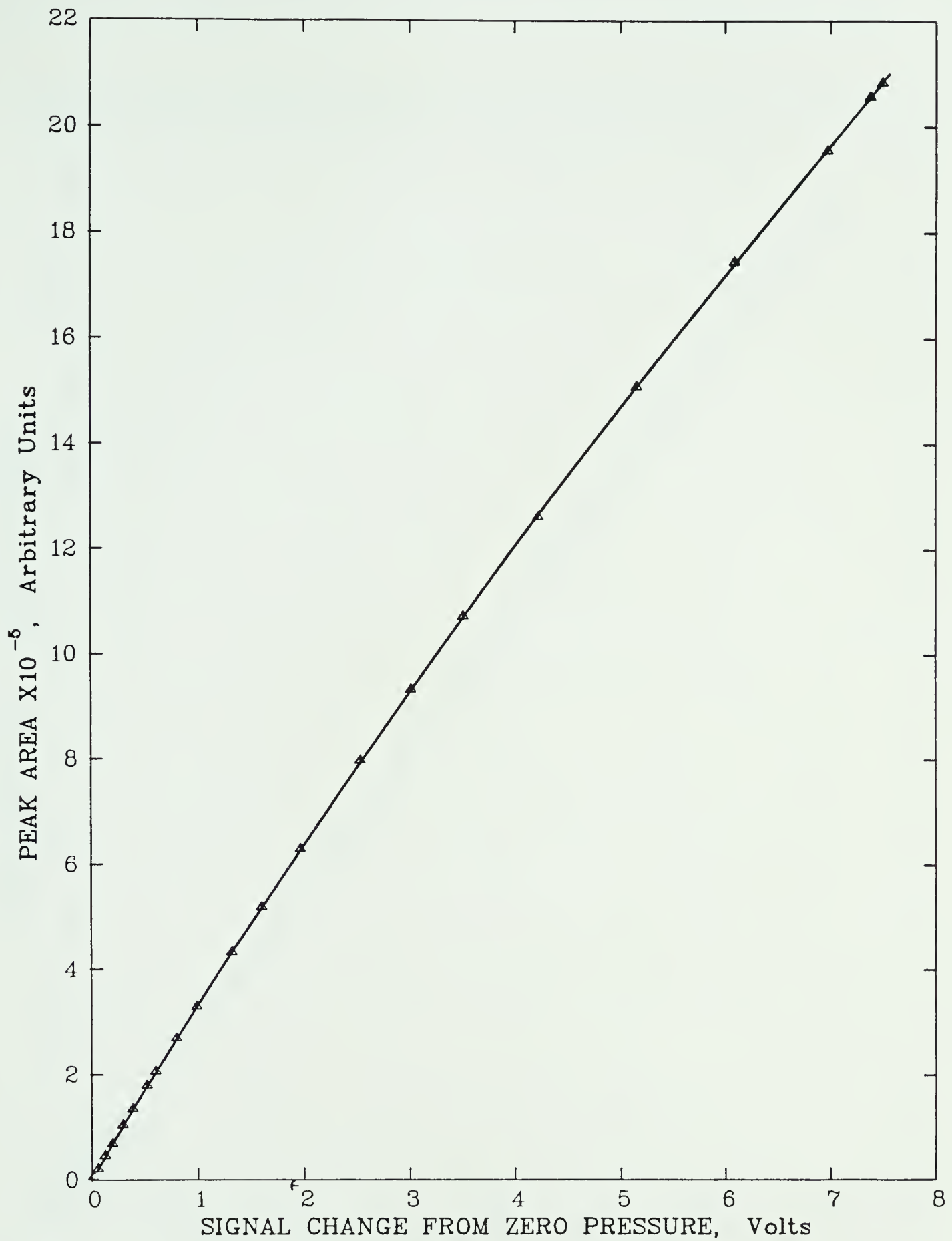


FIG. 16 CHROMATOGRAPH CALIBRATION — RELATIONSHIP BETWEEN PEAK AREA AND TRANSDUCER SIGNAL FOR HYDROGEN IN ARGON CARRIER GAS

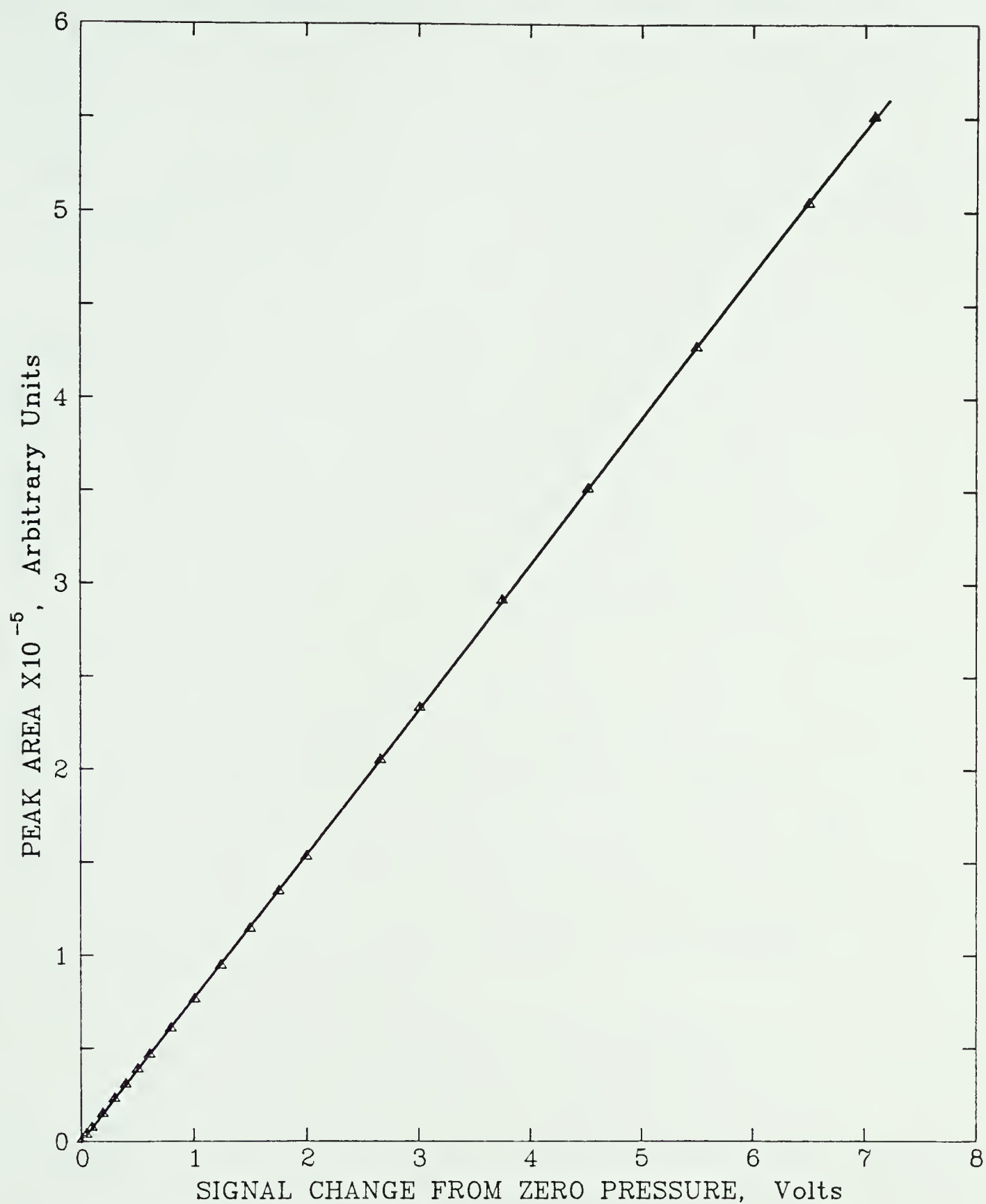


FIG. 17 CHROMATOGRAPH CALIBRATION — RELATIONSHIP BETWEEN PEAK AREA AND TRANSDUCER SIGNAL FOR METHANE IN ARGON CARRIER GAS

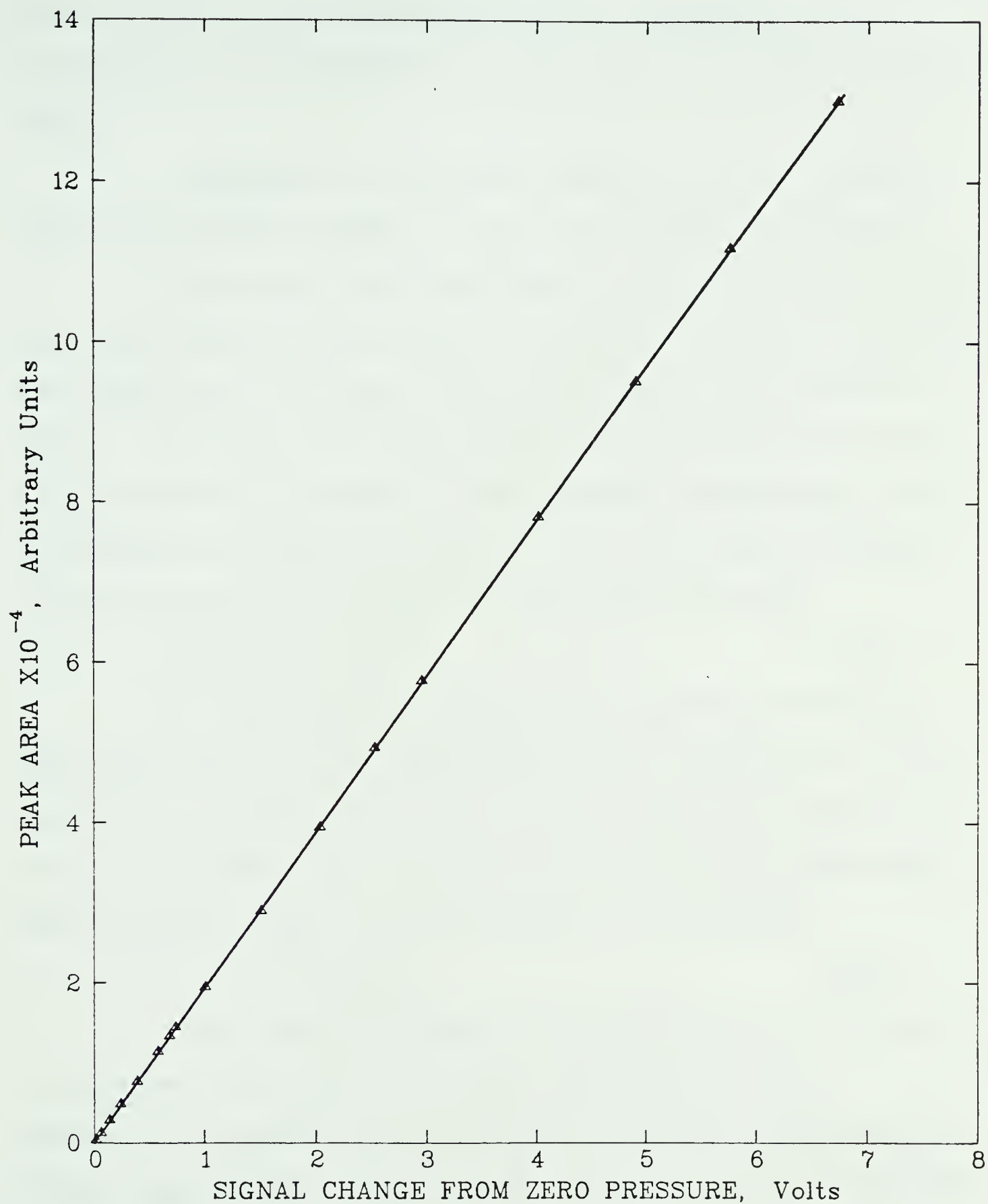


FIG. 18 CHROMATOGRAPH CALIBRATION — RELATIONSHIP BETWEEN PEAK AREA AND TRANSDUCER SIGNAL FOR CARBON DIOXIDE IN ARGON CARRIER GAS

where A_1 and A_2 are the peak areas of components 1 and 2, x_1 and x_2 are mole fractions, and a and b are weak functions of x_2 .

The case of a constant response factor is represented by setting b equal to zero and keeping a constant.

To obtain the composition of a binary mixture from the chromatograph peak areas, an iterative computer calculation was made as follows. Initial guesses were made for a and b . The peak area that component 2 would have if it responded exactly the same to the detector as component 1 was calculated from Equation (B-10). This was done by setting (x_2/x_1) equal to 1, giving the equivalent area A_e :

$$A_e = aA_2 + bA_2^2 \quad (\text{B-11})$$

If the initial guesses for a and b were correct, then the ratio A_1 (the observed area for component 1) to A_e would be in proportion to the ratio of the mole fraction x_1 to x_2 . To check this, the mole fractions of the two components were estimated from the areas. For example:

$$x_2 = A_e / (A_1 + A_e) \quad (\text{B-12})$$

With these estimates of x_1 and x_2 , new values of a and b were calculated from the correlations that follow. A revised value of A_e was calculated from Equation (B-11), and revised values of x_1 and x_2 were then calculated from Equation (B-12). The compositions were considered correct when the new value of x_2 differed by less than 0.01% from the previous value.

When a third component was present the mole

fractions from the above calculation provided only the ratio of component 1 to component 2. In this case, A_2 and x_2 in Equations (B-10) to (B-12) were replaced by A_3 and x_3 , and the above procedure was followed once more to find the ratio of x_1 to x_3 . The overall composition was then calculated by using component 1 as a tie component.

For each of the mixtures of known composition that was used, one value for each of the coefficients a and b was obtained. These values, which are plotted as circles in Figures 19 to 22, were obtained by a least squares fit to Equation (B-10) of the measured peak areas. The correlations of a and b versus mole fraction employed very simple functions, because more complicated functions were not justifiable in view of the random uncertainties that existed. These correlations appear as the solid lines in Figures 19 to 22.

For the component pair of n-pentane (component 1) and hydrogen (component 2) the following relationships were obtained:

$$\begin{aligned} a &= 7.362 + 5.443x_2 & x_2 < 0.16832 \\ a &= 8.175 + 0.613x_2 & x_2 \geq 0.16832 \\ b &= -12.02 \times 10^{-6} + 58.93 \times 10^{-6}x_2 & x_2 < 0.16623 \\ b &= -3.11 \times 10^{-6} + 5.33 \times 10^{-6}x_2 & x_2 \geq 0.16623 \end{aligned} \quad \begin{array}{l} \text{(B-13)} \\ \text{(B-14)} \end{array}$$

For n-pentane (component 1) and carbon dioxide (component 2):

$$a = 125.68 + 5.59x_2 \quad \text{(B-15)}$$

$$b = -5.58 \times 10^{-4} + 7.20 \times 10^{-4}x_2 \quad \text{(B-16)}$$

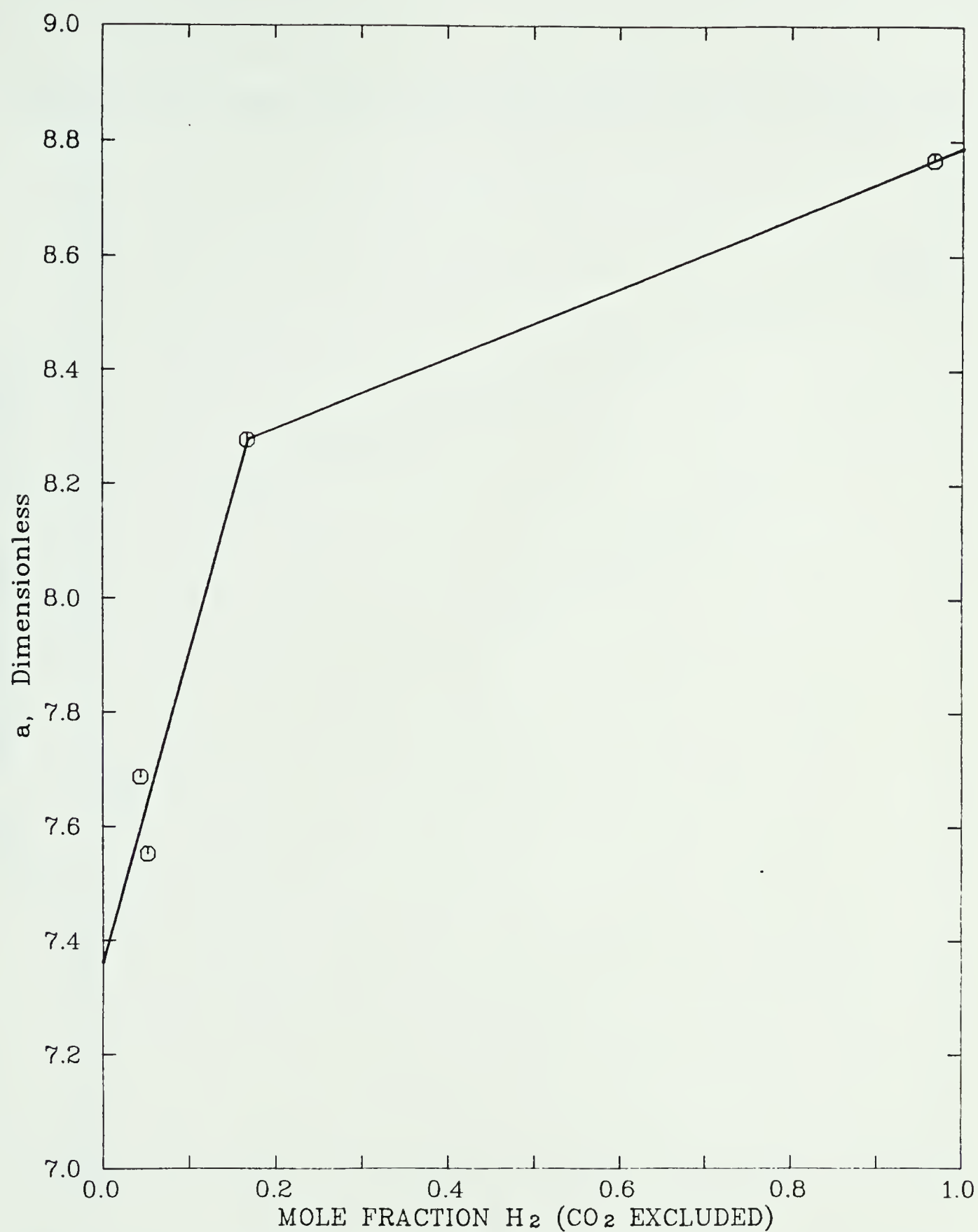


FIG. 19 COMPOSITION DEPENDENCE OF THE CONSTANT a IN THE EQUATION RELATING HYDROGEN TO n -PENTANE PEAK AREAS

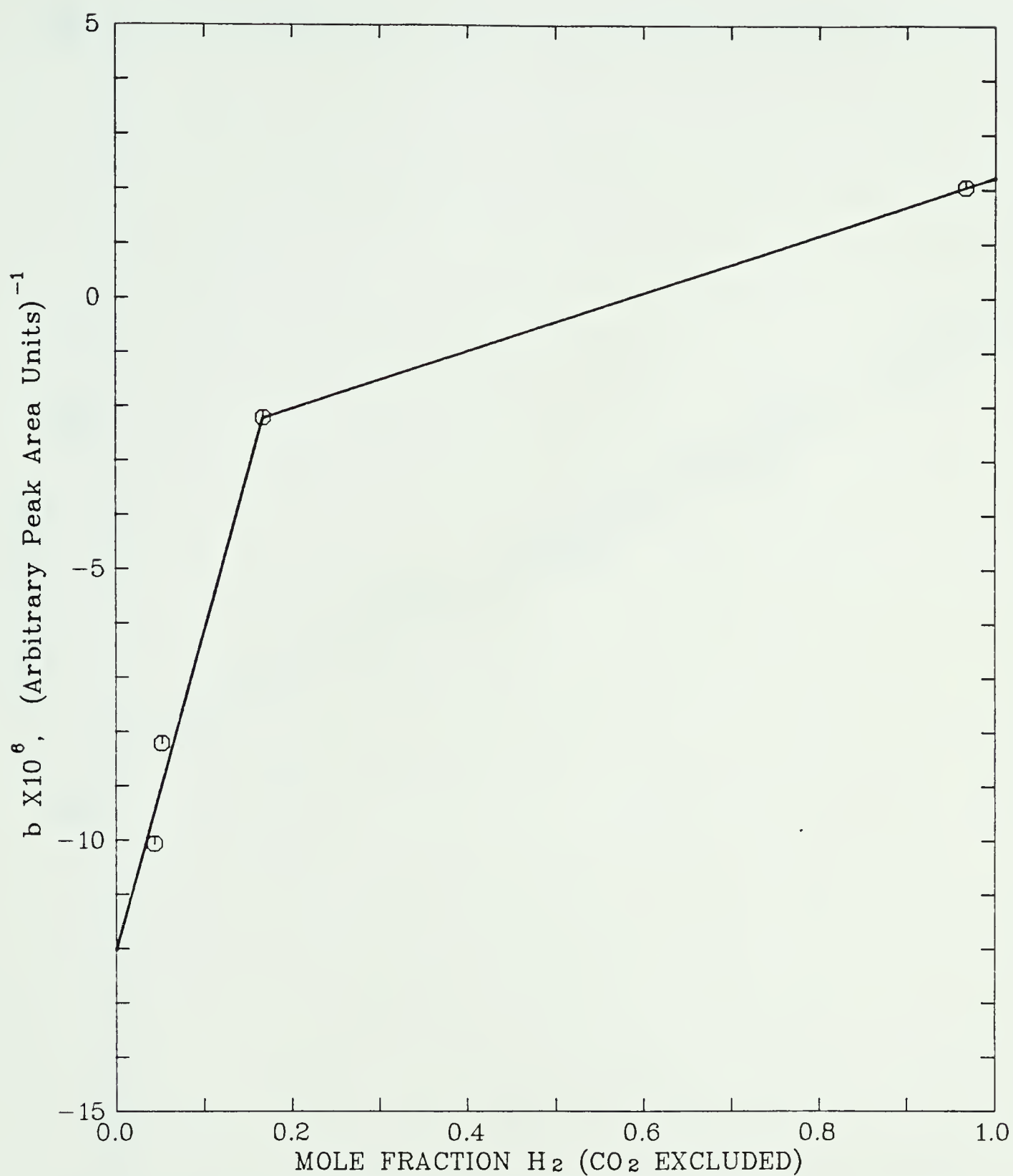


FIG. 20 COMPOSITION DEPENDENCE OF THE CONSTANT b IN THE EQUATION RELATING HYDROGEN TO n -PENTANE PEAK AREAS

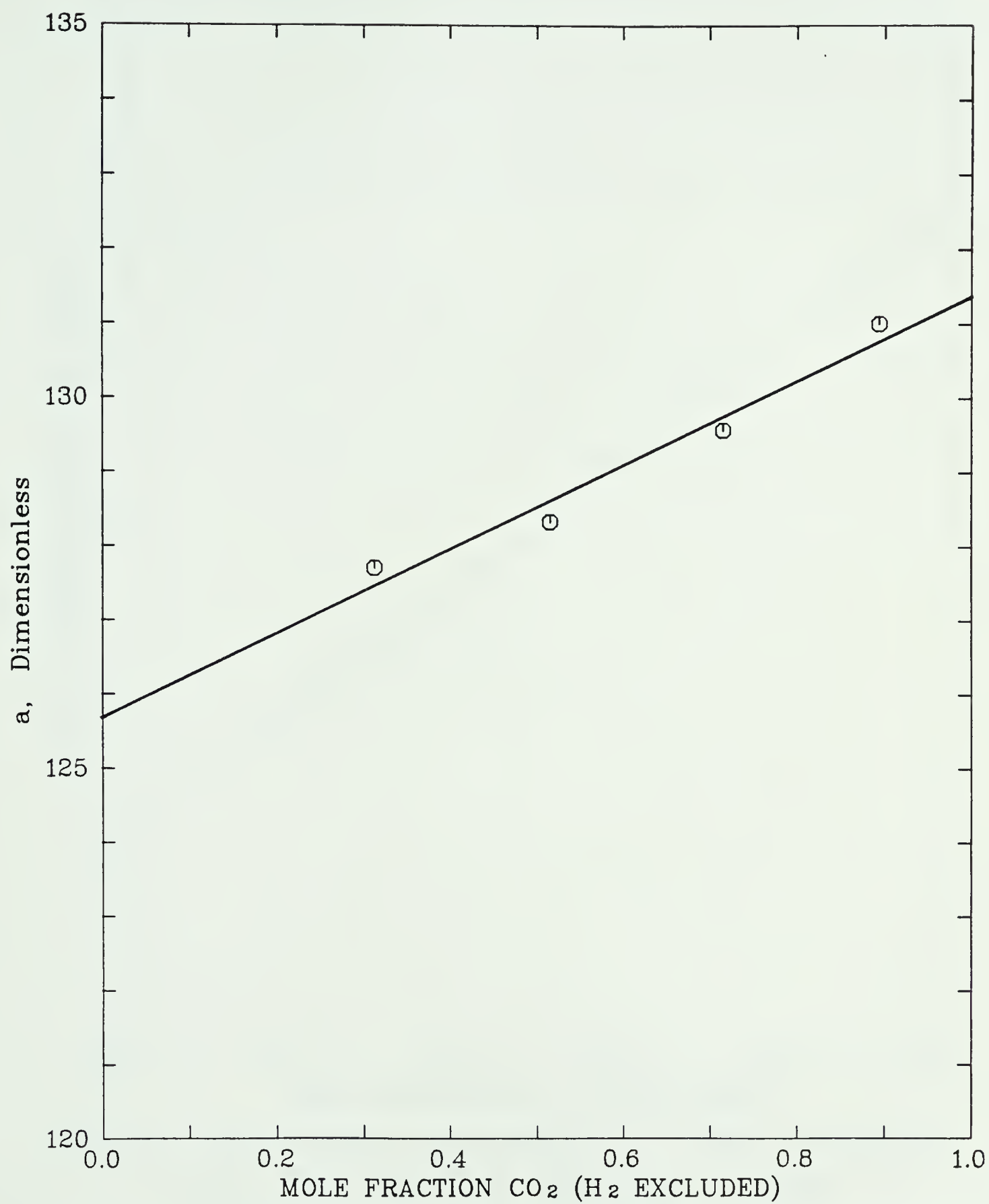


FIG. 21 COMPOSITION DEPENDENCE OF THE CONSTANT a IN THE EQUATION RELATING CARBON DIOXIDE TO n -PENTANE PEAK AREAS

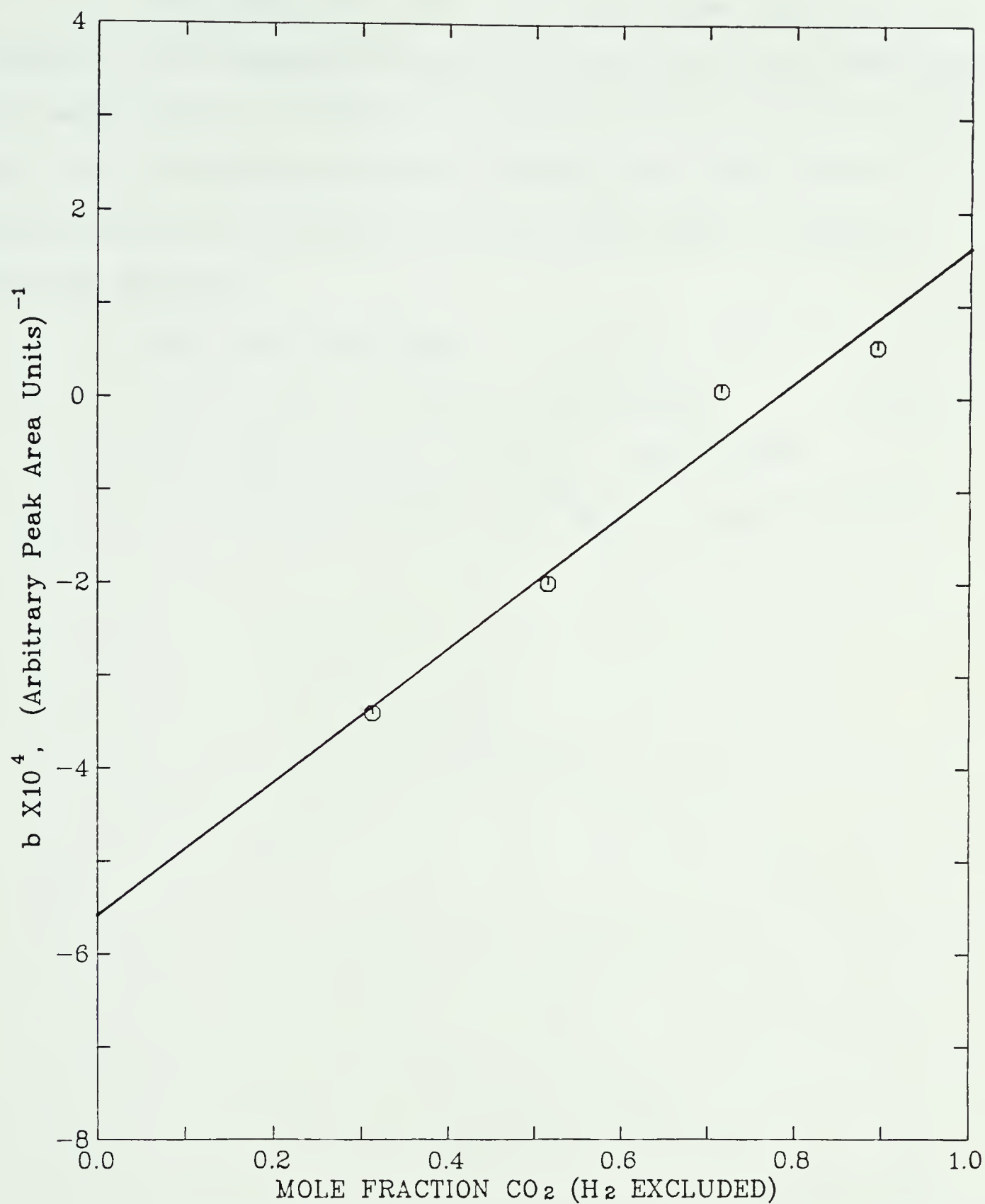


FIG. 22 COMPOSITION DEPENDENCE OF THE CONSTANT b IN THE EQUATION RELATING CARBON DIOXIDE TO n -PENTANE PEAK AREAS

The plots of a and b for the carbon dioxide (component 1) and hydrogen (component 2) pair are not presented, but were similar. They were used to calculate compositions for only the hydrogen-carbon dioxide binary data points. These points were used to establish the ends of several ternary diagrams.

The equations were:

$$a = 0.06920 - 0.02070x_2 + 0.01262x_2^2 \quad (\text{B-17})$$

$$b = 1.093 + 4.46 \times 10^{-9}x_{\text{H}_2} \quad x_{\text{H}_2} < 0.7623 \quad (\text{B-18})$$

$$b = 25.236 - 3.1226 \times 10^{-7}x_{\text{H}_2} \quad x_{\text{H}_2} \geq 0.7623$$

APPENDIX C
EXPERIMENTAL DATA

Table C-1. Experimental Equilibrium Ratios and Phase Compositions for the

Hydrogen-Methane-Carbon Dioxide System

-45.8 °C (227.35 K)

P	6900 kPa Isobar					13790 kPa Isobar				
	y_{H_2}	y_{CH_4}	y_{CO_2}	x_{H_2}	x_{CH_4}	x_{CO_2}	K_{H_2}	K_{CH_4}	K_{CO_2}	
6888	0.666	0.158	0.176	0.0176	0.0396	0.9428	37.8	3.99	0.187	
6909	0.534	0.284	0.182	0.0172	0.0782	0.9046	31.0	3.63	0.201	
6902	0.285	0.520	0.195	0.0149	0.1862	0.7989	19.1	2.79	0.244	
6936	0.130	0.661	0.209	0.0118	0.3118	0.6764	11.0	2.12	0.309	
6915	0.085	0.697	0.218	0.0104	0.3705	0.6191	8.1	1.88	0.352	
13790 kPa Isobar										
13769	0.752	0.130	0.118	0.0418	0.0532	0.9050	18.0	2.44	0.130	
13789	0.658	0.212	0.130	0.0448	0.0954	0.8598	14.7	2.22	0.151	
13803	0.414	0.416	0.170	0.0598	0.2560	0.6842	6.92	1.62	0.248	
13817	0.267	0.511	0.222	0.0865	0.4035	0.5100	3.09	1.27	0.435	
13803	0.236	0.519	0.245	-	-	-	-	-	-	

Units: P = kPa, y = mole fraction, x = mole fraction

P	y _{H2}	y _{CH4}	y _{CO2}	x _{H2}	x _{CH4}	x _{CO2}	K _{H2}	K _{CH4}	K _{CO2}
20680 kPa Isobar									
20712	0.8285	0.0644	0.1071	0.0599	0.0311	0.9090	13.8	2.07	0.118
20657	0.712	0.169	0.119	0.0714	0.0928	0.8358	9.97	1.82	0.142
20726	0.518	0.322	0.160	0.0994	0.2271	0.6735	5.21	1.42	0.238
20698	0.508	0.326	0.166	0.100	0.228	0.672	5.08	1.43	0.247
20670	0.415	0.384	0.201	0.125	0.301	0.574	3.32	1.28	0.350
-15.0 °C (258.15 K)									
6900 kPa Isobar									
6909	0.552	0.0	0.448	-	-	-	-	-	-
6915	0.551	0.0	0.449	0.0240	0.0	0.9760	23.0	-	0.460
6895	0.372	0.162	0.466	0.0201	0.0448	0.9351	18.5	3.62	0.498
6888	0.213	0.311	0.476	0.0149	0.0985	0.8866	14.3	3.16	0.537
6922	0.202	0.323	0.475	0.0146	0.1038	0.8816	13.8	3.11	0.539
6902	0.0809	0.4339	0.4852	0.0080	0.1641	0.8279	10.1	2.64	0.586
6895	0.0	0.507	0.493	0.0	0.233	0.767	-	2.18	0.643

P	y _{H2}	y _{CH4}	y _{CO2}	x _{H2}	x _{CH4}	x _{CO2}	K _{H2}	K _{CH4}	K _{CO2}
13790 kPa Isobar: Taken with Lower-Temperature Equipment									
13783	0.6417	0.0590	0.2993	0.0602	0.0244	0.9154	10.7	2.42	0.327
13789	0.545	0.133	0.322	0.0620	0.0606	0.8774	8.79	2.19	0.367
13782	0.318	0.305	0.377	0.0727	0.1862	0.7411	4.37	1.64	0.509
13782	0.236	0.348	0.416	0.0835	0.2481	0.6684	2.83	1.40	0.622
13782	0.233	0.348	0.419	0.0838	0.2480	0.6682	2.78	1.40	0.627
13790 kPa Isobar: Taken with Higher-Temperature Equipment									
13789	0.701	0.0	0.299	0.0595	0.0	0.9405	11.8	-	0.318
13789	0.5979	0.0831	0.3190	0.0605	0.0367	0.9028	9.88	2.26	0.353
13789	0.455	0.195	0.350	0.0625	0.0975	0.8400	7.28	2.00	0.417
13783	0.260	0.325	0.415	0.0732	0.2121	0.7147	3.55	1.53	0.581
13803	0.183	0.349	0.468	0.0871	0.2732	0.6397	2.10	1.28	0.732

P	y_{H_2}	y_{CH_4}	y_{CO_2}	x_{H_2}	x_{CH_4}	x_{CO_2}	K_{H_2}	K_{CH_4}	K_{CO_2}
	27580 kPa Isobar								
27558	0.758	0.0	0.242	0.132	0.0	0.868	5.74	-	0.279
27593	0.6797	0.0535	0.2668	0.1442	0.0360	0.8198	4.71	1.49	0.325
27593	0.531	0.137	0.332	0.180	0.104	0.716	2.95	1.32	0.464
27586	0.468	0.161	0.371	0.203	0.132	0.665	2.31	1.22	0.558
27607	0.411	0.176	0.413	0.227	0.152	0.621	1.81	1.16	0.665

Table C-2. Experimental Refractive Indices and Molar

Volumes for the Hydrogen-Methane-Carbon

Dioxide System

<u>P</u>	<u>n (vapor)</u>	<u>V (vapor)</u>	<u>n (liquid)</u>	<u>V (liquid)</u>
-45.8 °C (227.35 K)				
6900 kPa Isobar				
6888	(1.023)	(0.23)	1.2620	0.0395
6909	1.0248	0.250	1.2575	0.0401
6902	1.0317	0.253	1.2399	0.0429
6936	1.0506	0.180	1.2227	0.0461
6915	1.0560	0.168	1.2124	0.0483
13790 kPa Isobar				
13769	1.032	0.149	1.2560	0.0397
13789	1.0378	0.144	1.245	0.0412
13803	1.062	0.115	1.2229	0.0445
13817	1.0916	0.090	1.1900	0.0509
13803	1.1006	0.084	-	-
20680 kPa Isobar				
20712	1.041	0.105	1.2574	0.0390
20657	1.0513	0.099	-	-
20726	1.0794	0.081	1.2209	0.0436
20698	1.0776	0.084	-	-
20670	1.0965	0.075	1.2051	0.0460

Units: P = kPa, V = m³/kmol

<u>P</u>	<u>n (vapor)</u>	<u>V (vapor)</u>	<u>n (liquid)</u>	<u>V (liquid)</u>
----------	------------------	------------------	-------------------	-------------------

-15.0 °C (258.15 K)

6900 kPa Isobar

6909	1.0221	0.278	1.2336	-
6915	1.0215	0.286	1.2329	0.0439
6895	1.0280	0.265	1.2263	0.0474
6888	1.0356	0.239	1.2179	0.0470
6922	1.0367	0.234	1.2167	0.0473
6902	1.0460	0.205	1.2062	0.0498
6895	1.0570	0.175	1.1930	0.0533

13790 kPa Isobar: Taken with Lower-Temperature
Equipment

13783	1.0352	0.158	1.2242	0.0444
13789	1.0379	0.164	1.2177	0.0456
13782	1.0653	0.120	-	-
13782	1.0850	0.099	1.1728	0.0559
13782	1.0859	0.098	-	-

13790 kPa Isobar: Taken with Higher-Temperature
Equipment

13789	1.0334	0.154	1.2308	0.0432
13789	1.0404	0.145	1.2241	0.0444
13789	1.0517	0.133	1.2125	0.0466
13783	1.0780	0.105	1.1847	0.0528
13803	1.099	0.089	1.1636	0.0588

27580 kPa Isobar

27558	1.0567	0.0847	1.2249	0.0420
27593	1.0663	0.0806	1.2162	0.0432
27593	1.0879	0.0725	1.1954	0.0462
27586	1.1003	0.0685	1.1836	0.0481
27607	-	-	1.1717	0.0503

Table C-3. Experimental Equilibrium Ratios and Phase Compositions for the

Hydrogen-Carbon Dioxide-n-Pentane System

P	y _{H2}	y _{CO2}	y _{C5}	x _{H2}	x _{CO2}	x _{C5}	K _{H2}	K _{CO2}	K _{C5}
0.0 °C (273.15 K)									
6900 kPa Isobar									
6888	0.8947	0.0994	0.0059	0.0397	0.1015	0.8588	22.5	0.979	0.0069
6902	0.7327	0.2606	0.0067	0.0351	0.2923	0.6726	20.9	0.892	0.0100
6895	0.5709	0.4220	0.0071	0.0312	0.5533	0.4155	18.3	0.763	0.0171
6902	0.4461	0.5483	0.0056	0.0302	0.8416	0.1282	14.8	0.651	0.044
6895	0.3615	0.6385	0.0	0.0266	0.9734	0.0	13.6	0.656	-
13790 kPa Isobar									
13783	0.8665	0.1286	0.0049	0.0772	0.2207	0.7021	11.2	0.583	0.0070
13803	0.7475	0.2468	0.0057	0.0799	0.4908	0.4293	9.36	0.503	0.0133
13803	0.6750	0.3192	0.0058	0.0820	0.6943	0.2237	8.23	0.460	0.0259
13789	0.6211	0.3744	0.0045	0.0819	0.8320	0.0861	7.58	0.450	0.052
13796	0.550	0.450	0.0	0.0799	0.9201	0.0	6.88	0.489	-

Units: P = kPa, y = mole fraction, x = mole fraction

P	y _{H2}	y _{CO2}	y _{C5}	x _{H2}	x _{CO2}	x _{C5}	K _{H2}	K _{CO2}	K _{C5}
27580 kPa Isobar									
27565	-	-	-	0.157	0.200	0.643	-	-	-
27565	0.9129	0.0823	0.0048	0.155	0.198	0.647	5.89	0.416	0.0074
27579	0.8802	0.1142	0.0056	0.162	0.288	0.550	5.43	0.397	0.0102
27579	0.7894	0.2037	0.0069	0.171	0.542	0.287	4.62	0.376	0.0240
27607	0.7626	0.2298	0.0076	0.175	0.608	0.217	4.36	0.378	0.0350
27600	0.7046	0.2891	0.0063	0.187	0.730	0.083	3.77	0.396	0.076
27607	0.610	0.390	0.0	0.193	0.807	0.0	3.16	0.483	-
50.0 °C (323.15 K)									
6900 kPa Isobar									
6902	0.7873	0.1748	0.0379	0.0436	0.0977	0.8587	18.1	1.79	0.0441
6902	0.4754	0.4816	0.0430	0.0308	0.2806	0.6886	15.4	1.72	0.0624
6902	0.2023	0.7483	0.0494	0.0174	0.4857	0.4969	11.6	1.54	0.099
6895	0.0268	0.9184	0.0548	0.0036	0.6827	0.3137	7.4	1.35	0.175

P	y _{H2}	y _{CO2}	y _{C5}	x _{H2}	x _{CO2}	x _{C5}	K _{H2}	K _{CO2}	K _{C5}
	13790 kPa Isobar								
13796	0.8940	0.0814	0.0246	0.096	0.077	0.827	9.31	1.06	0.0297
13789	0.6339	0.3331	0.0330	0.086	0.324	0.590	7.37	1.03	0.0559
13796	0.4080	0.5483	0.0437	0.083	0.554	0.363	4.88	0.99	0.120
13789	0.227	0.710	0.063	0.096	0.732	0.172	2.38	0.97	0.364
	27580 kPa Isobar								
27586	0.9136	0.0651	0.0213	0.1895	0.0908	0.7197	4.82	0.717	0.0296
27586	0.7433	0.2264	0.0303	0.195	0.303	0.502	3.81	0.746	0.0604
27572	0.5697	0.3826	0.0477	0.222	0.485	0.293	2.57	0.790	0.163
27586	0.4419	0.4816	0.0765	0.271	0.547	0.182	1.63	0.880	0.421

Table C-4. Experimental Refractive Indices and Molar
 Volumes for the Hydrogen-Carbon Dioxide-
 n-Pentane System

<u>P</u>	<u>n (vapor)</u>	<u>V (vapor)</u>	<u>n (liquid)</u>	<u>V (liquid)</u>
0.0 °C (273.15 K)				
6900 kPa Isobar				
6888	1.0116	0.344	1.3599	0.1012
6902	1.0147	0.347	1.3417	0.0901
6895	1.0206	0.303	1.3078	0.0741
6902	1.0251	0.280	1.2503	0.0559
6895	1.0290	0.258	1.2143	0.0474
13790 kPa Isobar				
13783	1.0240	0.174	1.3466	0.0901
13803	1.0306	0.163	1.3121	0.0730
13803	1.0352	0.156	1.2734	0.0606
13789	1.0388	0.150	1.2368	0.0521
13796	1.0430	0.145	1.2091	0.0467
27580 kPa Isobar				
27565	1.0397	-	1.3458	0.0833
27565	1.0405	0.0951	1.3460	0.0840
27579	1.0438	0.0935	1.3365	0.0775
27579	1.0536	0.0893	1.2917	0.0610
27607	1.0566	0.0877	1.2727	0.0575
27600	1.0637	0.0840	1.2286	0.0503
27607	1.0723	0.0806	1.1954	0.0457

Units: P = kPa, V = m³/kmol

<u>P</u>	<u>n (vapor)</u>	<u>V (vapor)</u>	<u>n(liquid)</u>	<u>V (liquid)</u>
50.0 °C (323.15 K)				
6900 kPa Isobar				
6902	1.0143	0.392	1.3273	0.1107
6902	1.0224	0.352	1.3055	0.1015
6902	1.0328	0.304	1.2750	0.0917
6895	1.0462	0.246	1.2350	0.0833
13790 kPa Isobar				
13796	1.0218	0.207	1.3277	0.1066
13789	1.0352	0.186	1.2949	0.0935
13796	1.0529	0.159	1.2500	0.0820
13789	1.0845	0.122	1.1855	0.0787
27580 kPa Isobar				
27586	1.0385	0.112	1.3218	0.0962
27586	1.0556	0.103	1.2866	0.0840
27572	1.0802	0.0935	1.2368	0.0735
27586	-	-	1.1907	0.0714

Table C-5. Experimental Equilibrium Phase Properties of the Hydrogen-n-Pentane System

0.0 °C (273.15 K)

P	Vapor			Liquid			K_{H_2}	K_{C_5}
	y_{H_2}	n	V	x_{H_2}	n	V		
347	0.9222	(1.00049)	(11.9)	(0.0025)	1.3682	0.1114	(370.)	0.0780
1032	0.9669	1.0014	3.03	0.0064	1.3684	0.1109	151.	0.0333
1723	0.9815	1.0025	1.49	0.0113	1.3690	0.1101	86.9	0.0187
3440	0.9906	1.0048	0.714	0.0218	1.3688	0.1092	45.4	0.00961
5170	0.9932	1.0071	0.467	0.0332	1.3715	0.1073	29.9	0.00703
5170	-	-	-	-	1.3690	0.1080	-	-
6910	0.9944	1.0093	0.353	0.0457	1.3708	0.1063	21.8	0.00587
6910	-	1.0092	0.357	-	1.3688	0.1067	-	-
10350	0.9957	1.01365	0.238	0.0671	1.3706	0.1041	14.8	0.00461
10350	-	1.01361	0.239	-	1.3686	0.1046	-	-
13800	0.9961	1.01774	0.1828	0.0840	1.3683	0.1030	11.9	0.00426
13800	-	1.01782	0.1818	-	1.3684	0.1029	-	-
20650	0.9965	1.0255	0.1267	0.124	1.3678	0.0990	8.04	0.00400
27580	0.9964	1.0328	0.0989	0.161	1.3678	0.0951	6.19	0.00429

Units: P = kPa, y = mole fraction, x = mole fraction, V = m³/kmol

50.0 °C (323.15 K)

P	Vapor			Liquid				K _{H2}	K _{C5}
	y _{H2}	n	V	x _{H2}	n	V			
347	0.512	(1.0033)	(6.2)	0.00161	1.3384	0.1209		318.	0.489
693	0.749	1.0033	3.6	0.0044	1.3389	0.1204		170.	0.252
694	0.748	-	-	0.0045	-	-		-	-
1724	0.8945	1.0046	1.47	0.0124	1.3382	0.1197		72.1	0.107
3450	0.9418	1.0066	0.775	0.0258	1.3380	0.1183		36.5	0.0597
3450	0.9440	-	-	0.0265	-	-		-	-
5180	0.9589	1.0088	0.513	0.0386	1.3376	0.1170		24.8	0.0428
6890	0.9666	1.0107	0.398	0.0520	1.3372	0.1156		18.6	0.0352
10340	0.9746	1.0147	0.272	0.0783	1.3364	0.1130		12.4	0.0276
13790	0.9786	1.0186	0.208	0.1035	1.3359	0.1103		9.46	0.0239
13790	0.9762*	-	-	0.0975*	-	-		-	-
20680	0.9814	1.0255	0.147	0.146	1.3347	0.1058		6.72	0.0218
20720	-	1.0257	-	-	1.3346	-		-	-
27590	0.9823	1.0328	0.114	0.196	1.3333	0.1006		5.01	0.0220

* Reliability is uncertain

100.0 °C (373.15 K)

P	Vapor		Liquid			K _{H2}	K _{C5}
	y _{H2}	n	V	x _{H2}	n	V	
1036	0.373	1.0091	2.8	0.0047	1.3037	0.1337	0.630
1726	0.610	1.0101	1.67	0.0125	1.3032	0.1330	0.395
3450	0.793	1.0122	0.85	0.0314	1.3032	0.1307	0.214
5170	0.840	1.0143	0.61	0.0477	1.3024	0.1289	0.168
6890	0.875	1.0160	0.465	0.0666	1.3006	0.1259	0.134
10340	0.902	1.0200	0.325	0.101	1.2992	0.1222	0.109
13790	0.923	1.0240	0.242	0.137	1.3002	0.1174	0.0892
20680	0.9374	1.0320	0.166	0.203	1.2953	0.1109	0.0785
27590	0.942	1.0400	0.129	0.259	1.2946	0.1042	0.0783

APPENDIX D

CALCULATION OF MOLAR VOLUME

The molar volumes of the co-existing phases were calculated according to Equation (D-1), which is a rearrangement of the formula for the Lorentz-Lorenz refractivity:

$$V = \frac{R_{LLm}(n^2+2)}{(n^2-1)} \quad (D-1)$$

In the above equation n is the refractive index, R_{LLm} is the Lorentz-Lorenz refractivity for the mixture in units of $m^3/kmol$ and V is the molar volume, also in units of $m^3/kmol$

R_{LLm} was calculated for each mixture from Equation (D-2):

$$R_{LLm} = \sum_{i=1}^N z_i R_{LLi} \quad (D-2)$$

where z_i is the mole fraction of the i^{th} component, R_{LLi} is the molar refractivity of pure component i , and N is the number of components in the mixture. For those components for which the pure component refractivity varied with temperature and density, the values of R_{LLi} used in Equation (D-2) were taken to be the refractivities of the pure components at the same temperature and molar density as the experimental mixture.

As a result of the above approximation an iterative procedure was required to calculate molar volumes. A mixture density was calculated from assumed refractivities. This density was then used to obtain better estimates of the pure component refractivities. Because refractivity varies only slightly with density, agreement within the convergence limit of 0.001% change between iterations was usually obtained by the third calculation.

The calculations were performed on a digital

computer, and as a convenience the pure component refractivities were represented in equation form. These equations and the sources used in forming them are provided below.

For pure hydrogen, the refractivity is given by:

$$R_{LL} = 0.0020649 + \frac{0.03471\rho}{T} + \frac{1.732\rho^2}{T} \quad (D-3)$$

where ρ is density in kmol/m^3 , and T is the temperature in kelvins. The equation coefficients were found by least squares fitting of the data of Diller (11) for normal hydrogen at 98 and 298 K. The form of Equation (D-3) is taken from the same article, and is based on the more extensive data for parahydrogen. The refractivities reported by Diller were measured by using light of wavelength 546.2 nm. To correct his results to make them apply to the wavelength used in this work (632.8nm) the equation for R_{LL} from Diller's data was multiplied by the factor 0.99371. This factor is the ratio of the refractivity of hydrogen at 632.8 nm to the refractivity at 546.2 nm, when hydrogen is at standard temperature and pressure. The ratio was obtained by calculating refractivities from refractive index data from the literature (32) and the calculated density of hydrogen, then plotting these values of refractivity against wavelength, and calculating the ratio from the refractivities interpolated at 632.8 nm and 546.2 nm. As no data were found for the dispersion of hydrogen at densities other than at standard conditions, this correction factor was of necessity assumed to remain constant with changes of density.

For pure methane the refractivities were determined

from

$$R_{LL} = 0.006572 + 0.00546\rho - 0.288\rho^2 \quad (D-4)$$

This equation was obtained by least squares fitting of Olson's data (31) for R_{LL} of methane at 546.2 nm. The correction factor for wavelength was based upon data from the literature (46), and was obtained in the same manner as for hydrogen. In this case, the correction factor was 0.9935.

For carbon dioxide and n-pentane the Lorentz-Lorenz refractivities at 632.8 nm have been reported by Besserer and Robinson (6), who used optical equipment that was the same in principle as the apparatus used for this work (see Chapter III). For carbon dioxide they reported R_{LL} to be constant at 0.00660 m³/kmol. For n-pentane they observed a small temperature dependence of R_{LL} , which is well represented by the expression

$$R_{LL} = 0.02439 + 0.0000027T \quad (D-5)$$

where T is in kelvins.

APPENDIX E

DIMENSIONS OF NEW EQUILIBRIUM CELL

(All dimensions are in inches)

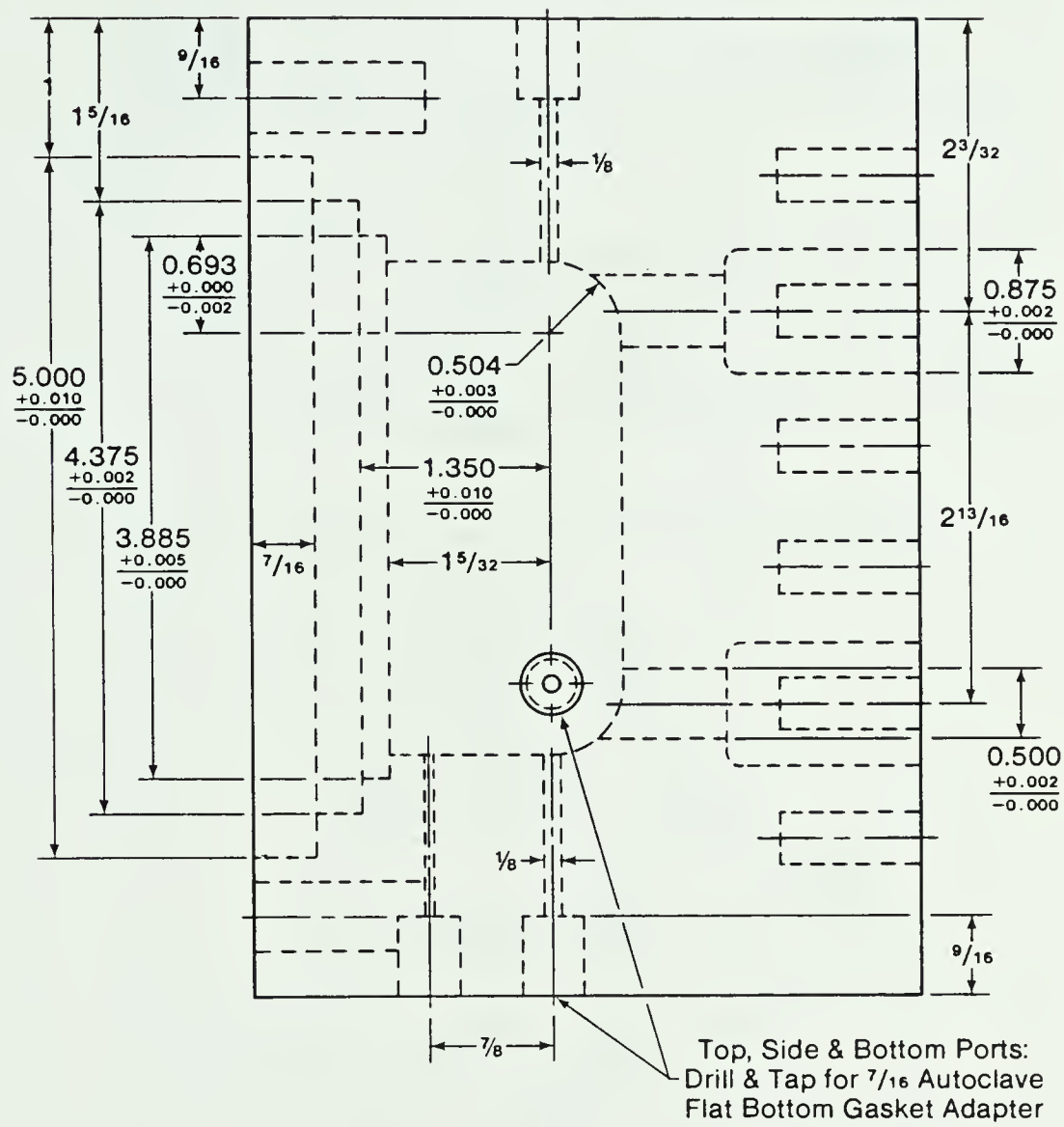


FIG. 24 Side View of Equilibrium Cell

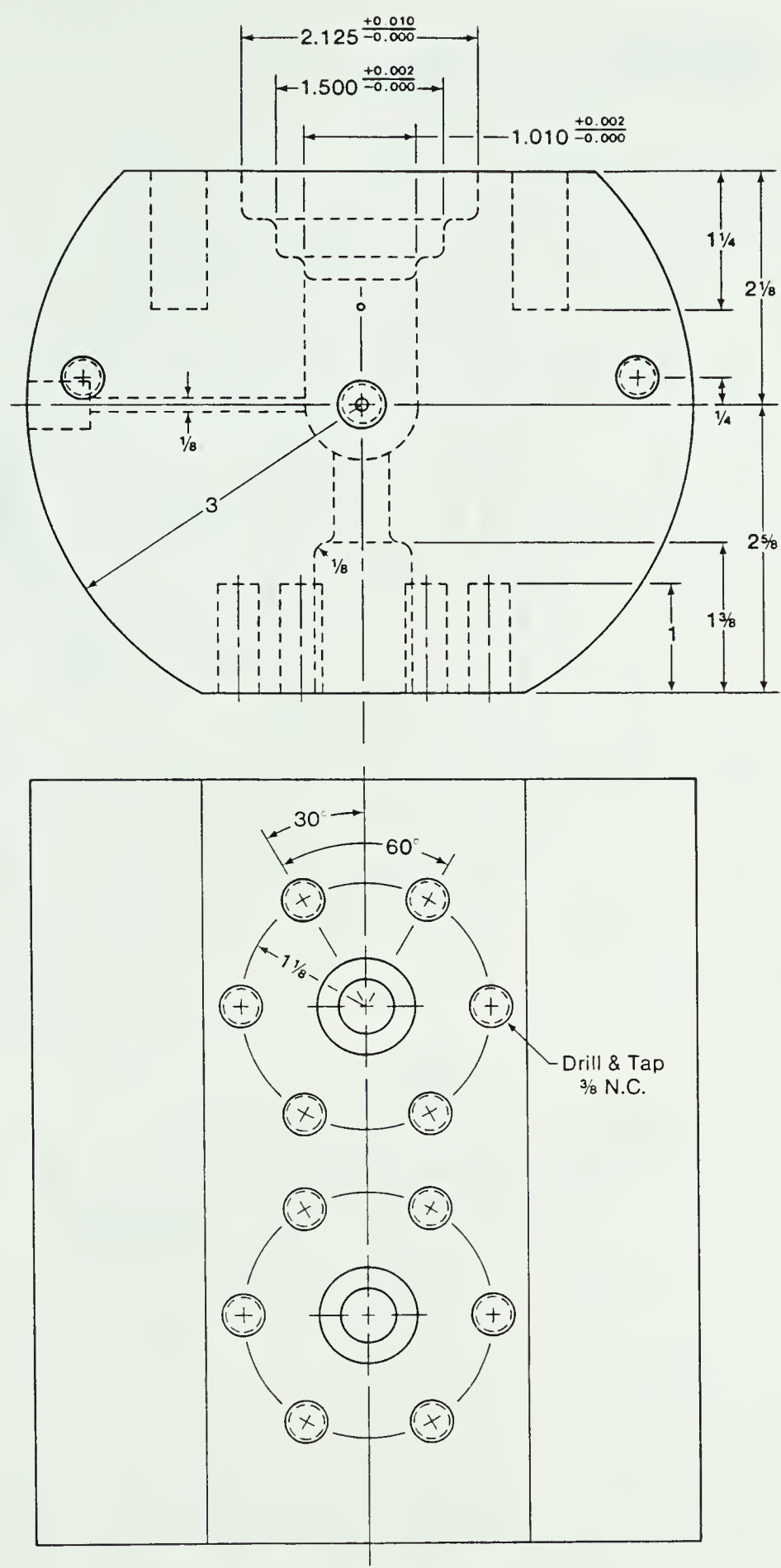


FIG. 25 Top and Rear Views of Equilibrium Cell

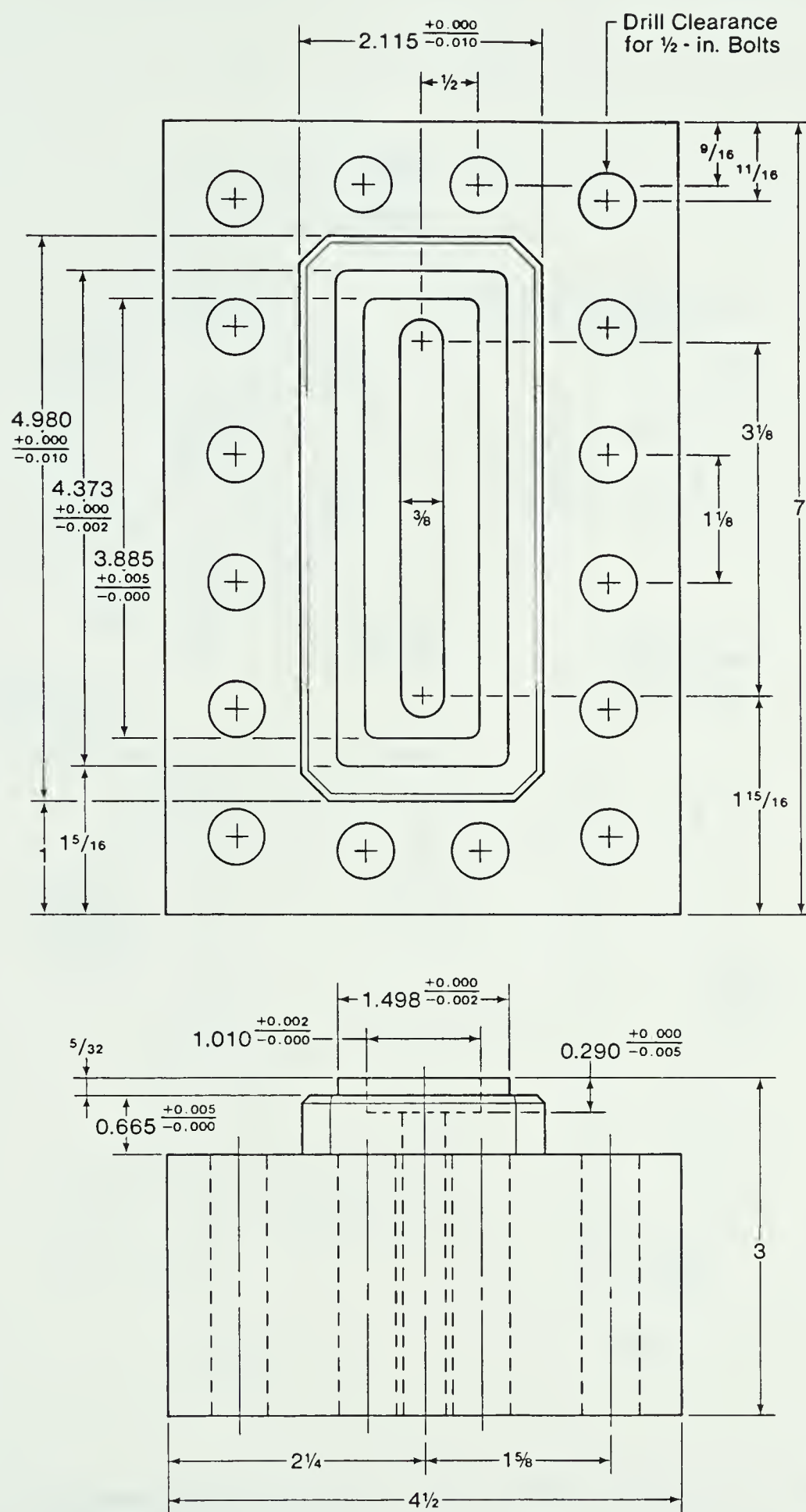


FIG. 26 Dimensions of the Window Cover Plate for the Equilibrium Cell

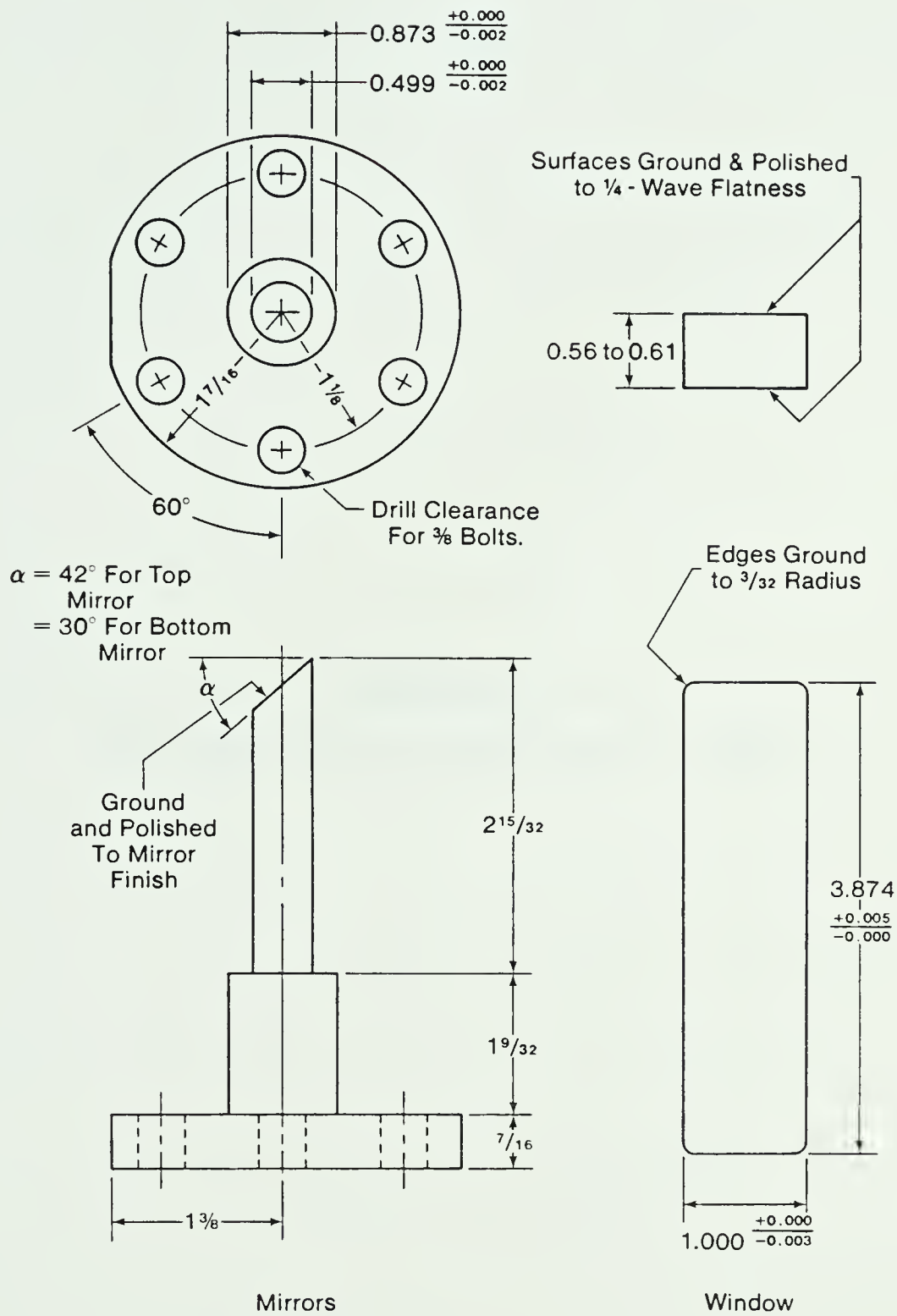


FIG. 27 Dimensions of the Mirrors and Window for the Equilibrium Cell

APPENDIX F

THE PENG-ROBINSON EQUATION OF STATE

The Peng-Robinson equation of state has the form

$$P = \frac{RT}{V-b} - \frac{a(T)}{V(V+b)+b(V-b)} \quad (F-1)$$

To evaluate the constants $a(T)$ and b the derivative conditions at the critical point are applied. These conditions are that the first and second derivatives of pressure with respect to temperature are equal to zero at the critical point when temperature is held constant. When applied to Equation (F-1) the result is

$$a(T_c) = 0.45724 \frac{R^2 T_c^2}{P_c} \quad (F-2)$$

$$b = 0.07780 \frac{RT_c}{P_c} \quad (F-3)$$

At other than the critical temperature

$$a(T) = a(T_c) \alpha(T_r, \omega) \quad (F-4)$$

$$\alpha(T_r, \omega) = [1 + \kappa(1 - T_r^{\frac{1}{2}})]^2 \quad (F-5)$$

$$\kappa = 0.37464 + 1.54226\omega - 0.26992\omega^2 \quad (F-6)$$

The mixing rules used to calculate $a(T)$ and b for a mixture are

$$a_m = \sum_i \sum_j x_i x_j (a_i a_j)^{\frac{1}{2}} (1 - k_{ij}) \quad (F-7)$$

$$b_m = \sum_i x_i b_i \quad (F-8)$$

where k_{ij} is the binary interaction parameter determined empirically from vapor-liquid equilibrium data of the binary system formed by components i and j .

The application of equations of state to vapor-liquid equilibrium calculations follows from the condition for equilibrium and the application of a thermodynamic relationship. The equilibrium condition is that for every component i , the fugacity f in each phase must obey

$$f_i^V = f_i^L \quad (F-8)$$

where superscripts V and L refer to the vapor and liquid phases respectively. When Equations (F-1) to (F-8) are substituted into the following rigorous thermodynamic equation

$$\ln \frac{f_i}{x_i P} = \int_V^\infty \left[\frac{1}{RT} \left(\frac{\partial P}{\partial n_i} \right) - \frac{1}{V} \right] dV - \ln Z \quad (F-9)$$

the result is

$$\begin{aligned} \ln \frac{f_i}{x_i P} = & \frac{b_i}{b_m} (Z_m - 1) - \ln(Z_m - B_m) - \\ & \frac{A_m}{2\sqrt{2}B_m} \left(\frac{2\sum x_i a_{ij}}{a_m} - \frac{b_i}{b_m} \right) \ln \left(\frac{Z_m + 2.414B_m}{Z_m - 0.414B_m} \right) \end{aligned} \quad (F-10)$$

where

$$A_m = \frac{a_m P}{R^2 T^2} \quad (F-11)$$

and

$$B_m = \frac{b_m P}{RT} \quad (F-12)$$

B30356